

Diamonds are a girl's best friends

Minerals have a definite chemical composition ; e.g. magnetite Fe_3O_4

However, many if not most fixed chemical compositions can assume more than one xtal structure

One speaks of different phases

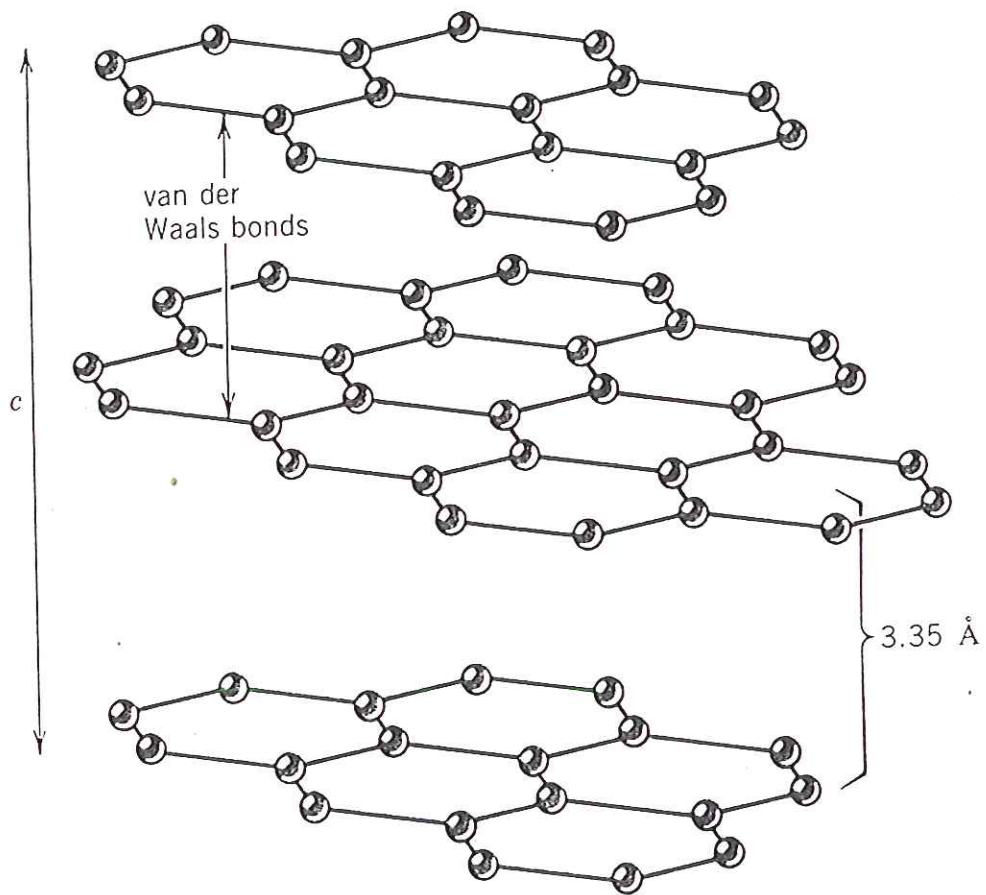
Familiar example — pure carbon C — two forms

- graphite — hexagonal symmetry — sheets of ~~hexagons~~ C hexagons linked by very weak van der Waals bonds — extremely soft — pencil lead
Fig 4.38 KH

van der Waals — weakest type of chemical bond — graphite is so soft that it can be abraded by rubbing on paper

- diamond — hardest substance known
KH Fig 10.8 Fig 5.1a Putnis
3-d tetrahedral framework — equally strong in all directions

FIG. 4.38 Perspective sketch of the graphite structure with covalent bonding between carbon atoms within layers and residual (van der Waals) bonding between layers. Note large separation (3.35 \AA) between layers.



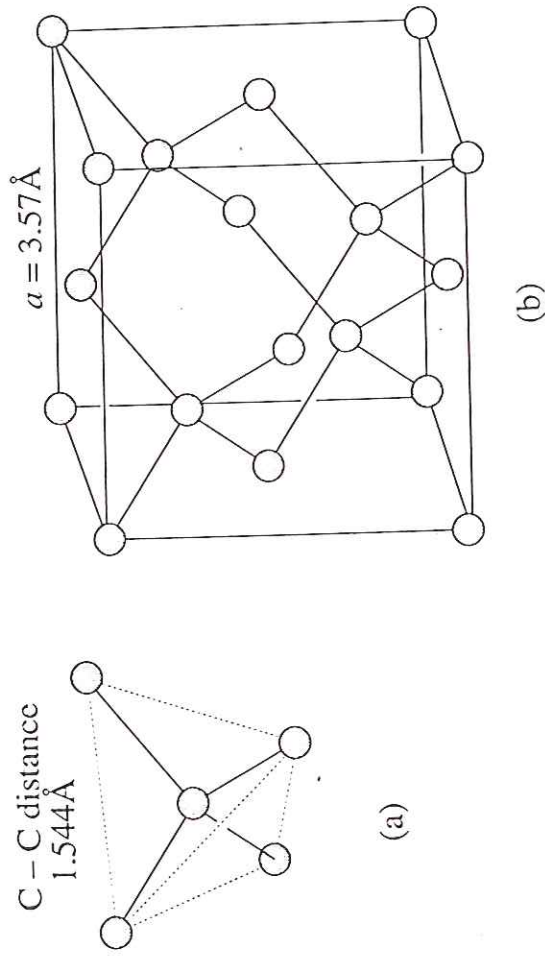


Figure 5.1. (a) The carbon atom at the centre is tetrahedrally coordinated to four neighbouring carbon atoms. These four carbon atoms lie on the corners of a regular tetrahedron (shown in the dashed line). (b) The diamond structure is built up from these tetrahedra, and every carbon atom is coordinated in this way.

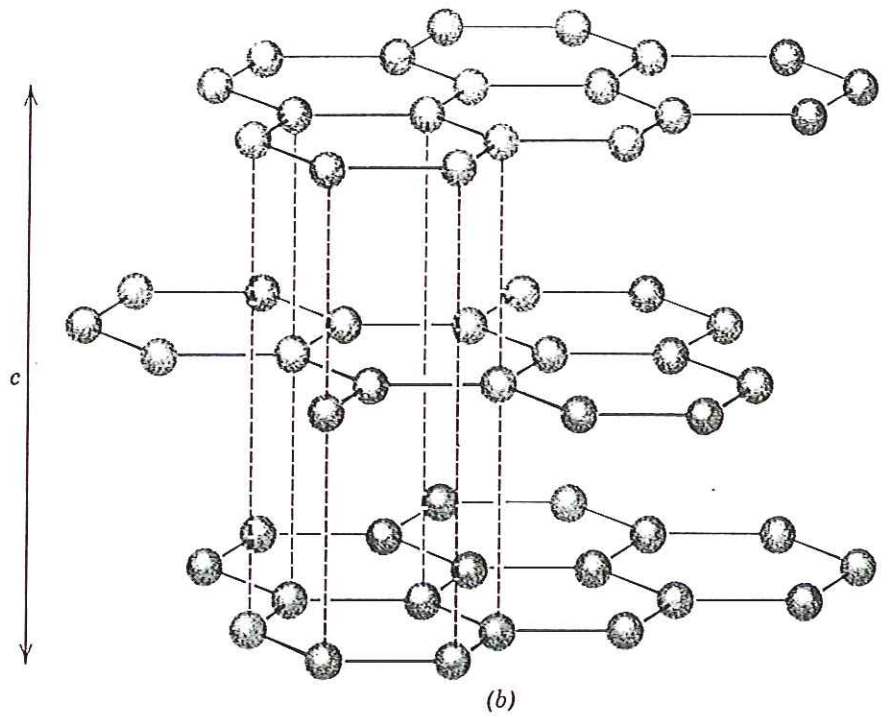
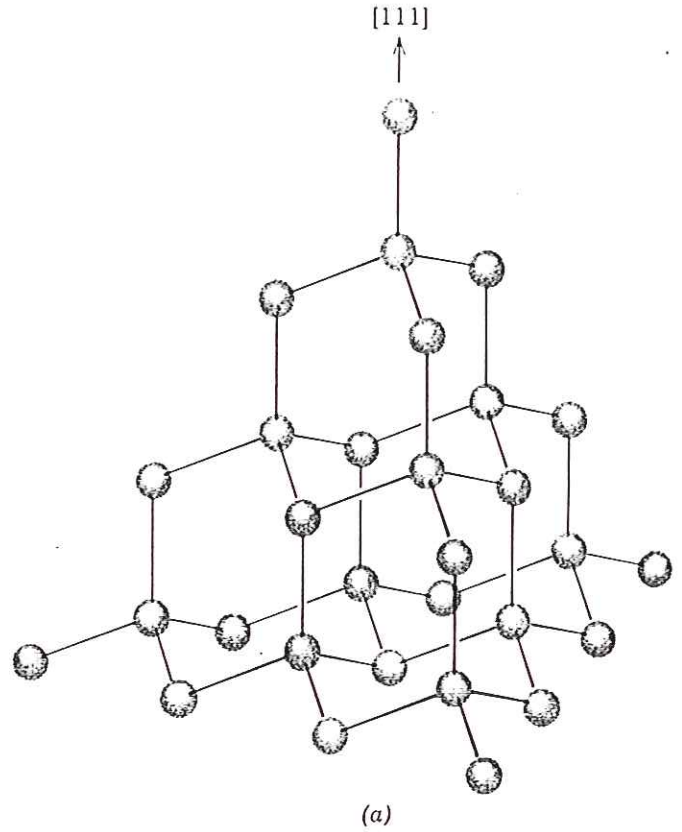


FIG. 10.8. (a) Partial representation of the structure of diamond. The horizontal plane is (111). (b) The structure of graphite with sheets // {0001}. Dashed vertical lines link atoms in successive sheets; these lines do not represent bonds.

The World's Great Diamonds

The diamonds that are called great are both physically large, usually more than 50 carats for near colorless stones or 30 for blues and pinks, and have an additional claim to fame, such as their history, cut, uniqueness, or sheer magnificence. On the pages that follow, we present a number of diamonds that are universally accepted as "great" because of their grandeur and grand histories.

The Hope

A 45.52-carat antique cushion-cut blue diamond mounted in a pendant surrounded by smaller white diamonds, the Hope is perhaps the best-recognized gem in the world. It is a recut version of the Great Blue that was part of the French crown jewels. It is one of the Indian diamonds, probably from the Kollur deposits, brought back to Louis XIV by Jean-Baptiste Tavernier in 1668. Originally weighing 112 $\frac{3}{4}$ carats (about 110.5 metric carats), the Tavernier Blue was recut from an irregular form to a heart shape of 67 $\frac{1}{2}$ carats by the king's diamantier, Pitau, and set in an Order of the Golden Fleece.¹ Stolen during the French Revolution and probably recut in London in its present form, it was acquired by the banker Henry Philip

Hope sometime after 1830 for an estimated £18,000. The Hope family sold it in 1901 after which its history is complicated. It came into the hands of jeweler Pierre Cartier in 1909. By refaceting its girdle and creating a new mounting, Cartier endeavored to interest Mrs. Evalyn Walsh McLean, daughter-in-law to Edward B. McLean, owner of the *Washington Post*, in the Blue. The deal was completed in 1910 or 1911. In 1949, two years after Mrs. McLean's death, Harry Winston bought the Hope, which had been evaluated for \$176,920, and in 1958 presented the fabulous blue diamond to the Smithsonian Institution. It is displayed in the Harry Winston Gallery at the National Museum of Natural History, where it is the most revered object in all the Smithsonian collections. (Courtesy of National Museum of Natural History, Smithsonian Institution.)

The Regent

A 140.5-carat cushion-cut water-clear, yet faintly blue, diamond. The original stone weighed 410 carats and was discovered in 1701 at the Partial mine along the Krishna River. By an unresolved set of transactions, it was sold to Thomas Pitt, a merchant and

Regent 140.5 carats
(1 carat = 200 mg)
≈ 1 ounce



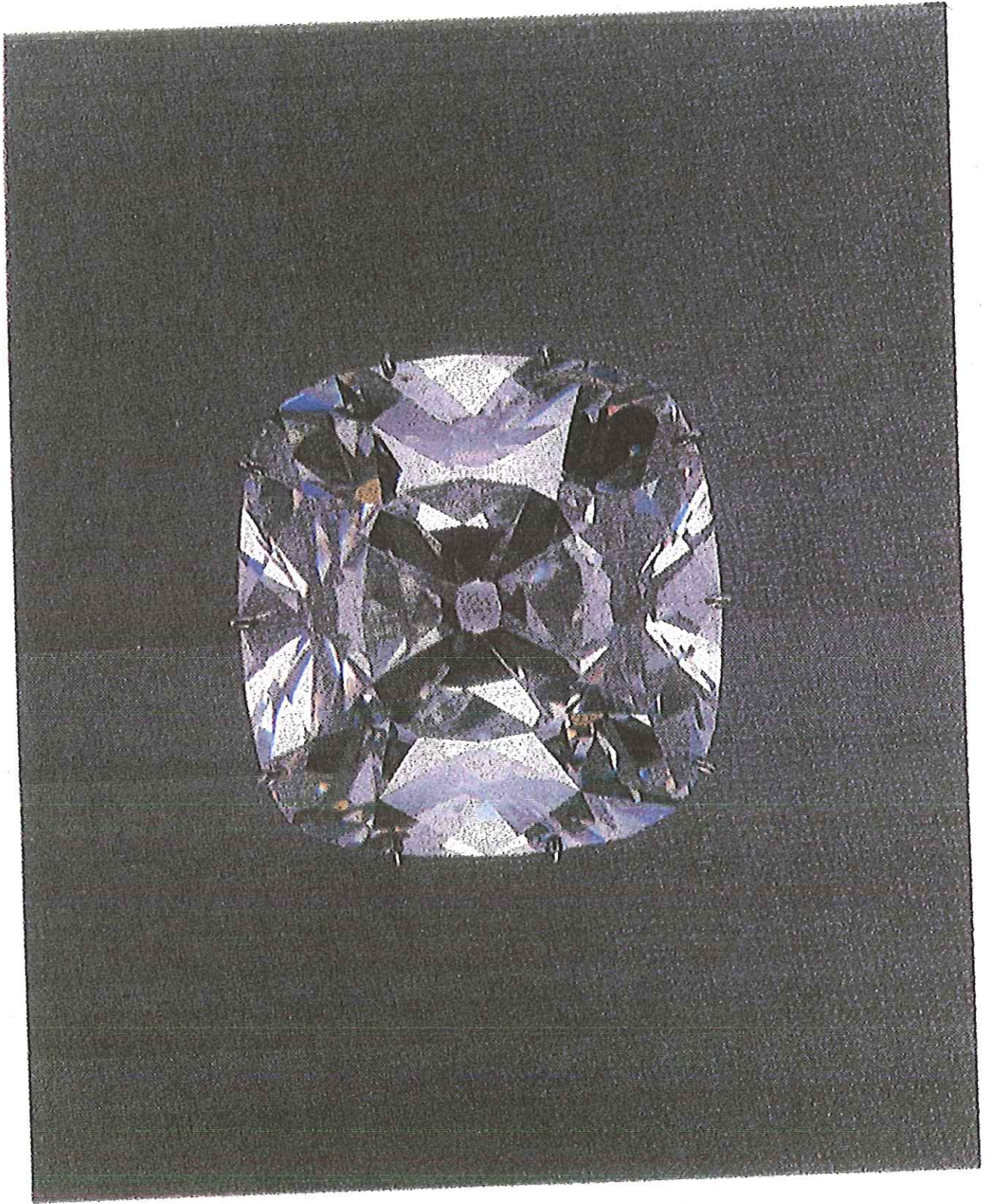
The Hope

president of Fort Madras, for the equivalent of about £20,000. In 1702, Pitt's son brought the stone to England and had it cut to its present form by Joseph Cope. But the elder Pitt was the subject of unflattering rumors about how he acquired the diamond, then known as the Pitt. Disputes ensued which led him to sell the gem to Philippe d'Orléans, regent of France, in 1717 for £135,000, the highest price paid for a gem to that time. With the name of Regent, the diamond was set above the rim of the coronation crown of Louis XV in 1722. Stolen in 1792 with the other French crown jewels, the Regent was found in the attic of a Parisian house and was used as collateral for several loans to finance the French Revolution and ensuing wars. Napoleon treasured the Regent as a talisman and had it

mounted in the guard of his ceremonial consular sword and later in his imperial sword. Last set in a Greek-style diadem for Empress Eugénie in the 1880s, the Regent was one of the several diamonds not auctioned by the Third Republic in 1887. It is displayed today in the Galerie d'Apollon at the Louvre. (Courtesy of Réunion des Musées Nationaux.)

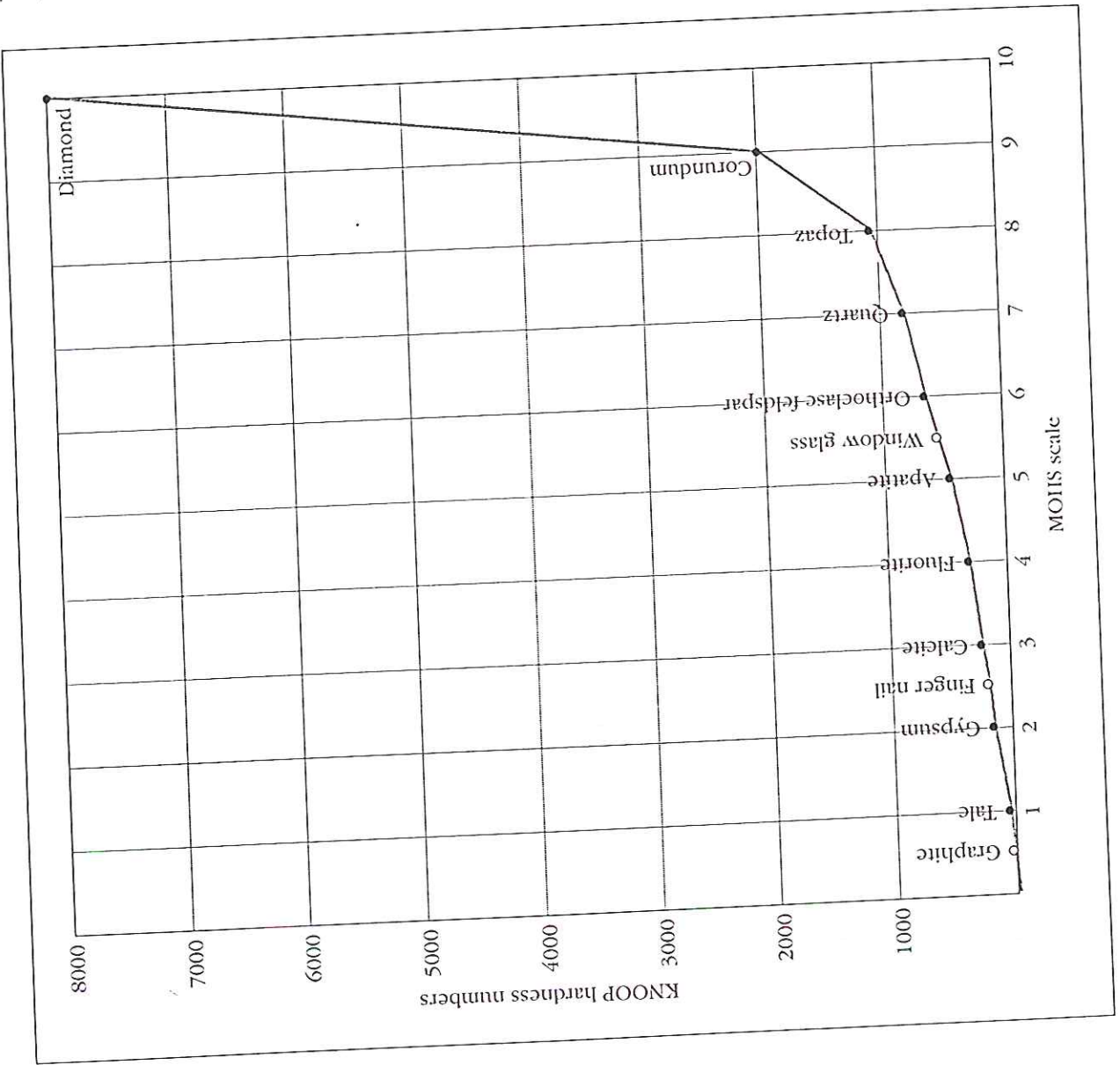
The Sancy

This pale-yellow pear-shaped diamond weighing 55.23 carats has a bewildering history. Its origin in India is lost, so the tale begins with French diplomat Nicolas Harlay de Sancy (1546–1627) who acquired several



The Regent

Figure 7. Comparison of the Mohs scale of hardness and the Knoop indenter hardness scale shows the dramatically greater hardness of diamond, as compared with the nearly linearly related hardnesses of other minerals. (Adapted from Bruton, 1978.)



MOHS HARDNESS SCALE

1. Talc
2. Gypsum
3. Calcite
4. Fluorite
5. Apatite
6. Feldspar
7. Quartz
8. Topaz
9. Corundum
10. Diamond

each C linked to each other C
by a covalent bond

C-C bond length 1.54 Å

In contrast, interplanar van der
Waals bonds in graphite ~~3.35 Å~~ 3.35 Å

insert

Fig. 7 Harlow shows mineral
hardnesses — measured by
size of indentation made by
a diamond indenter



Diamond is ~ 1000 times harder
than graphite

Phase diagrams: used to show which
phase of a substance is
thermodynamically stable under
given P, T and other
environmental conditions



Picture of Regent from Harlow
William Pitt → Philippe d'Orleans (Regent
of France → Napoleon's sword — now in
Gabriele d'Apollon 140 carats = 200mg
1 carat = 1/5 gm

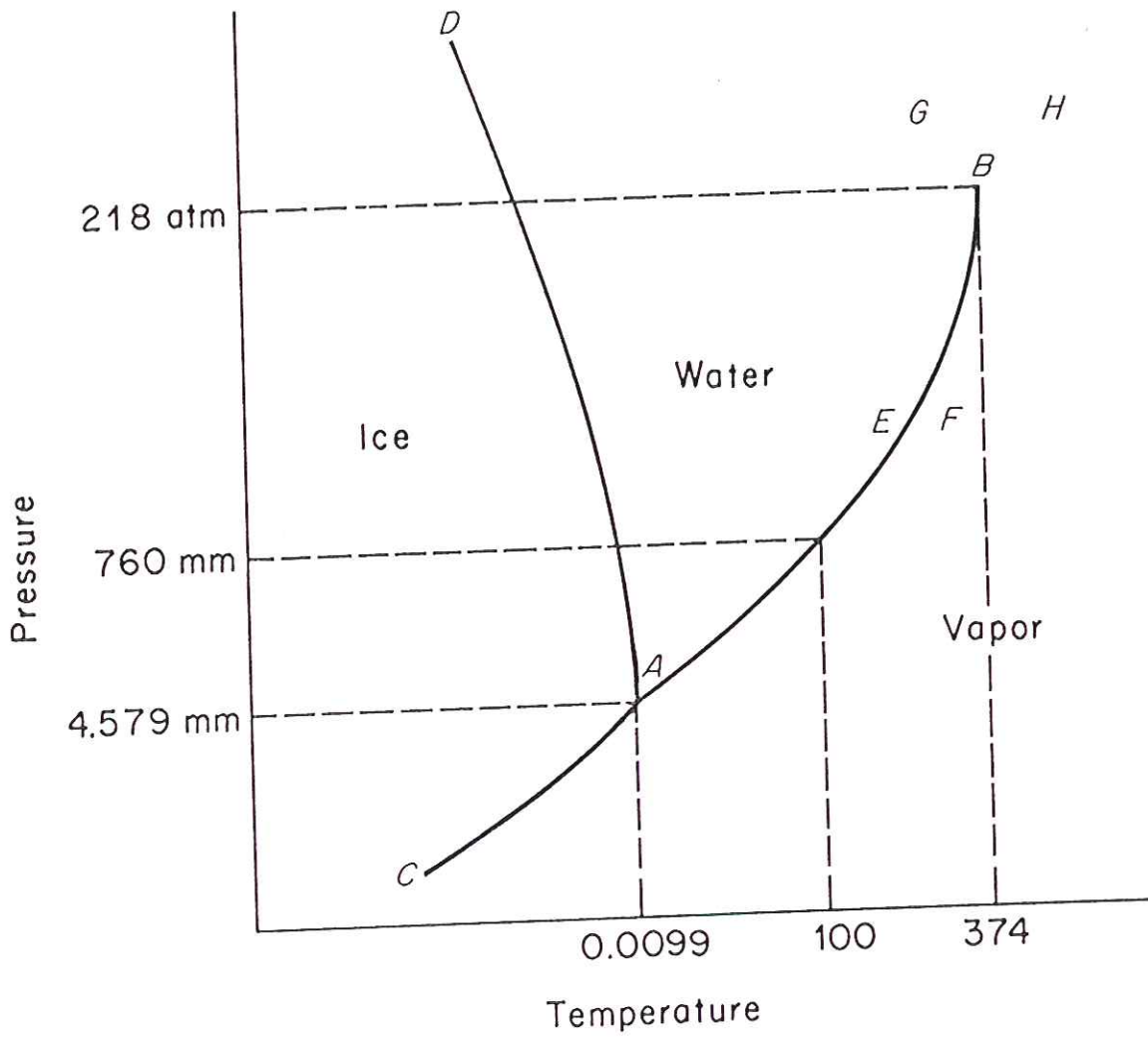


FIGURE 147
 Schematic *PT* diagram, showing the relations
 between ice, water, and vapor.

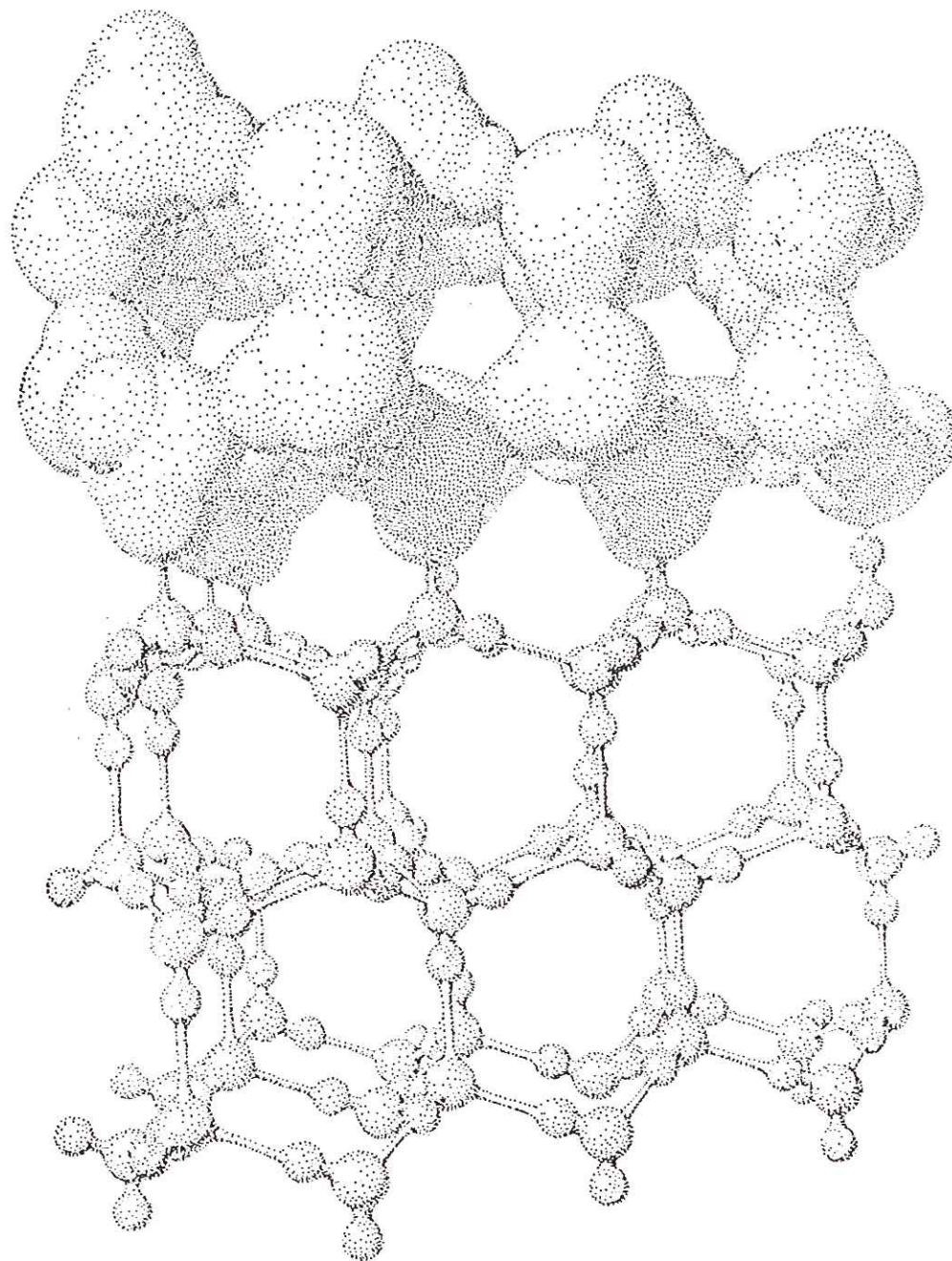


FIG. 15-11 *A small part of a crystal of ice. The molecules above are shown with approximately their correct size (relative to the interatomic distances). Note hydrogen bonds, and the open structure which gives ice its low density. The molecules below are indicated diagrammatically as small spheres for oxygen atoms and still smaller spheres for hydrogen atoms.*

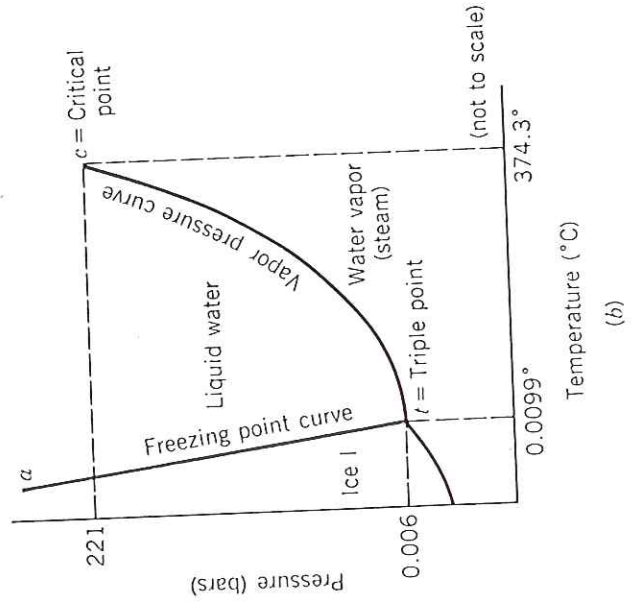
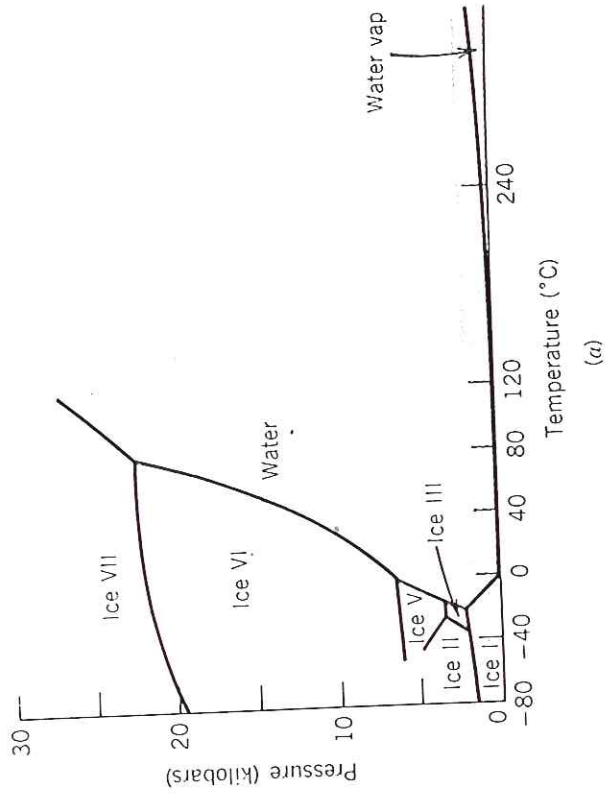


FIG. 9.1 (a) P - T diagram for H_2O . Six polymorphic types of ice are indicated by I, II, III, V, VI, and VII. (After Bridgeman, P. W., *Jour. Chemical Physics*, 1937, v. 5, p. 965, and *Phase Diagrams for Ceramists*, copyright © American Ceramic Society, Columbus, Ohio, 1964.) For clarity the water/ice vapor curve has been offset slightly toward higher pressure. The shaded region in figure (a) is enlarged, but not to scale. in (b).

Q & A



Victoria Roberts

Freezing Water

Q. Is the freezing point of water altered by pressure? Why does deep sea water not freeze?

A. The freezing temperature of water drops about one degree for every 75 of the units of pressure called atmospheres, but the change is small compared with the difference even one atmosphere of pressure makes in raising the boiling point, said Dr. Alan J. Friedman, director of the New York Hall of Science in Queens. (One atmosphere is equal to 14.69 pounds per square inch.)

Why deep sea water does not freeze depends less on pressure than on two other factors, he said: "The ocean is salt water, which interferes with the freezing process and lowers the freezing point, and at depths of a mile or so, there is considerable heating from inside the earth."

At normal atmospheric pressure, water freezes at 32 degrees. But when water is compressed to about 20,000 atmospheres and cooled, other varieties of ice form, with different molecular arrangements and linkages among hydrogen and oxygen atoms.

The form called Ice II is 12 percent denser, and Ice III is 3 percent denser. The known types go up to Ice X, beyond the infamous "Ice Nine" in Kurt Vonnegut's 1963 novel "Cat's Cradle."

"Ice IX exists, but does not have the properties Vonnegut gave it, like forming at room temperature, and being contagious," Dr. Friedman said. "It was found after the novel came out, so his version was based on good speculation." C. CLAIBORNE RAY

Readers are invited to submit questions by mail to Question, Science Times, The New York Times, 229 West 43rd Street, New York, N.Y. 10036-3959, or by e-mail to question@nytimes.com.

Ice IX exists!

Jellyfish Damage in Gulf

By BEN RAINES

Swarms of jellyfish consumed so many fish eggs and larvae in the Gulf of Mexico this summer that some scientists are talking about the potential for serious future threats to commercial and recreational fisheries in the northern Gulf.

The jellyfish, a native species and an invading one, appeared in prime spawning areas just as breeding season for many of the Gulf's most important species kicked into high gear.

According to the National Marine Fisheries Service, the number of jellyfish in the Gulf has been rising for at least 13 years, since scientists started studying their population.

Scientists say the jellyfish are exploiting three major human-induced changes in the environment: thousands of oil rigs and artificial reefs established to attract game fish have greatly increased the breeding habitat for jellyfish, which need a hard surface for spawning; nitrogen pollution from farm runoff and industrial sources feeds plankton blooms, providing extra food for jellyfish; and commercial fishermen in the Gulf take great numbers of menhaden, a soft-finned, bony fish that competes with jellyfish for the plankton.

Dr. Monty Graham, a researcher at the Dauphin Island Sea Lab in Alabama, worries that with all these advantages jellyfish cannot help but multiply at an astonishing rate.

Making matters much worse, he said, is the advent of *Phyllorhiza punctata*, or Australian spotted jelly-

fish. The giant species, previously unreported in the Gulf, *Phyllorhiza punctata* is a 25-pound bruiser of a jellyfish native to the Pacific.

Some time ago the basketball-size jellyfish established themselves in the Caribbean. This summer, after apparently riding ocean currents north, they concentrated themselves in the passes between the barrier

Big eaters exploit changes in the environment.

islands that separate the Mississippi Sound from the Gulf of Mexico.

The Australian jellyfish, whose numbers normally peak in the Caribbean in August and September, have now mostly died off in the Gulf. But fishery scientists worry that their egg and larvae consumption may already have affected next year's fish populations. And scientists say the animals were spawning prodigiously, broadcasting millions of their own eggs as they ate the eggs and larvae of native species.

Popular sport fish, including redfish, speckled trout, white trout and Spanish mackerel, as well as commercially important species like crabs and menhaden, spawn just outside the barrier islands in August and September. This year, their eggs and larvae had to drift with tidal currents through the jellyfish-choked passes to reach the estuaries that

Effort to Return Rare Ferret

MALTA, Mont., Oct. 2 (AP) — Hopes of reintroducing one of North America's rarest mammals, the black-footed ferret, into Montana have diminished this year — the indirect victim of a plague outbreak and of land management politics.

For the first time in six years, officials at the Charles M. Russell National Wildlife Refuge in north-central Montana, about 50 miles south of Malta, have decided not to set loose any more ferrets there.

"I don't think there's much more potential for ferrets to do much more there than they already are," said Mike Lockhart, a ferret recovery coordinator for the United States Fish and Wildlife Service in Laramie,

Wyo. "The habitat, frankly, is pretty limiting. It's too small and too fragmented."

The decision not to release ferrets this year has less to do with them than it does with prairie dogs, the rodents that make up more than 90 percent of the ferret's diet. Both hunting and illness have reduced the prairie dog's numbers.

Sylvatic plague, known as the bubonic plague in humans, has killed prairie dogs on thousands of acres in the region since the early 1990's, most recently on the Fort Belknap Indian Reservation in northern Montana, another reintroduction site.

In addition, some wildlife officials say, the hunting of prairie dogs has

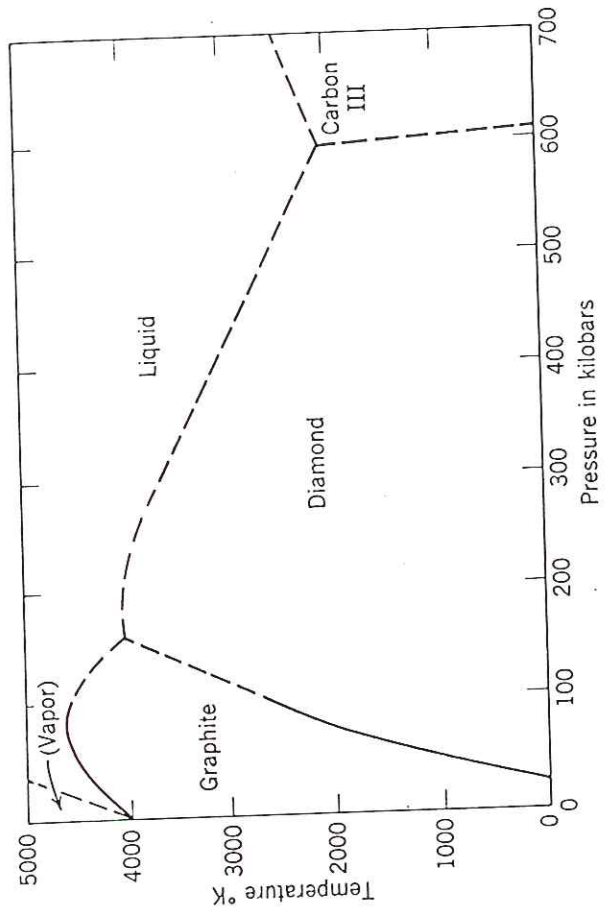


FIG. 10.14. Pressure-temperature phase diagram for carbon, based on experimental data from various sources.

Familiar example of a phase diagram
Water - H_2O

ice - liquid water - steam

Figure 147 Shlens shows triple point

1 atm = 760 mm Hg - freeze at $0^\circ C$
boil at $100^\circ C$

Note that freezing temperature decreases
with pressure - principle of ice skate

Ice is an crystalline structure
Pauling Fig 15-11

Openness \rightarrow less dense than liquid
 $\rho_{ice} = 900 \text{ kg/m}^3 = 0.9 \times \rho_{liquid}$

At even higher pressures, this
open structure is unstable - other
forms of ice Ice I - Ice VII
Fig. 9.1 KH

These diagram of C shown KH Fig. 10.14

Note P-T axes now interchanged

Pressure P in kilobars

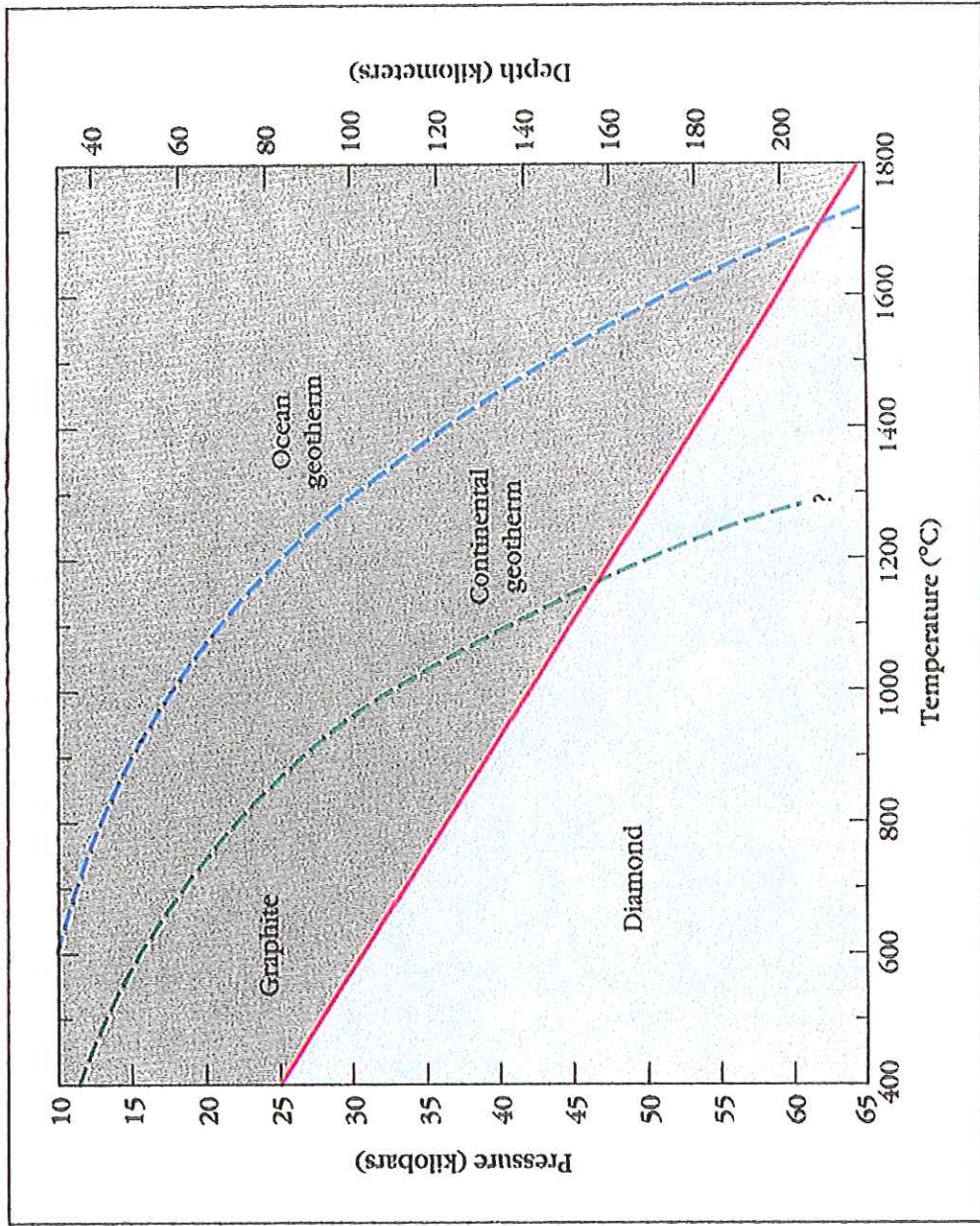
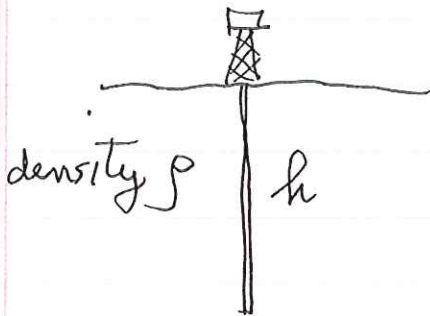


Figure 7. P-T diagram for the stability of diamond-graphite. The average geotherms beneath continents and oceans are shown as dashed curves.

$$1 \text{ bar} = 1 \text{ atm} = 0.1 \text{ MPa}$$

Diamond is the high-pressure —
it is metastable at \oplus surface —
way down in lower left corner

How does pressure increase with
depth in the Earth?



$$p = \rho g h$$

$$\rho \approx 3000 \text{ kg/m}^3$$

$$g = 9.8 \text{ m/sec}^2$$

~~p increases by $\sim 3 \text{ MPa}$ for every km depth increase. $\sim 0.3 \text{ kbar}$~~

~~p increases by $\sim 3 \text{ MPa}$ for every km increase in depth. $\sim 0.03 \text{ kbar}$~~

p increases by ~~$\sim 3 \text{ MPa}$~~ $\sim 30 \text{ MPa}$
 $\sim 0.3 \text{ kbar}$ for every km
increase with depth h

SUMMARY

The picture as we understand it for diamond formation involves relatively cool harzburgite keels at the base of the thickest, oldest parts of the Earth's crust. Those keels probably were formed in the earliest stages of the growth of the continents. From carbon in the mantle, diamonds crystallized in these keels during or shortly following their formation (Figure 12), some 3 billion years ago. Later subduction of the basaltic oceanic crust resulted in some portions of it adhering to the bases of the continental keels and recrystallizing there as eclogite. The basaltic crust contained carbon, some of organic origin, that recrystallized as diamond. Heating beneath or fluid infiltration of the continental keel caused kimberlite melts to form and, under the right conditions, they ascended the 200–300 km distance to the Earth's surface, bringing samples of the Earth's mantle for scientists to study and diamonds for us to use and enjoy.

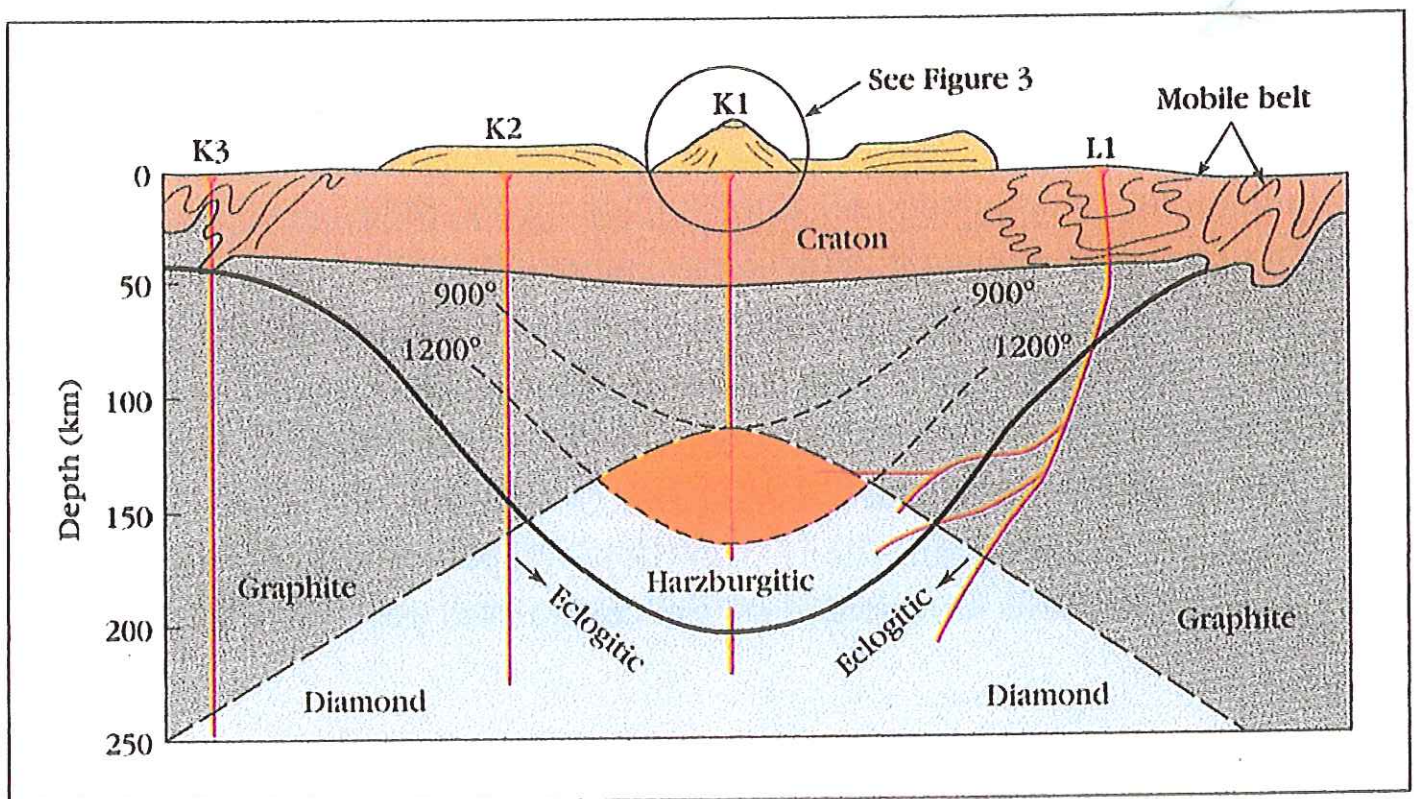
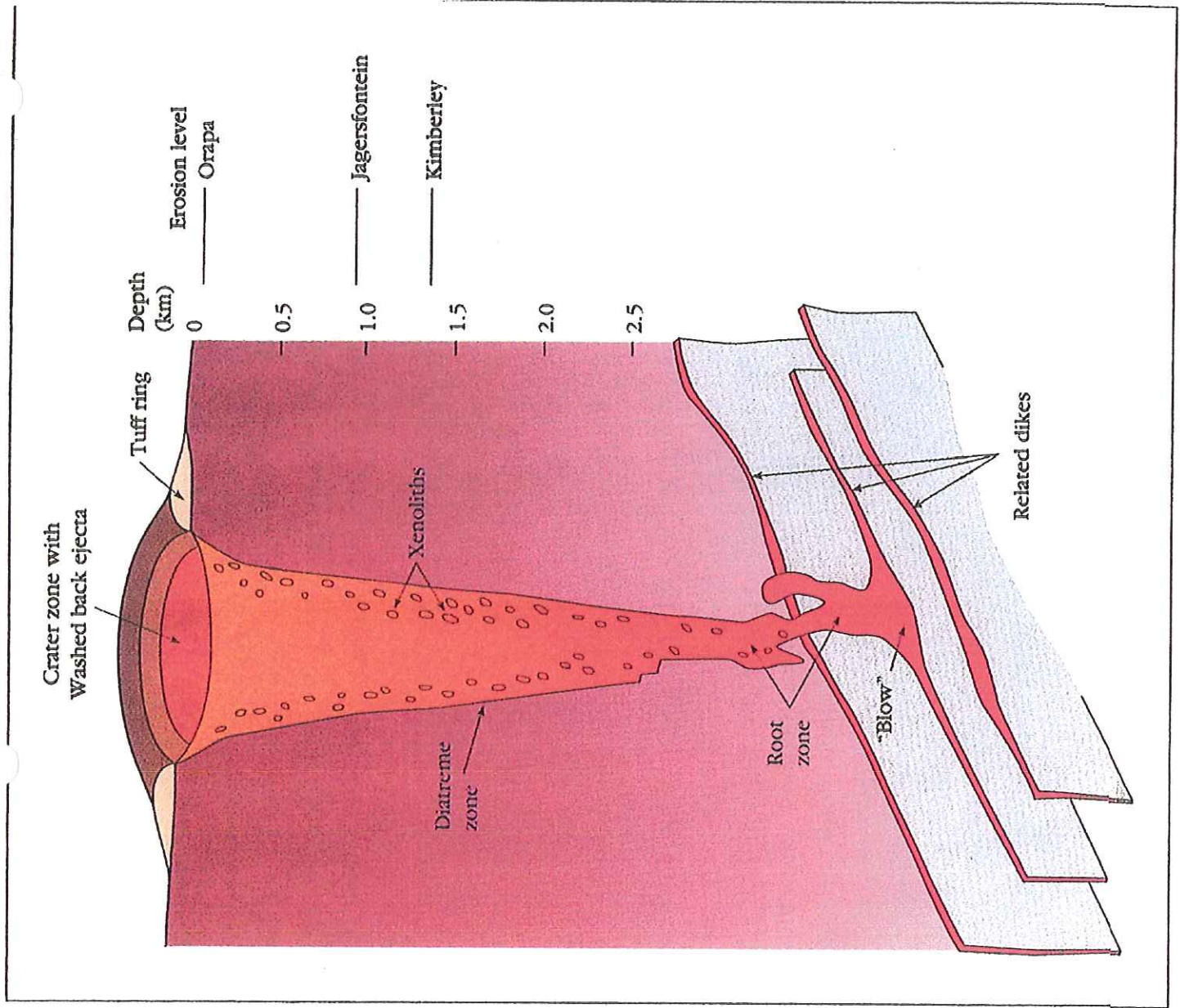


Figure 3. This cross section sketch of a typical kimberlite pipe shows the carrot-shaped profile. The root zone is the point where the high velocity eruption commences, in which exsolved gases blow out the fragmented kimberlite (tuff breccia) including volcanoclastics that form the volcano's tuff ring. The crater zone partially refills with ejecta that falls or washes into the crater. Depth measurements show the levels of erosion for various kimberlite pipes in South Africa. (Adapted from Haurhorne, 1975, and Mitchell, 1995.)



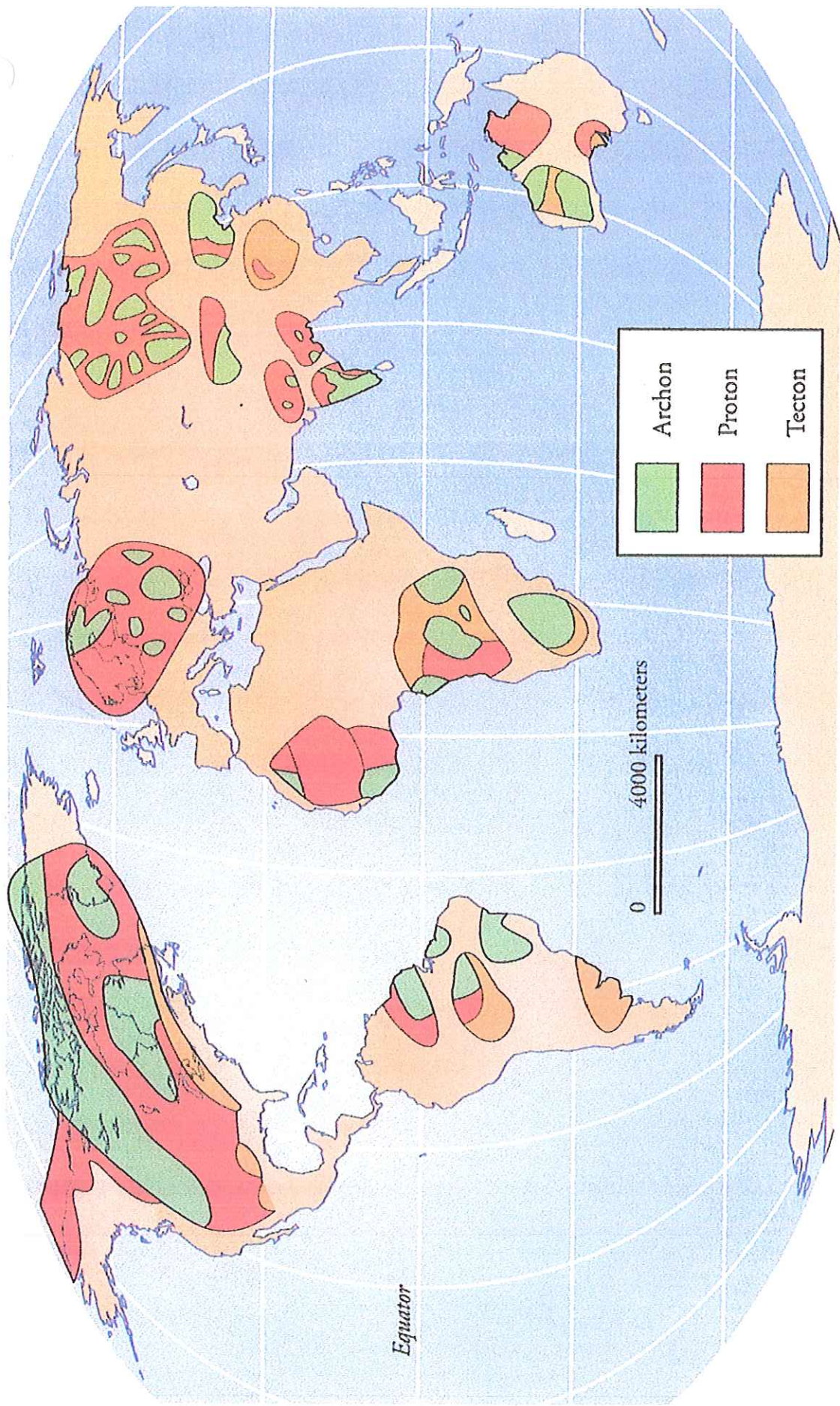
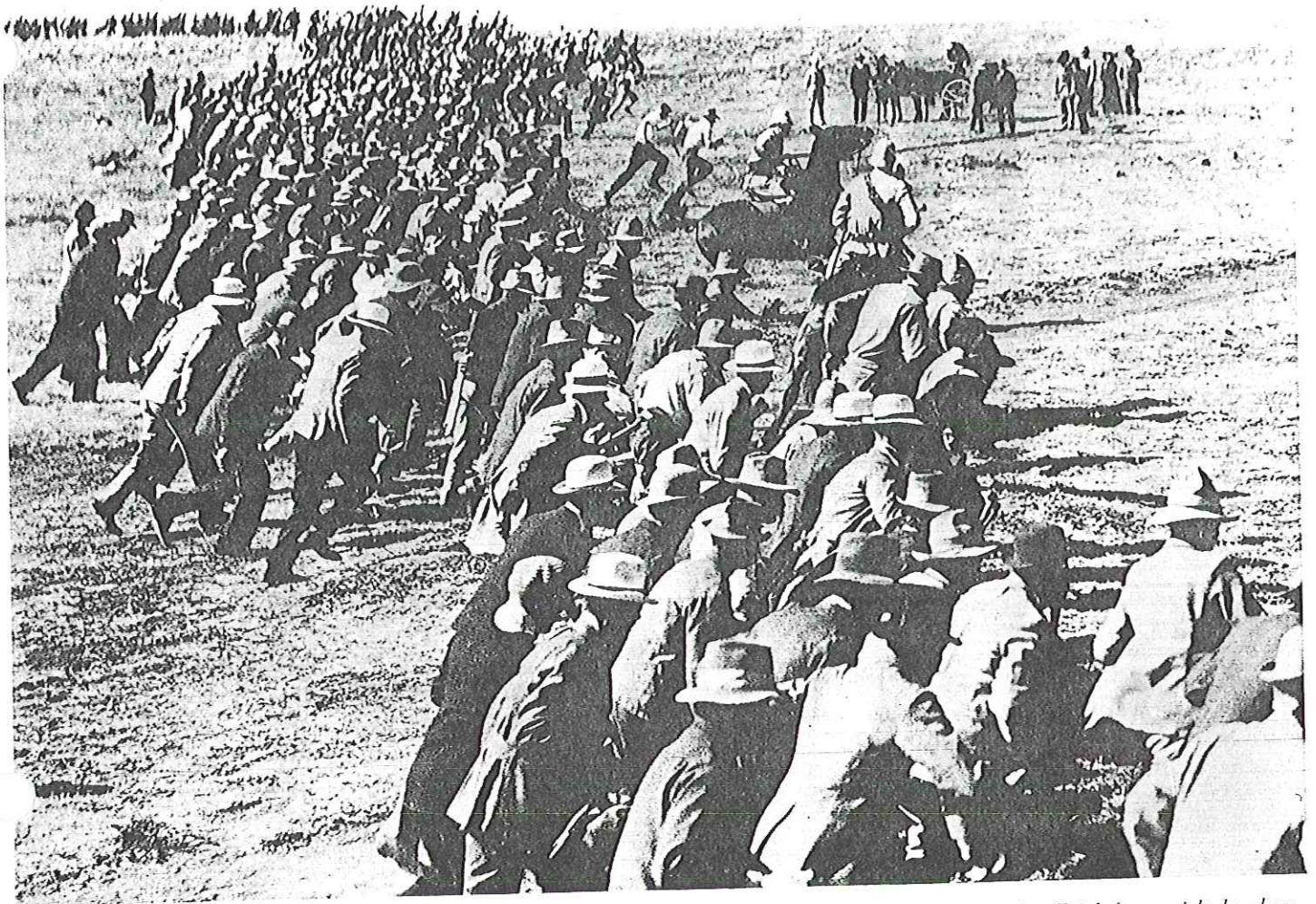


Figure 1. World distribution (except for Antarctica) of cratons. (Adapted from Levinson et al., 1992.)



Discovery and Characteristics of Kimberlite Pipes

In late 1869, diamonds were discovered about 20 km (12 miles) from the nearest Vaal River diggings, totally remote from any streams or rivers. That discovery forced everyone to rethink the theories about the origin and occurrence of diamonds – theories that had been in place for more than 2,000 years. The diamond-containing rock was compact and hard, so that it had to be crushed and the diamonds extracted by hand. We now refer to that kind of rock as kimberlite. Further, because the new deposits were not close to water sources, washing the diamond-bearing ore as part of the extraction process was not possible. Thus the deposits were referred to as dry diggings, in contrast to the wet diggings along the Orange, Vaal, and other rivers, where diamonds were easily recovered from the unconsolidated sands and gravels.

There are several versions of the sequence in which the various dry diggings were discovered. The most recent study, by A. J. A. Janse, gives the order Bultfontein (September 1869), Dutoitspan (October 1869), Jagersfontein

Figure 12. The officials (upper right-hand corner) have read the formal proclamation, and the starting flag has been dropped for the rush to stake claims near Lichtenburg on August 20, 1926, where diamond-bearing alluvial deposits had been discovered earlier that year. The rush drew 10,000 prospective mine-owners. (Courtesy of De Beers.)

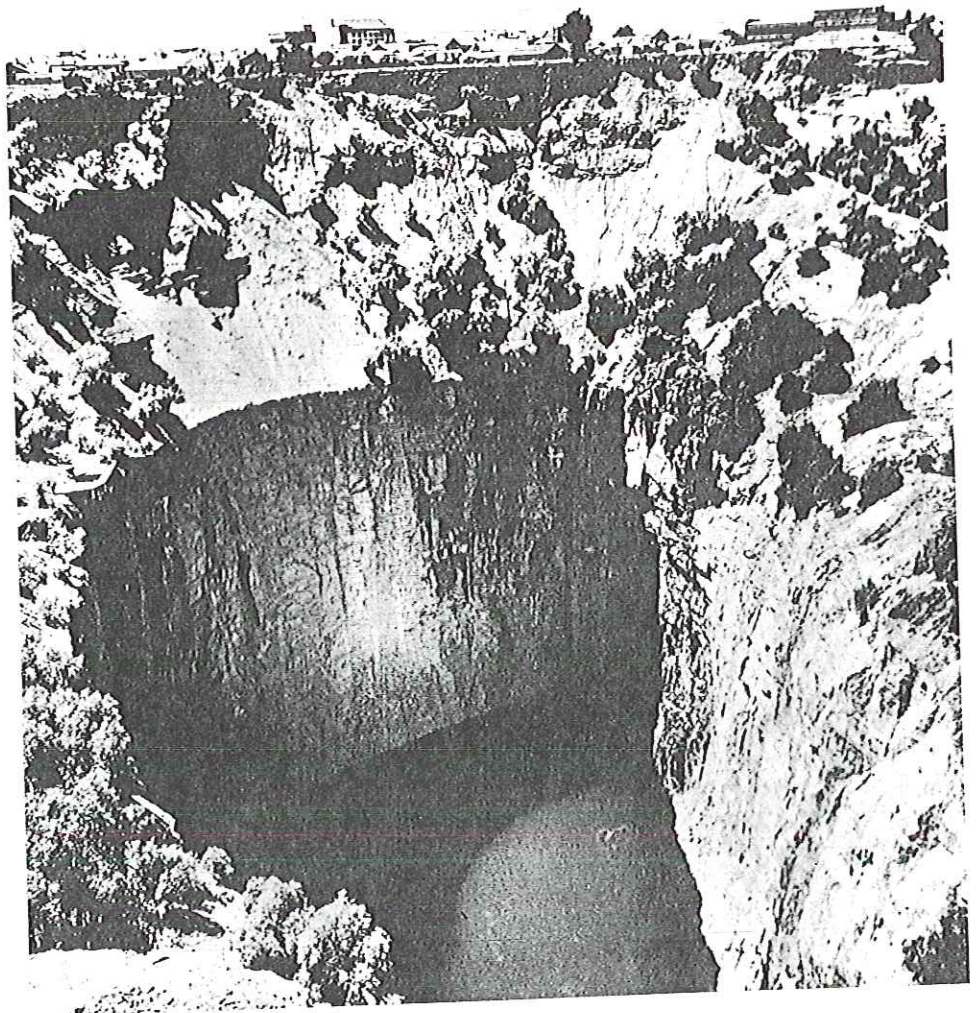


Figure 13. The main onshore and offshore areas where diamonds are being mined along the coasts of Namaqualand (South Africa) and Namibia. The broken line trending northwest above the Orange River in Namibia represents the inland boundary (approximately 100 km, or 62.5 miles, from the Atlantic Ocean) of the Sperrgebiet, established in 1908 by the German government, where exploration for diamonds was prohibited, and still is, except in specific situations. (Adapted from Janse, 1995.)

Figure 14. The Big Hole (Kimberley mine) began production in July 1871 and produced continually until it was closed permanently in July 1914. It yielded 14.5 million carats of diamonds. (Courtesy of De Beers.)

(July 1870), Koffiefontein (July 1870), De Beers (May 1871), and Kimberley, also known as the Big Hole (July 1871; Figure 14). Four of those deposits – Bultfontein, Dutoitspan, De Beers, and Kimberley – fell within a circle 5 km (3 miles) in diameter, within which the city of Kimberley was established in 1871. The other two, Koffiefontein and Jagersfontein, were 90 and 150 km (55 and 92 miles) to the southeast. Up to 15 other kimberlites, only some of which contained diamonds, were known in the vicinity of Kimberley, but it was not until 1890 that another large pipe of economic significance (the Westelton) was discovered only about 3 km (2 miles) from Bultfontein and Dutoitspan.

The diamond deposits of the dry diggings were initially found in various soft, friable, yellowish and reddish weathered surface materials that became known as “yellow ground.” When the mines began to reach depths of 17 to 27 meters (55–90 feet), the nature of the rock changed. Under the soft yellow ground was a harder, compact bluish rock, initially called “blue ground,” but beginning in 1897 it began to be referred to as “kimberlite” in various publica-



Big Hole
Kimberley

tions. As mining progressed deeper, the conical nature of the kimberlite pipes became evident, and therefore the traditional explanation that diamonds occurred in surface deposits (i.e., relatively shallow and extensive alluvial deposits), or else in rocks compressed from ancient surface deposits, was not applicable to the occurrences in the vicinity of Kimberley.

In 1872, Emil Cohen, a German mineralogist, was the first to suggest that the dry diggings were actually cylindrical columns that represented volcanic conduits and that the diamonds contained in them were brought up from far below and had no necessary relationship to rivers. The term "pipe" was first applied to these volcanic conduits in 1874, and since 1897, when the term "kimberlite" first appeared in print, the term "kimberlite pipe" has gradually gained universal acceptance.

The five mines in the Kimberley cluster and the nearby Koffiefontein and Jagersfontein mines were sources of fabulous wealth. From 1872 to 1903 they provided about 95 percent of the diamonds that entered the world market, generally about 2 to 3 million carats per year.

The Kimberley mine, the richest in the Kimberley area, operated continuously until 1914, when it was closed because its kimberlite ore was mined out. The six others in the Kimberley area have been closed from time to time since 1908 because of the world wars, the Great Depression, and oversupply. Today, four are still active more than 100 years after their discovery: Bultfontein, Dutoitspan, Wesselton, and Koffiefontein. However, their combined production in recent years has averaged only about 700,000 carats annually, a mere 0.7 percent of the present world production of about 108 million carats annually (1995 data). It is likely that all the mines still active in the Kimberley area will close permanently by about 2010 because they are already close to the bottom of their kimberlite ore reserves.

Formation of the De Beers Consolidated Mines

When the pipes were discovered, in 1869 through 1871, an individual was permitted one claim, 31 feet by 31 feet. For example, the Kimberley mine, the Big Hole, consisted of about 430 such claims, but each claim could be divided into fractional parts, with the result that in 1872 there were about 1,600 separate holdings, some as small as one-sixteenth of a claim, or about 7 square yards. It is obvious that it would be difficult and dangerous to work such a small claim to any significant depth (Figures 15 and 16). In the interest of efficiency and safety, the rules prohibiting amalgamation of claims were relaxed in 1872 and totally eliminated in 1876. That paved the way for small companies to take over claims from individual miners and attracted the attention of many entrepreneurs (Figure 17). Two of them, Cecil Rhodes and Barney Barnato, would play major roles in the world of diamonds.

Cecil John Rhodes arrived in South Africa from England in 1870 at the age

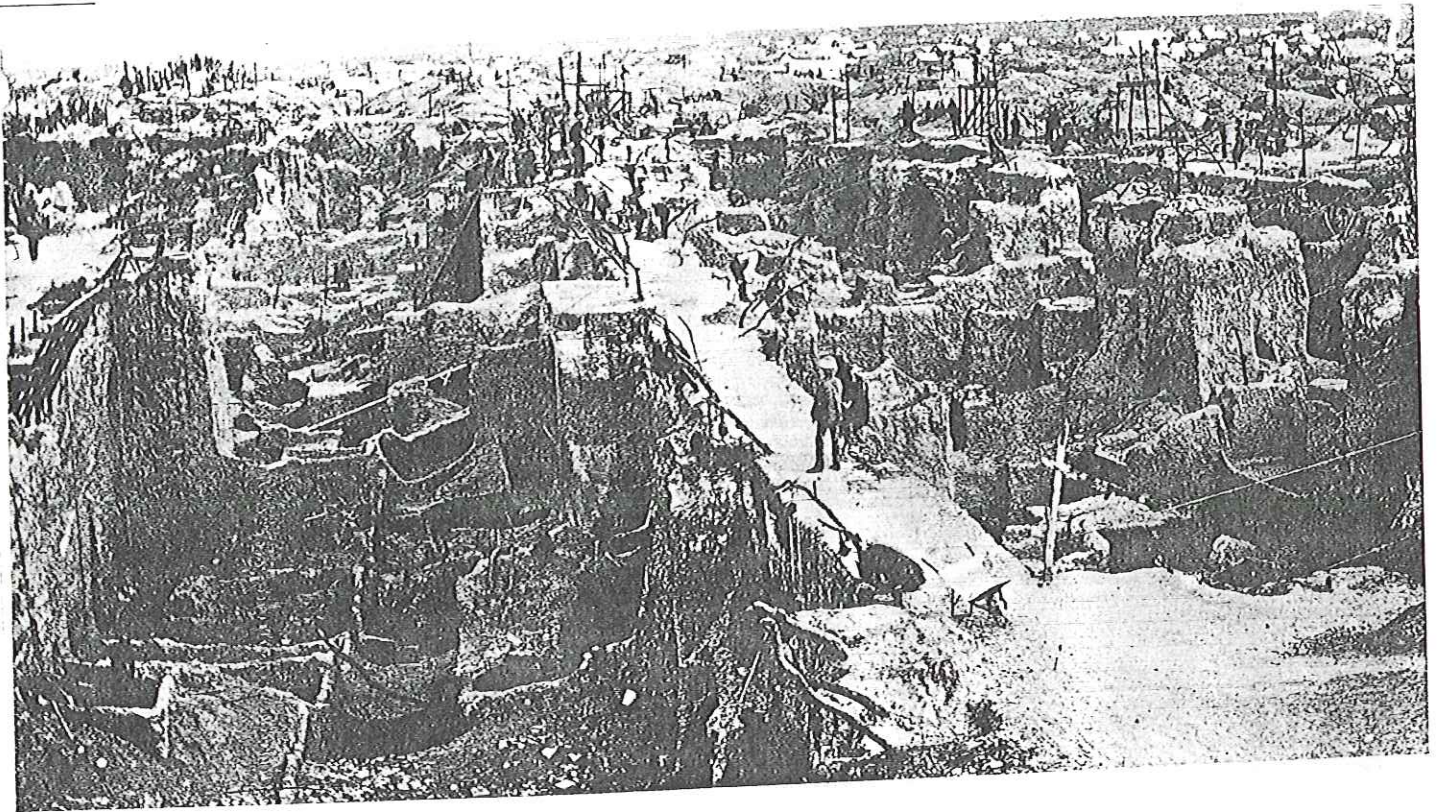


Figure 15. By 1872, as miners dug deeper, the walls that served as roadways between the claim pits at the Kimberley mine had started to collapse, making mining difficult and unsafe. The roadways, which ran north-south, were 15 feet wide, with 7.5 feet taken from the sides of each bordering claim (31×31 feet), making the working surface of each claim 31×23.5 feet. (From Williams, 1906; Jackie Beckett/courtesy of American Museum of Natural History.)

of 17 and soon migrated to Kimberley. He purchased a mining claim in the De Beers mine and, in addition, made considerable money in partnership with others by pumping water from flooded claims. He returned to England in 1873 to enroll at Oxford, but left considerable assets in South Africa in the care of friends, who continued the pumping business and bought more claims with the profits. When Rhodes graduated in 1881, he returned to South Africa, where he and his associates formed the De Beers Mining Co. Ltd.,

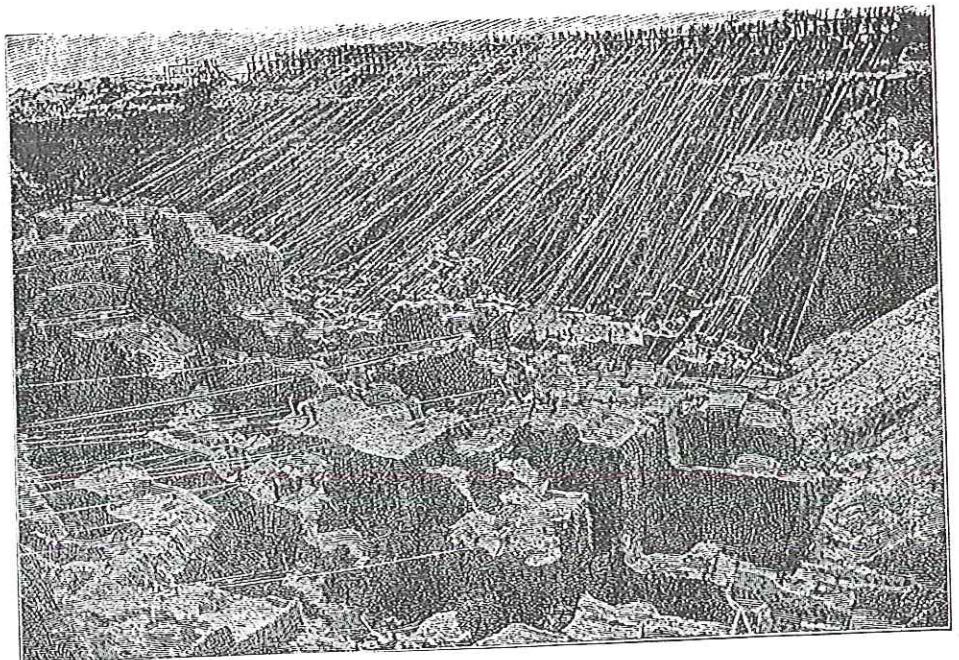


Figure 16. The Kimberley mine in 1874 was a mass of ropeways ingeniously constructed to rush buckets of extracted material to the top, where they were quickly dumped and the buckets sent back into the mine. (From Williams, 1906; Jackie Beckett/courtesy of American Museum of Natural History.)

Diamond Sources and Their Discovery

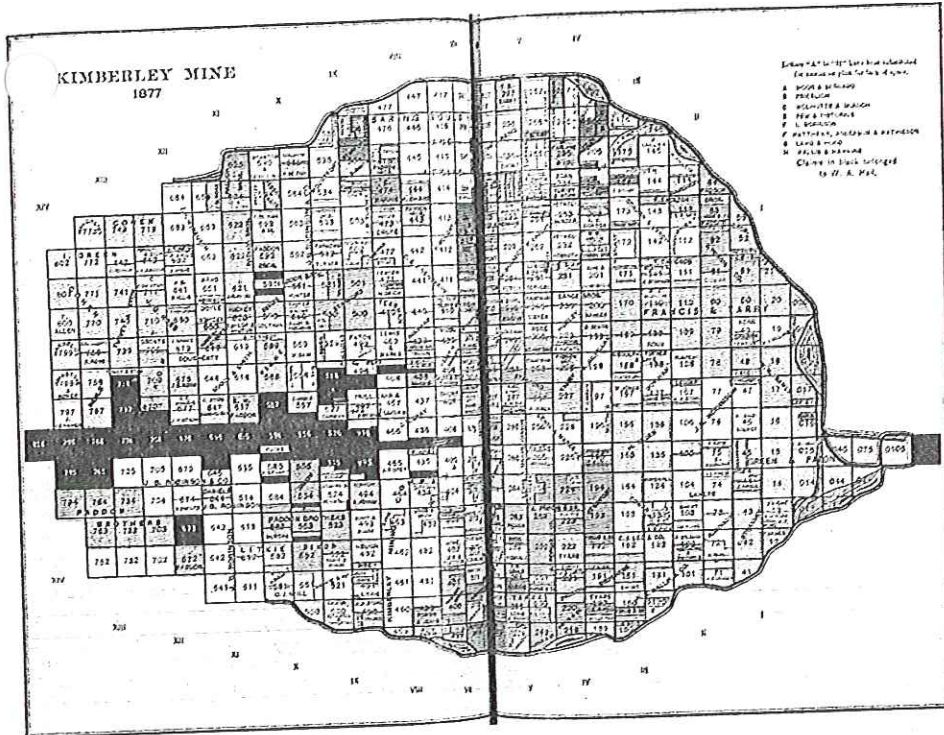


Figure 17. The Kimberley mine in 1877, when the prohibition on amalgamating claims was fully lifted, was still divided into many small claims. The central vertical distortion in the image is the result of this two-page spread reproduction. (From Williams, 1906; Jackie Beckett/courtesy of American Museum of Natural History.)



Who actively continued to buy claims. Abetted by a drop in world prices because of oversupply and the expensive technical problems of mining ever deeper, Rhodes and his associates were able to buy more and more claims. By 1887 he had gained complete control of the De Beers mine (Figure 18).

Analogous, in some ways, was the history of Barney Barnato. He arrived in South Africa in 1873 at the age of 20, also from England, and in 1876 bought four mining claims in the Kimberley mine. He soon made a huge profit. In 1881 he formed the Barnato Diamond Mining Co., which he enlarged and eventually merged with Kimberley Central Mining Co., making it the largest company in the Kimberley mine by 1883. However, he never did gain complete control of the Kimberley mine, whose remaining claims were held by a French company that refused to sell to Barnato.

To take control of the Kimberley mine from Barnato, Rhodes initiated a series of brilliant financial maneuvers. First, Rhodes had his De Beers Mining purchase the French company. Then Rhodes sold the French company to Barnato's Kimberley Central for 20 percent of the shares of the latter plus £300,000 in cash. Barnato remained the largest, although not the majority, shareholder in Kimberley Central, and he thought he could still control the company. Rhodes next began to buy up the outstanding shares in Kimberley Central. When Barnato realized what was happening, a vicious bidding battle ensued, driving shares of Kimberley Central to great heights. Ultimately Barnato capitulated. He sold Kimberley Central to Rhodes for £5,338,650 [\$25 million (U.S.)], paid for by what was at that time the largest check ever issued.

Figure 18. Cecil John Rhodes, master entrepreneur of the South African diamond mines and founder of De Beers Mining Co. Ltd., controlled 90 percent of the world's diamonds at the end of the nineteenth century. At his death in 1902 he left most of his fortune to Oxford University, funding the prestigious Rhodes scholarships that bear his name. (From Williams, 1906; Jackie Beckett/courtesy of American Museum of Natural History.)



C. J. Rhodes

In 1888 Rhodes merged Kimberley Central into a new company, De Beers Consolidated Mines Ltd., which he controlled.

The stage was then set for one company, De Beers Consolidated Mines Ltd. (henceforth, De Beers), to control almost all of the world's diamond production, except for some South African alluvial production and minimal production from Brazil, and to adjust the supply of diamonds to fluctuations in world demand. But there were, and continue to be, two factors that might threaten that dominant position: a serious drop in the demand for diamonds, and the discovery of new mines that would operate beyond the direct control of De Beers.

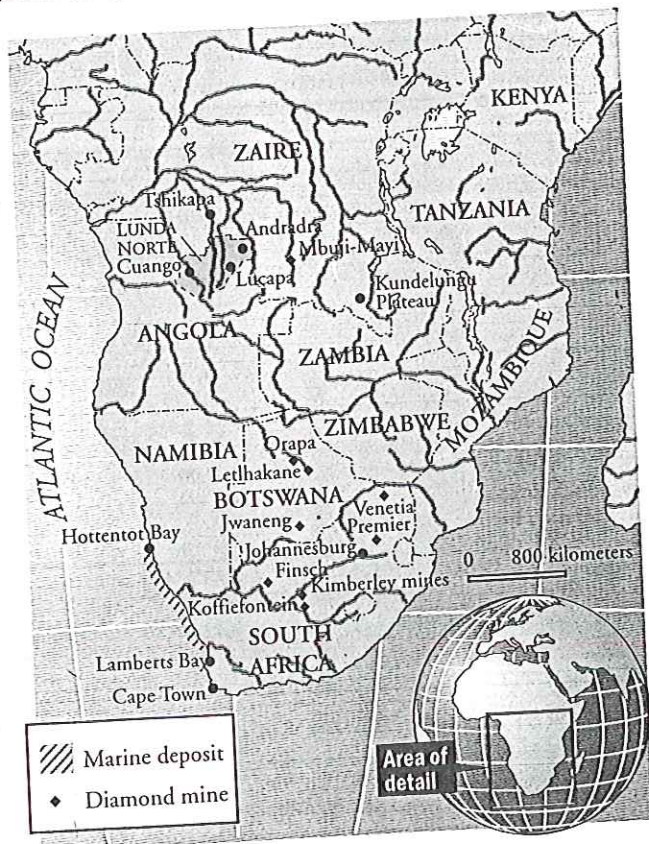
The Premier Mine

The dominance of the Kimberley mines controlled by De Beers as the only important source of the world's diamonds was not challenged until 1902, the year Rhodes died. In that year the Premier mine was discovered by Thomas Cullinan, who later became chairman of the Premier Diamond Mining Company. The mine was located about 500 km (300 miles) northeast of Kimberley and about 30 km (18 miles) east of Pretoria (Figure 19). With a surface area of 32.2 hectares (80 acres), it was three times as large as Dutoitspan (10.6 hectares, 26 acres), the largest pipe known prior to 1902.

Production started in May 1903, and on January 25, 1905, the famous Cullinan diamond, named after the mine's discoverer, was found. It weighed 3,106 carats. More than 300 other stones larger than 100 carats were recovered from 1903 to 1930. In 1904, its first full year of operation, the Premier mine produced almost 750,000 carats, and that increased to an average of almost 2 million carats per year from 1907 to 1914, when the mine was closed for 2 years during World War I. The annual production from the Premier mine was the largest in the world in each year of its first decade; its production was comparable to the combined annual production from all of the De Beers mines.

The Premier mine was the first major challenge to De Beers, which had enjoyed virtually complete control of rough-diamond production since its formation in 1888. The effect of that huge production on prices in the world market was further exacerbated when the management of the Premier mine chose to establish their own marketing organization rather than use the channels already established by De Beers. It was not until 1917 that De Beers managed to acquire the majority of shares in the Premier mine, but from that time on De Beers was in a position to control the production at Premier and integrate it into the overall De Beers production strategy. De Beers purchased the remainder of the Premier shares in 1977. Today, the Premier mine is per-

Figure 19. Major diamond mines currently producing in South Africa, Namibia, Botswana, Angola, and Zaire. (Adapted from Janse, 1995.)



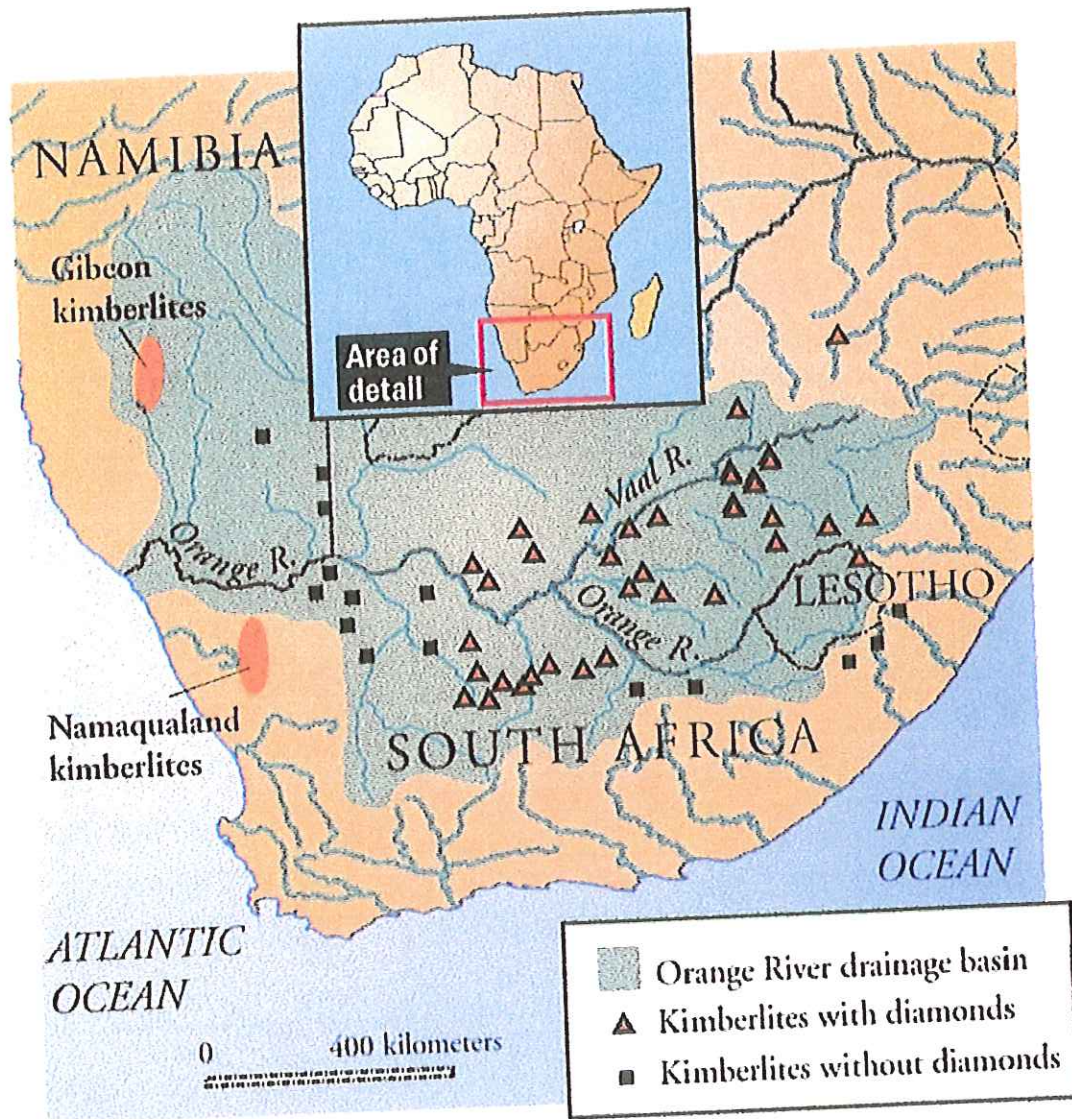
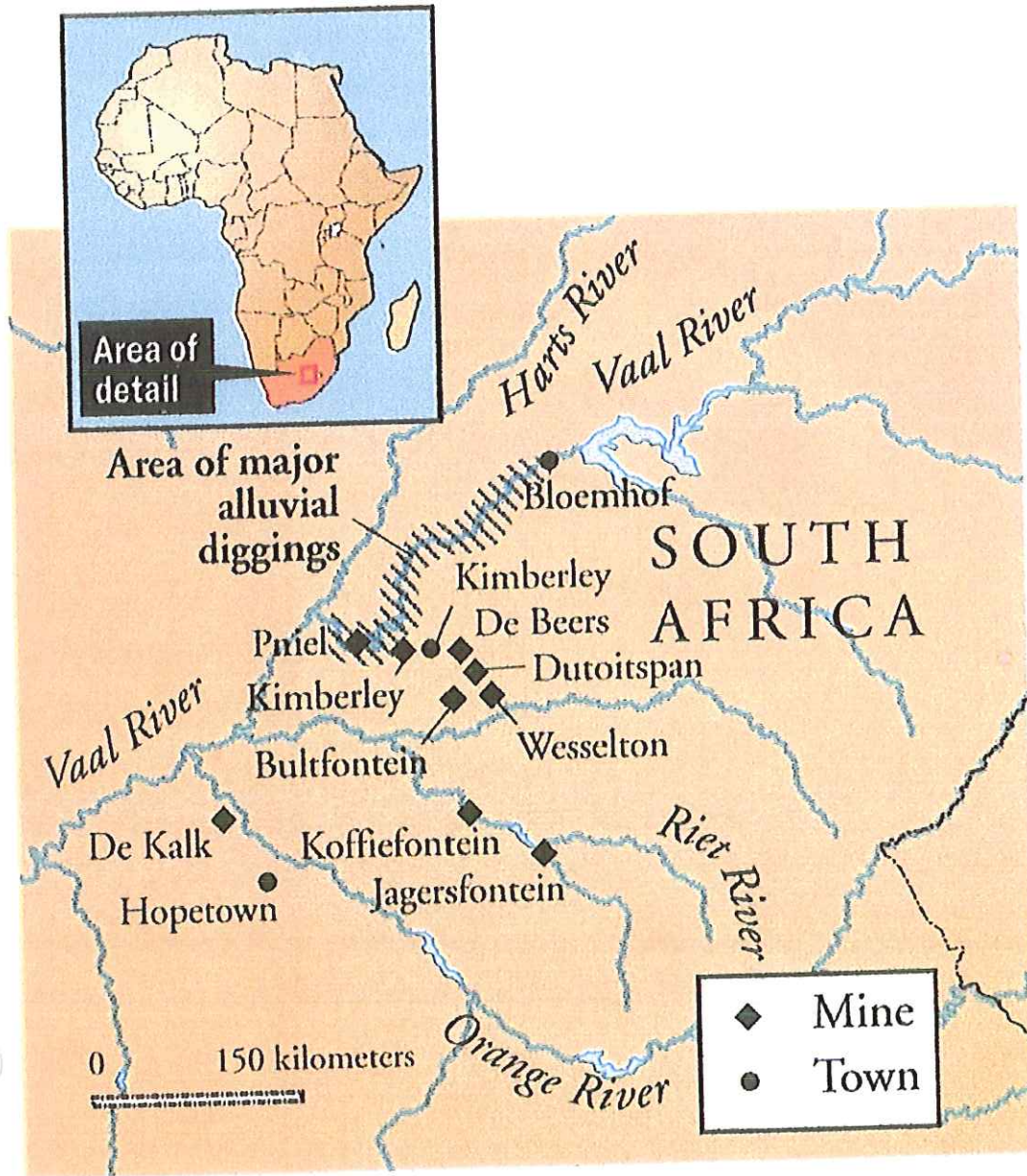


Figure 24. The Orange River drainage basin in southern Africa showing the present position of the Orange and Vaal rivers, the locations of kimberlites with and without diamonds in the Orange River basin and the Gibeon (Namibia) and Namaqualand (South Africa) kimberlite fields, both of which are barren of diamonds. Alluvial-deposit diamonds have been found throughout the basin, but the vast majority has been transported west to the Atlantic Ocean, where they now rest in marine, beach, and related deposits. (Adapted from Gurney et al., 1991.)

Figure 9. The first diamonds reported in South Africa (and all subsequent major finds until 1903, when the Premier mine was discovered) were located between the Orange and Vaal rivers. Note that the mines in the Kimberley vicinity are shown here in relative positions, because they are clustered in such a small area that their locations cannot be shown precisely. The inset indicates the area shown in the map. (Adapted from Janse, 1995.)



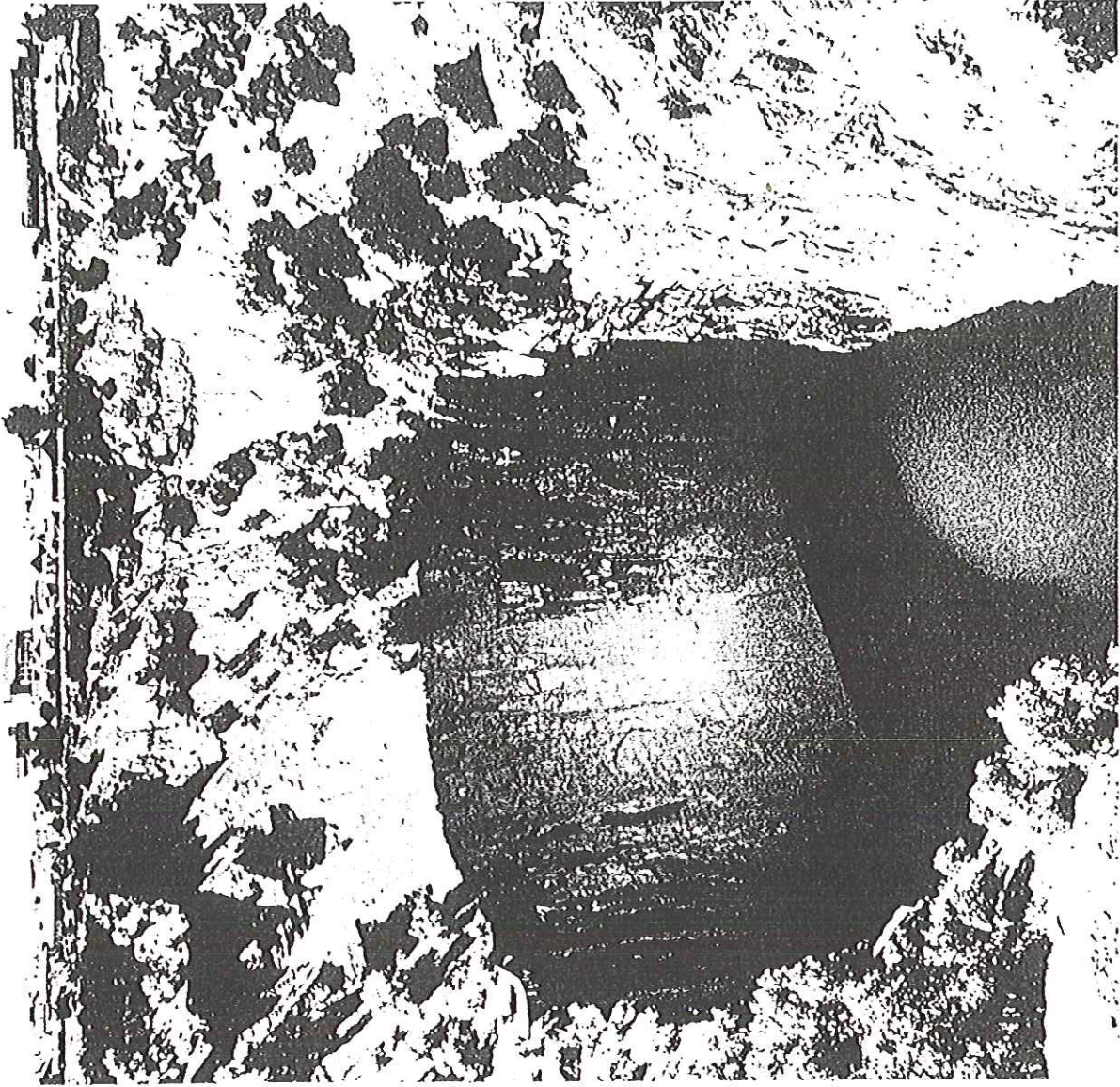


Figure 14. The Big Hole (Kimberley mine) began production in July 1871 and produced continually until it was closed permanently in July 1914. It yielded 14.5 million carats of diamonds. (Courtesy of De Beers.)

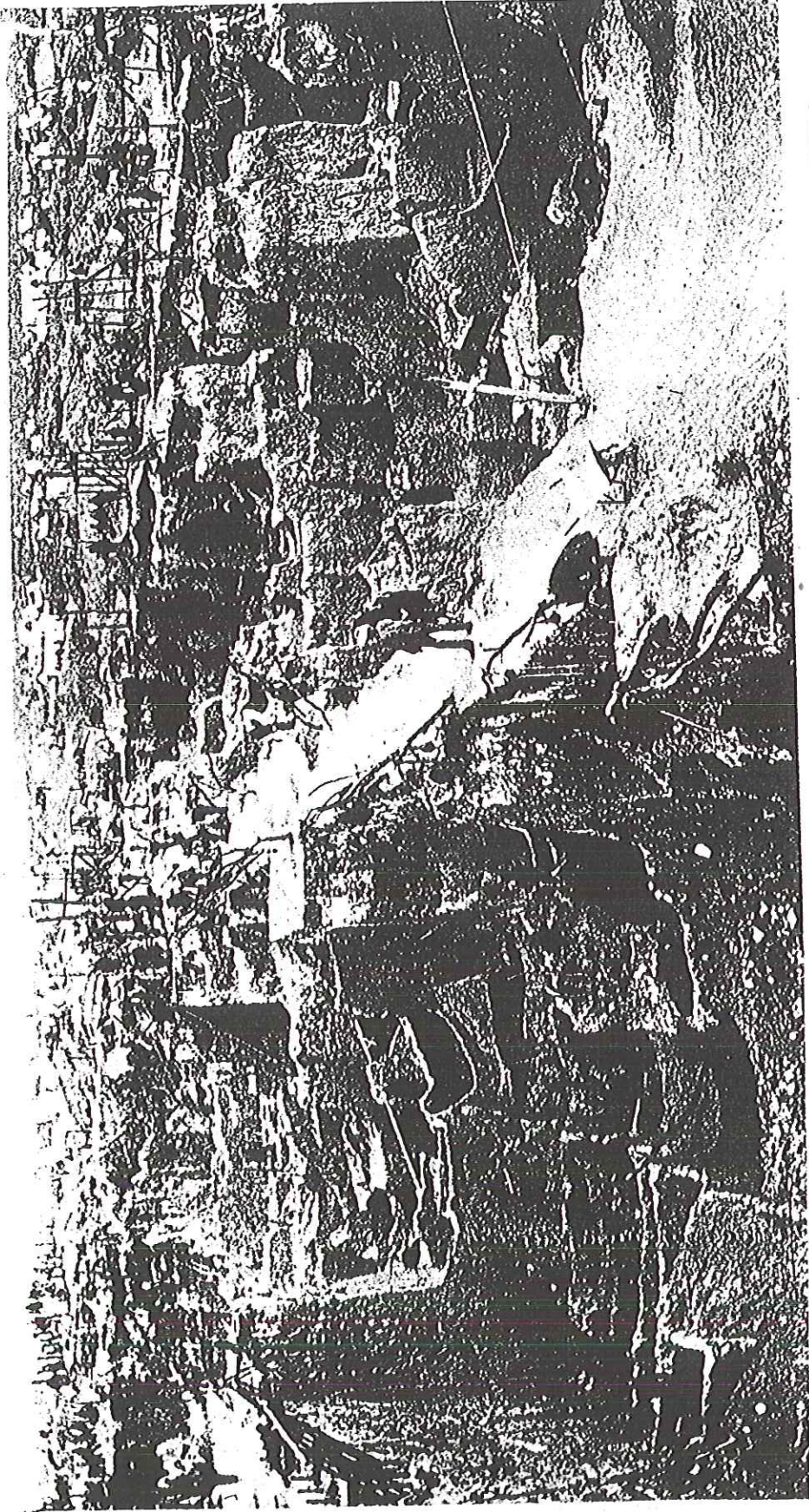
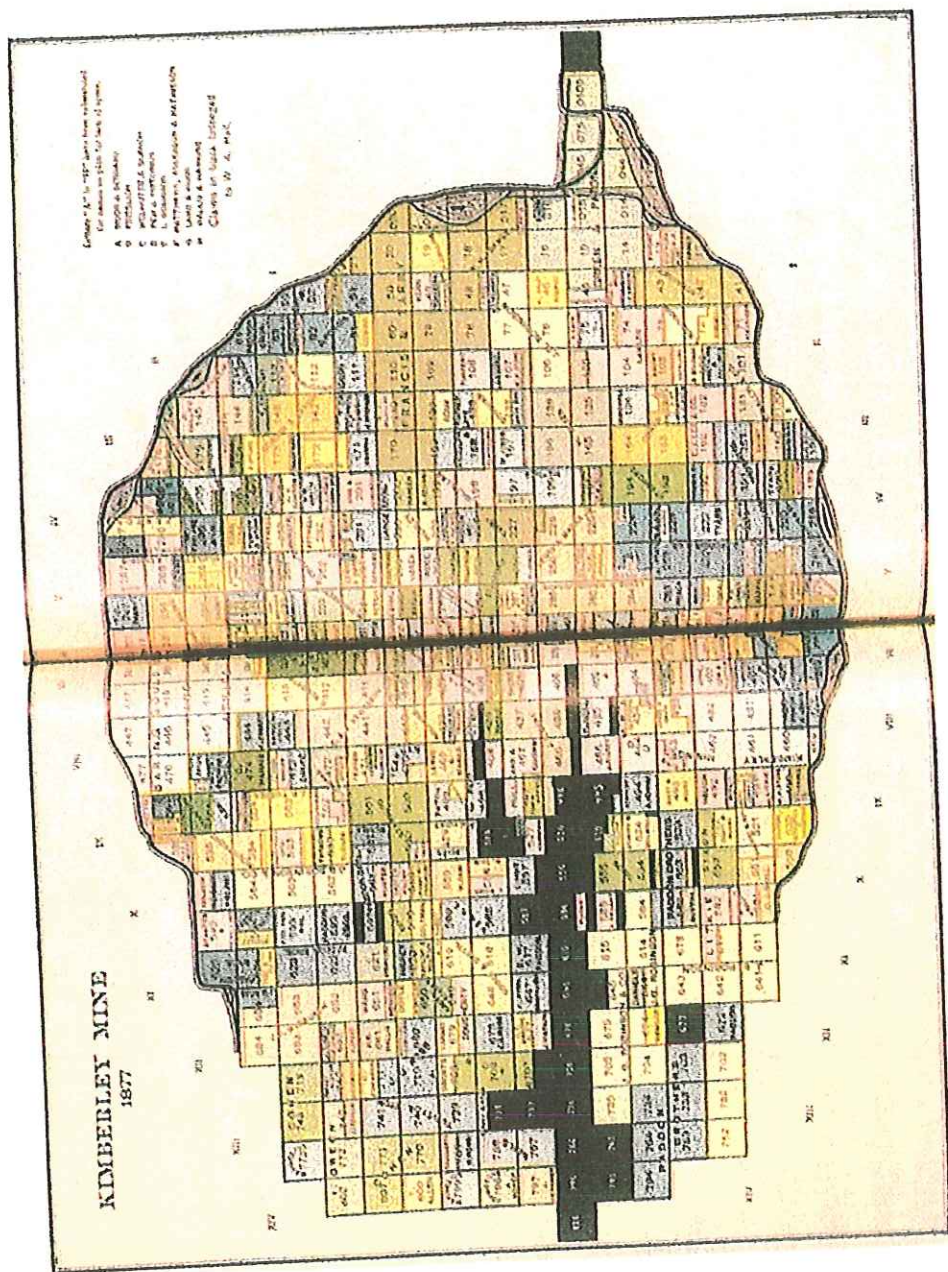


Figure 15. By 1872, as miners dug deeper, the walls that served as roadways between the claim pits at the Kimberley mine had started to collapse, making mining difficult and unsafe. The roadways, which ran north-south, were 15 feet wide, with 7.5 feet taken from the sides of each bordering claim (31 × 31 feet), making the working surface of each claim 31 × 23.5 feet. (From Williams, 1906; Jackie Beckett/ courtesy of American Museum of Natural History.)

Figure 17. The Kimberley mine in 1877, when the prohibition on amalgamating claims was fully lifted, was still divided into many small claims. The central vertical distortion in the image is the result of this two-page spread reproduction. (From Williams, 1906; Jackie Beckett/courtesy of American Museum of Natural History.)



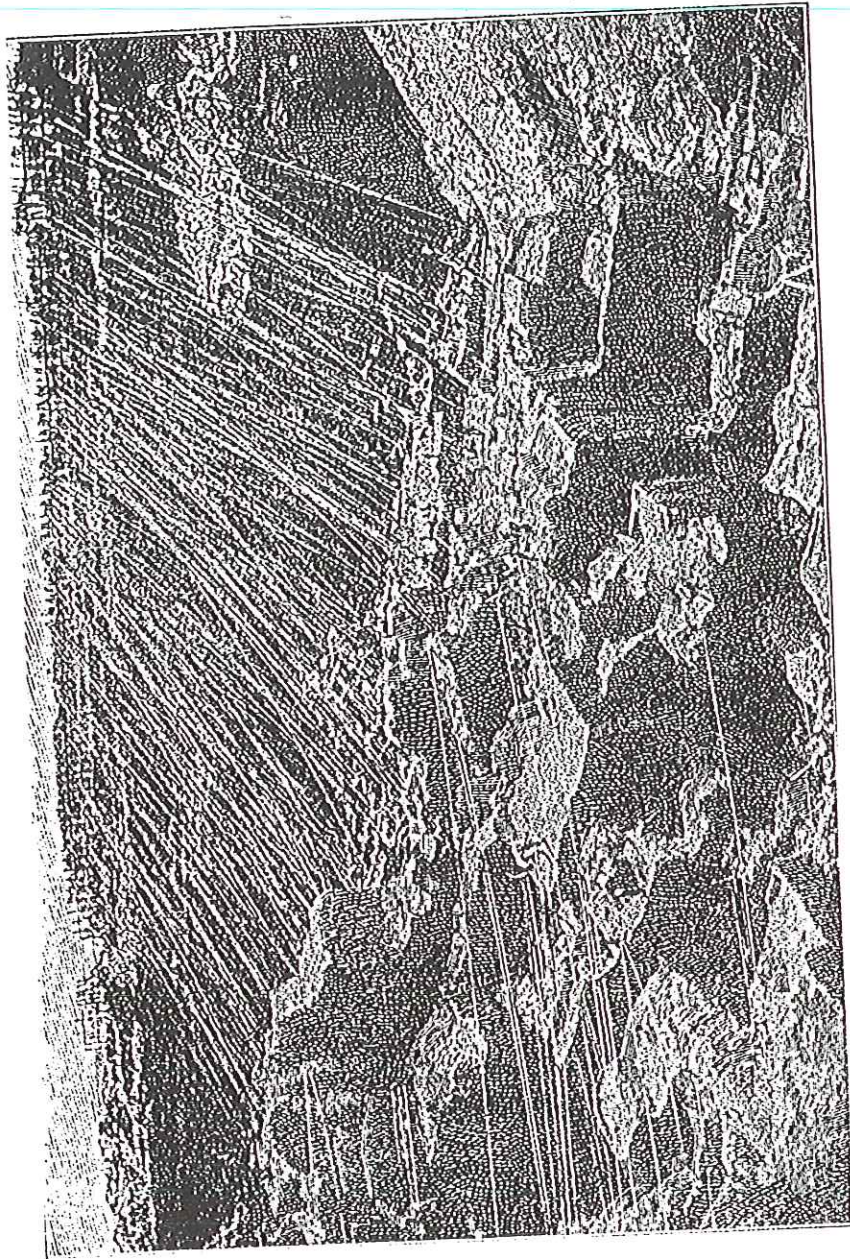


Figure 16. The Kimberley mine in 1874 was a mass of ropeways ingeniously constructed to rush buckets of extracted material to the top, where they were quickly dumped and the buckets sent back into the mine. (From Williams, 1906; Jackie Beckett/courtesy of American Museum of Natural History.)

Figure 18. Cecil John Rhodes, master entrepreneur of the South African diamond mines and founder of De Beers Mining Co. Ltd., controlled 90 percent of the world's diamonds at the end of the nineteenth century. At his death in 1902 he left most of his fortune to Oxford University, funding the prestigious Rhodes scholarships that bear his name. (From Williams, 1906; Jackie Beckett/courtesy of American Museum of Natural History.)



C. J. Rhodes

Figure 1. The Finsch pipe is one of the major working kimberlite mines in South Africa. The open pit operation employs benches that are 12 meters high. (Courtesy of De Beers.)



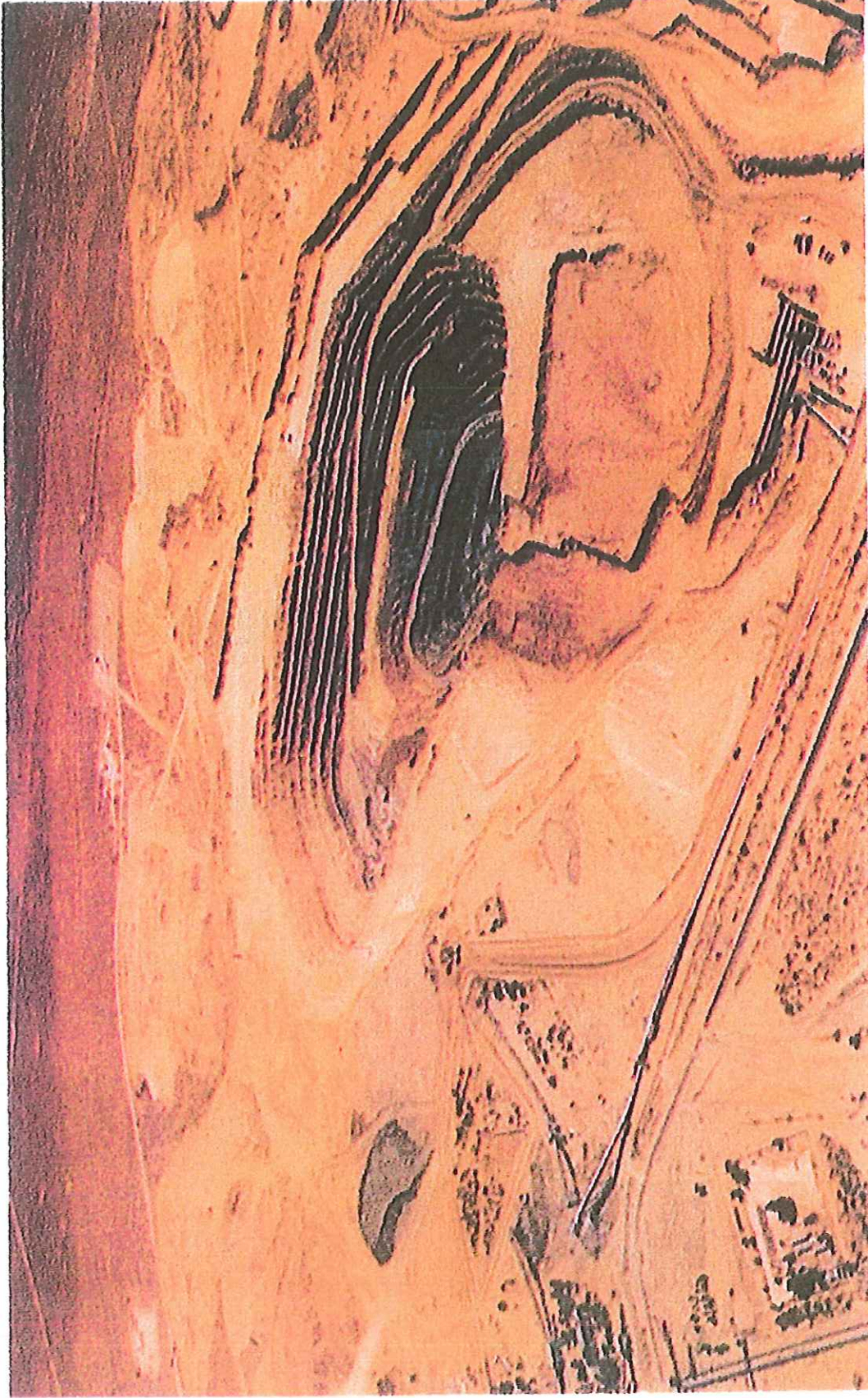


Figure 25. The Swaneng open pit mine in Botswana is the most valuable diamond mine in the world. Its production of about 10.5 million carats in 1995 had a value of about \$1.2 billion (U.S.). (Rory O. Moore.)

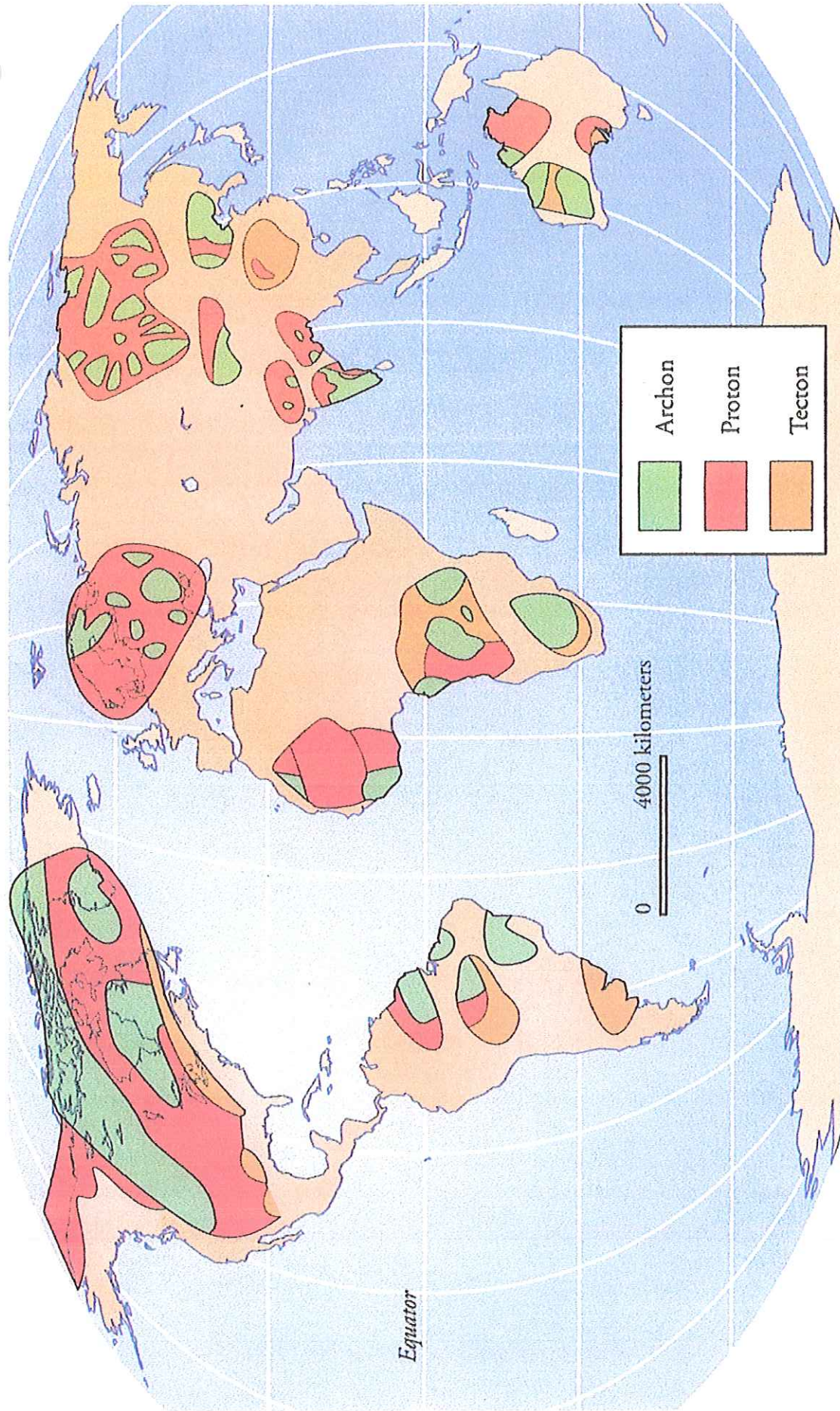


Figure 1. World distribution (except for Antarctica) of cratons. (Adapted from Levinson et al., 1992.)

the future. That suggestion gains plausibility from the fact that ever since the early 1840s, diamonds, usually as isolated alluvial occurrences, have been found in such widely separated parts of the United States as the Appalachian and Great Lakes regions and California.

There are numerous kimberlites or lamproites in scattered parts of the United States, ranging from New York to Wyoming in an east-west direction, and from the Upper Peninsula of Michigan to Arkansas in a north-south direction, but most do not contain diamonds. All can be correlated with various cratons that underlie the United States. The most famous of those bodies are the diamond-bearing lamproite near Murfreesboro, Arkansas, and the recently discovered kimberlite cluster close to the Colorado-Wyoming border.

In 1906, the first diamond from a primary host rock in the United States was found at Prairie Creek, near Murfreesboro, Arkansas. That rock was classified as lamproite in 1984. From 1907 to 1933, more than 100,000 stones, averaging 0.25 carat per stone, were produced from that locality. Although a large percentage of the diamonds were of gem quality (40 percent were considered white) and the pipe was large (29 hectares, 72 acres), the mine was not profitable, and formal mining ended in 1919.

In recent years, that locality has been designated the Crater of Diamonds State Park, and it has been a mecca for hobbyists and tourists who pay a small fee to search for diamonds, which are theirs to keep. A 4.23-carat faceted canary yellow from that locality was worn by Hillary Rodham Clinton to presidential inaugural activities in 1993. Recent studies have shown that the pipe is not economically viable as a mine.

Kimberlites were first identified along the Colorado-Wyoming border known as the "state-line kimberlite district," in 1964, and since then more than 100 kimberlites have been identified within 80 km north and 150 km south of the border. Diamonds were first identified from those rocks in 1975. Several large companies evaluated the pipes in the 1980s, but concluded that they would be unprofitable.

In June 1996, a mine was opened at Kelsey Lake, Colorado, with anticipated production of about 20,000 carats for 1996, and as much as 100,000 carats annually at peak production, starting in 1997. It is the first operating diamond mine in the United States since the end of formal mining at the Prairie Creek mine in Arkansas in 1919.

Canada

Most of Canada is underlain by cratons, making occurrences of diamond-bearing primary rocks such as kimberlite seem likely (Figure 1). In eastern Canada, the first kimberlite was found in 1946. Subsequently, numerous kimberlite pipes and dikes have been discovered in several areas in Ontario and Quebec. Some are diamondiferous, but none shows economic promise at present. Exploration is continuing.

In western Canada, diamond exploration was begun in the 1970s by several large companies, particularly in Saskatchewan and the Northwest Territories. In Saskatchewan, a diamond-bearing, but noneconomic, kimberlite was found in 1988 about 30 km (18 miles) northwest of the city of Prince Albert. In 1989, about 100 km (62 miles) east of Prince Albert, the first of about 100 kimberlites was discovered. Many of those kimberlites are large, and many contain diamonds, but none appears economically promising at this time. Exploration for additional pipes in that region is continuing.

In the Northwest Territories, intermittent explorations by major companies for kimberlites were unsuccessful, and most of the companies had withdrawn from that area by the end of the 1980s. Dia Met Minerals, a small company whose chairman, Charles E. Fipke, had a decade of experience in diamond exploration in various parts of the world, continued the search. Fipke followed the trail of diamond-indicator minerals to the Lac de Gras region, about 300 km (186 miles) northeast of the territorial capital at Yellowknife, and in April 1990 a kimberlite was located under Point Lake (Figure 30). Eventually, Dia Met and its Australian partner, BHP Minerals, found at least 77 kimberlites on their claims, of which at least 42 contain diamonds, with several showing economic promise.

Five of those relatively small pipes (1.8–4 hectares, 4.4–9.9 acres), being operated as if they were one mine, are scheduled to begin production in the second half of 1998. Annual production of 3 million carats (about 30 percent gems) from that mine is expected by 2000. It is believed that in later years that production could double. The projected mine life is 25 years. That one mining project should propel Canada into the position of sixth leading producer of diamonds, on a weight basis, with about 3 percent of the world's production.

The spectacular discoveries by Dia Met/BHP sparked the greatest rush to

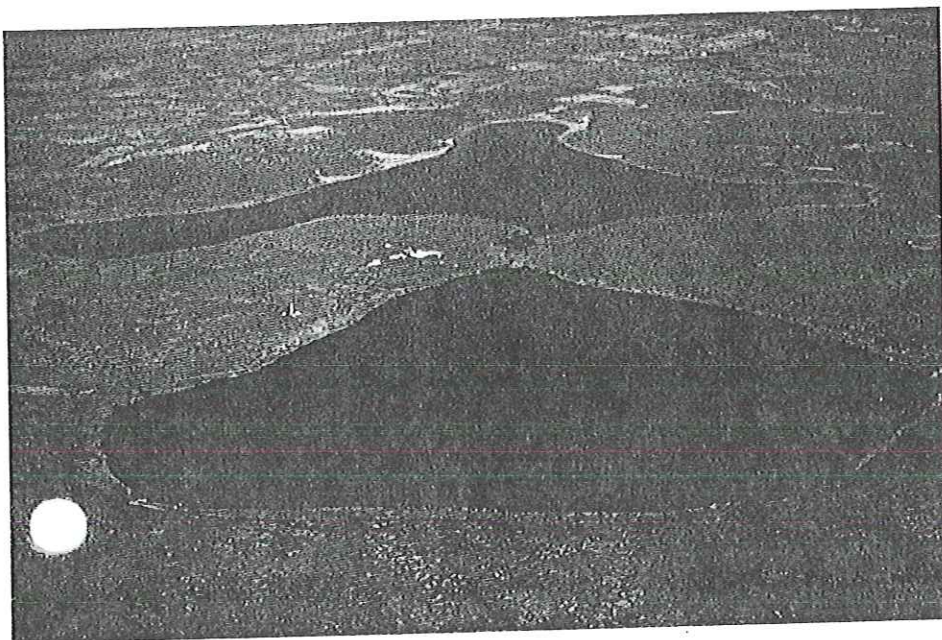


Figure 30. The first kimberlite pipe discovered in the Northwest Territories is under Point Lake. The surface of the kimberlite lies about 50 m (165 feet) below the surface of the lake, which is 600 m (1,969 feet) wide. The white objects on the far shore are trailers, on the property as of 1992. (B. T. Evans.)

Jan. 21

stake claims ever seen in Canada, and possibly the world. More than 100 kimberlites have now been found in the Northwest Territories alone, many of which are diamondiferous and are now being evaluated by several companies for their economic viability.

The Canadian discoveries are only the latest in what has been a fabulous century of diamond production. The improved understanding of diamond sources, both pipes and their weathered products, combined with improved technology and a steady demand, means that the future is bright for discovering diamonds.

BIBLIOGRAPHY

- Blakey, G. G. (1977). *The Diamond*. Paddington Press, London.
- Bruton, E. (1978). *Diamonds*, 2nd ed. Chilton Book Co., Radnor, Pa.
- Cassedanne, J. P. (1989). Diamonds in Brazil. *Mineralogical Record* 20:325-36.
- Gurney, J. J., Levinson, A. A., and Smith, H. S. (1991). Marine mining of diamonds off the west coast of southern Africa. *Gems & Gemology* 27:206-19.
- Janse, A. J. A. (1995). A history of diamond sources in Africa: Part I. *Gems & Gemology* 31:228-55.
- Janse, A. J. A. (1996). A history of diamond sources in Africa: Part II. *Gems & Gemology* 32:2-30.
- Legrand, Jacques. (1980). *Diamonds: Myth, Magic, and Reality*. Crown Publishers, New York.
- Lenzen, G. (1970). *The History of Diamond Production and the Diamond Trade*. Barrie & Jenkins, London. (English translation from the German, first published by Duncker & Humboldt, Berlin, 1966.)
- Levinson, A. A., Gurney, J. J., and Kirkley, M. B. (1992). Diamond sources and production: past, present, and future. *Gems & Gemology* 28:234-54.
- Mawe, John (1812). *Travels in the Interior of Brazil*.
- Mawe, John (1823). *Treatise on Diamonds and Precious Stones*. London.
- Reclus, Elis  e (1891). *The Earth and Its Inhabitants: Asia*. New York.
- Sevdermish, M., and Mashiah, A. (1996). *The Dealer's Book of Gems and Diamonds*, 2 vols. Kal Printing House, Israel.
- Webster, R. (1994). *Gems: Their Sources, Descriptions and Identification*, 5th ed., revised by P. G. Read. Butterworth-Heinemann, London.
- Williams, Gardner Fred (1906). *Diamond Mines of South Africa*. B. F. Buck & Co., New York.

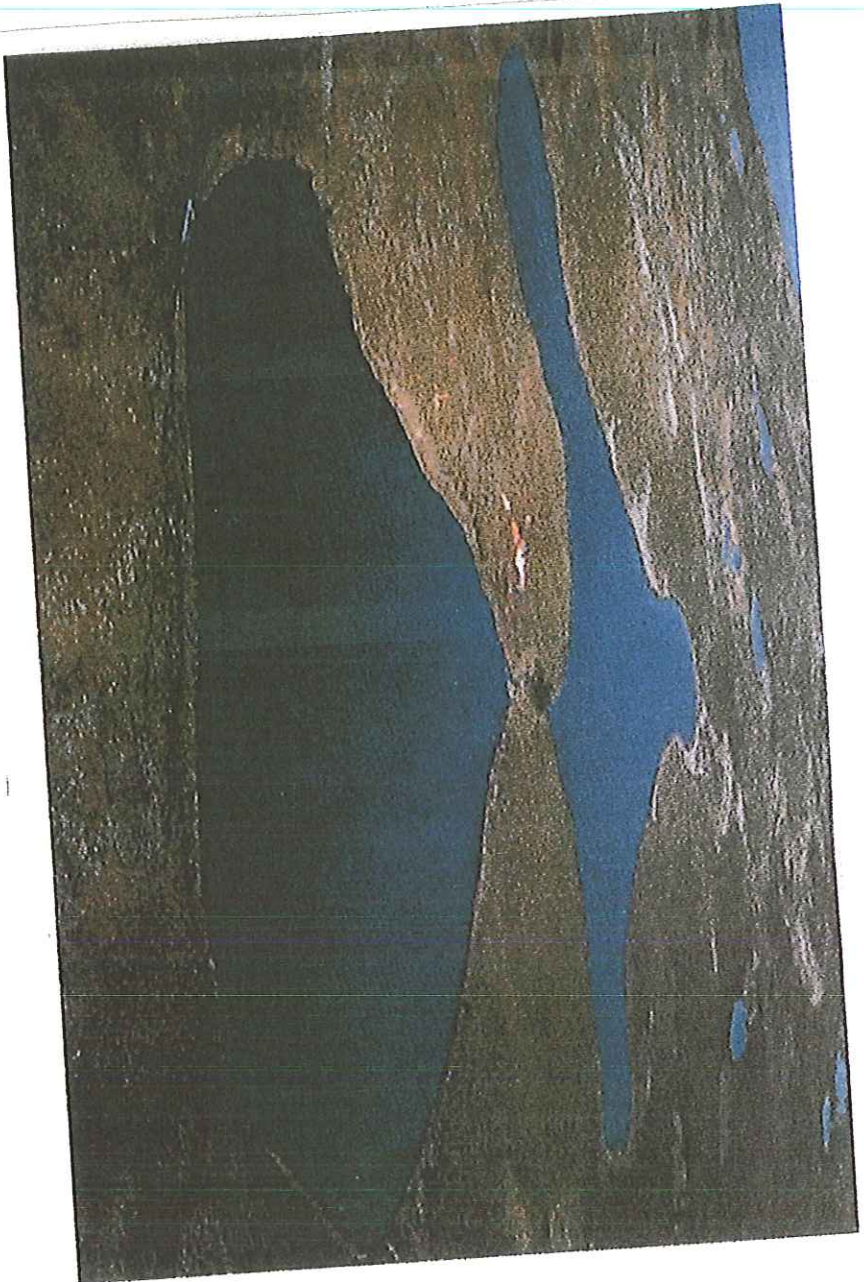


Figure 30. The first kimberlite pipe discovered in the Northwest Territories is under Point Lake. The surface of the kimberlite lies about 50 m (165 feet) below the surface of the lake, which is 600 m (1,969 feet) wide. The white objects on the far shore are trailers, on the property as of 1992. (B. T. Evans.)

hopefully whoever
is swatting blackflies
in those prefects
will leave his/her
\$ to Princeton rather
than Oxford

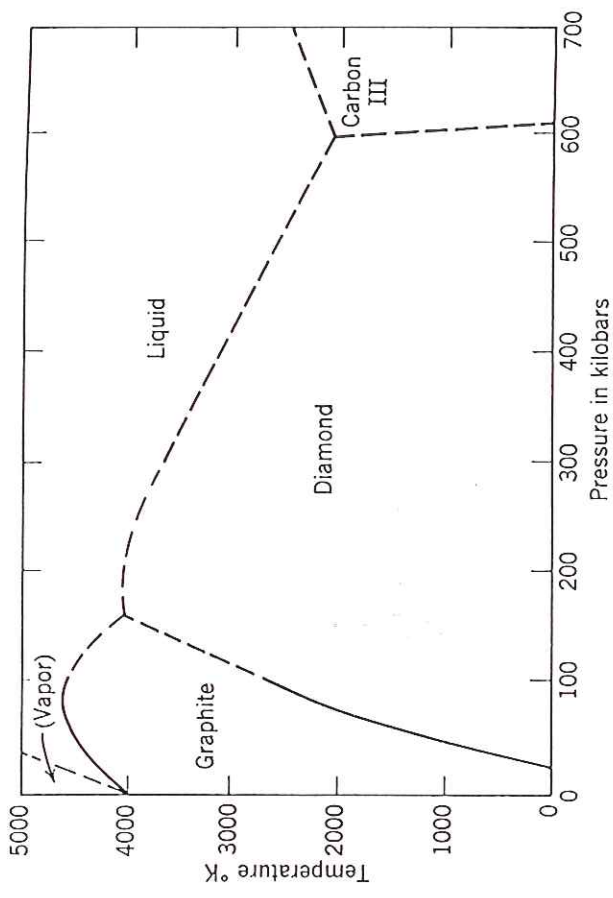


FIG. 10.14. Pressure-temperature phase diagram for carbon, based on experimental data from various sources.

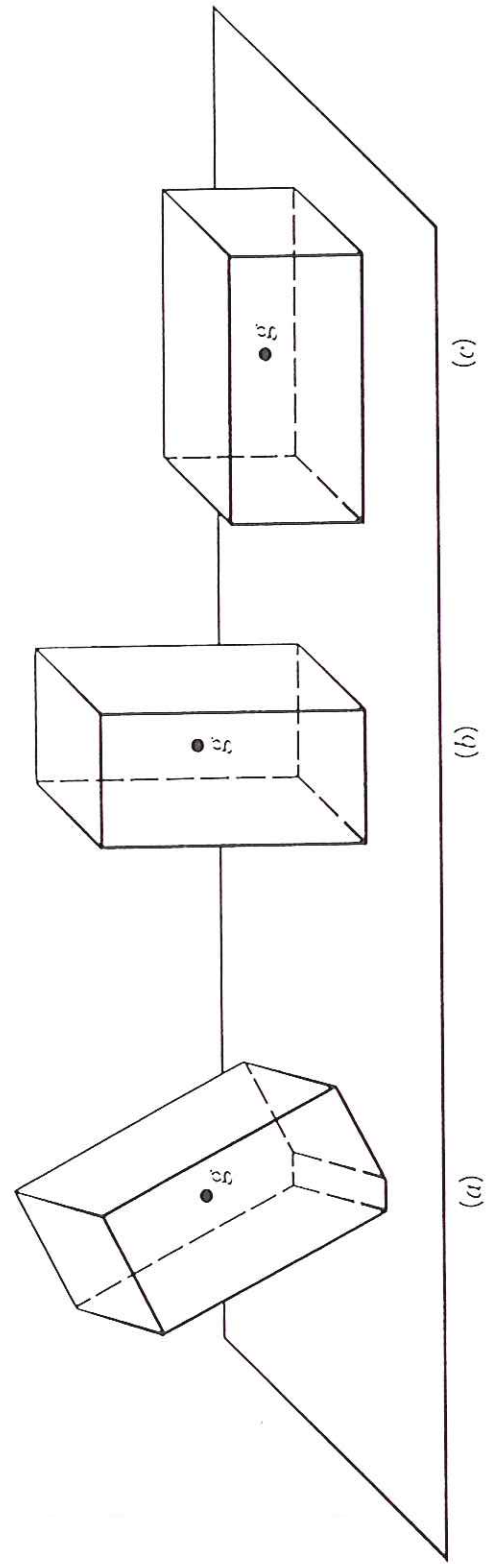


FIG. 9.2. Illustration of various degrees of stability for the same block in different orientations: (a) unstable, (b) metastable, and (c) stable (see text for discussion). The center of gravity is marked as g .

Fig. 7 Harlow superimposes diamond-graphite stability line on model oceanic and continental geotherms

Source of diamonds at great depth — 160 km beneath continents

Model for diamond formation shown in Fig. from p. 65

Form at base of deepest oldest parts of ~~crust~~ continental crust — in regions of ~~steepened~~ steepened thermal gradient — at depths in excess of 100 km

Brought to surface via kimberlite eruptions — see Fig. 3 — mining operations completely excavate these, e.g. The Big Hole Kimberly, SA — at one point individual claims ~~31~~ 31 feet x ~~31~~ 31 feet — many subdivided — a total of 1600 claimants — Cecil Rhodes — formation of de Beers — The Big Hole now abandoned

origin of term kimberlite

kimberlites contain nodules — sample or mantle

Fig. 1 shows a modern de Beers mine

Next two frontiers — offshore Atlantic —
alluvial diamond-bearing gravels
eroded from kimberlites — Orange
River Basin — Fig. 24

NWT Canada — biggest rush to
stake claims in history — now
more than 100 kimberlites — first
discovery 1990

~~Final note — diamonds are forever?~~

Final note — diamonds are forever?

Note that diamonds are highly unstable
at surface of \oplus

Why don't they revert to graphite
upon being brought to surface in
a kimberlite eruption

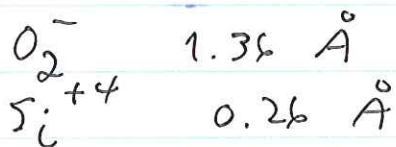
Answer — they are metastable — sluggish
kinetics — analogy of a block —
Fig 9.2

Silicate Minerals ← crystal (low pressure) minerals first

As we have seen, these are the dominant minerals comprising the \oplus why? KH Fig. 5.1

Eight most common elements - most minerals made from these Fig 13.1 - only 8% non-silicates

Recall $[\text{SiO}_4]^{4-}$ tetrahedron - most stable way to bond Si & O why? Because of ionic radii



Si-O bond length ~~1.62 Å~~ 1.62 Å

Common for silica tetrahedra to polymerize ~~by~~ by sharing a bridging oxygen

This leads to a wide variety of structures

K & H Fig 13.3

Putnis Fig. 6.3

Single-chain, double-chain, sheet silicates, 3-d framework silicates

Figure 2. Cross section of the Earth with detail of crustal structure. The Earth is divided into a central inner and outer core, mantle, and crust (below). The thinnest crust lies under the ocean basins, and thick crust forms the continents (bottom). The lithosphere (rock sphere) below the crust is shown darker than the more mobile asthenosphere (weak sphere).

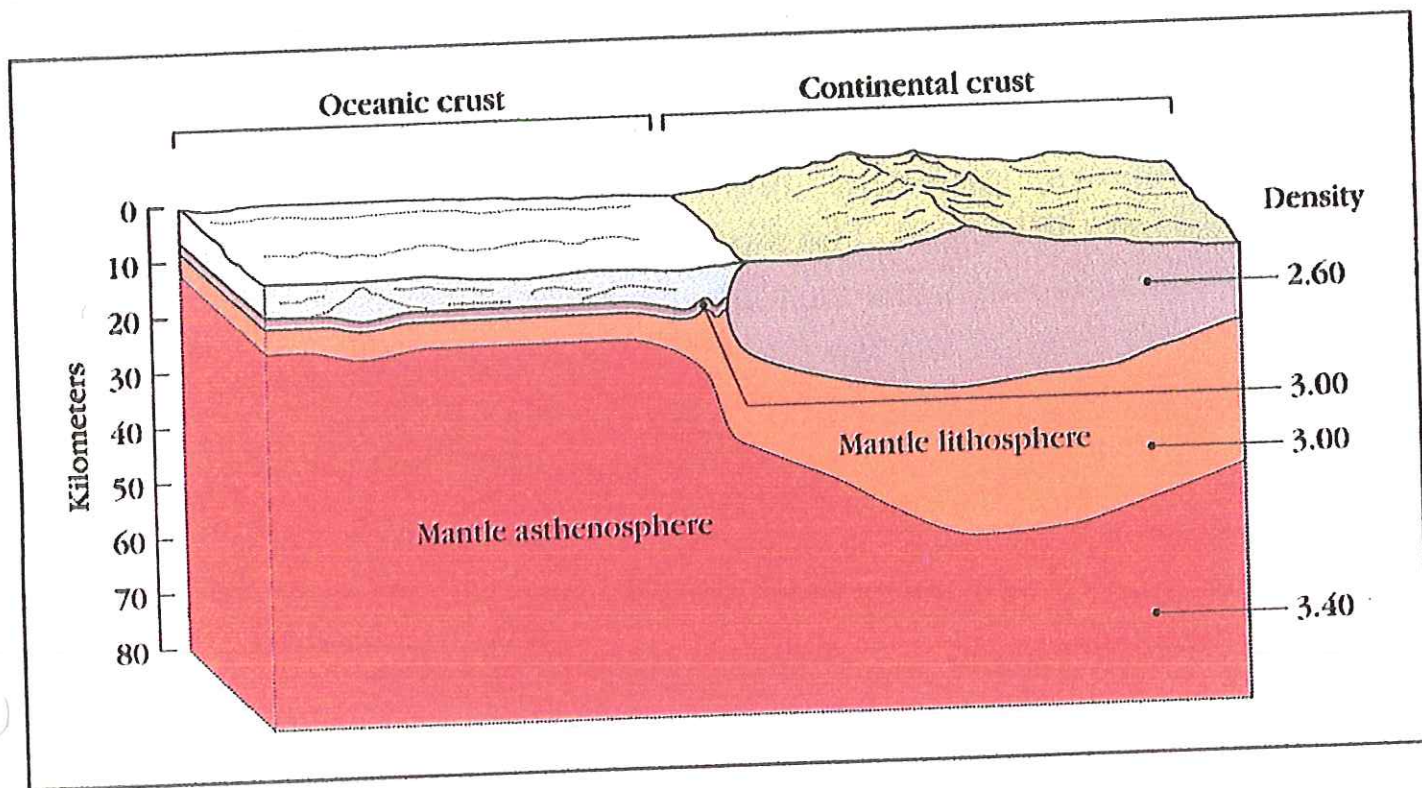
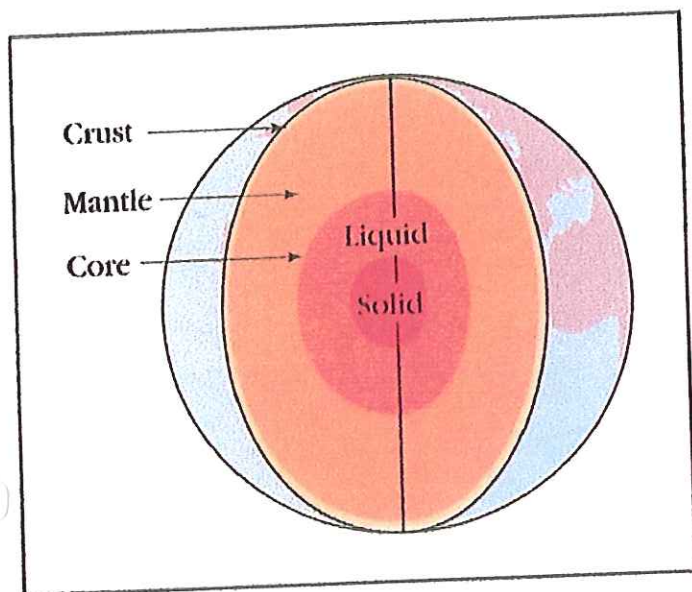


FIG. 5.1 The eight most common elements in the Earth's crust. (*From Mason, B. and Moore, C. B., 1982, *Principles of Geochemistry*, 4th ed. John Wiley & Sons, Inc., New York. †Ionic radii taken from Table 4.8. Numbers in parentheses refer to coordination number.)

NIB

Element	Weight percent*
O	46.60
Si	27.72
Al	8.13
Fe	5.00
Ca	3.63
Na	2.83
K	2.59
Mg	2.09
	<u>98.59</u>

weight %
 $\frac{1}{2}$ oxygen
 $\frac{1}{4}$ Si
 $\frac{1}{4}$ cations

Atom percent	Ionic radius (Å)	Volume percent
62.55	1.36	~94
21.22	0.26 (4)	
6.47	0.39 (4)	
1.92	0.78 (6)	
1.94	1.00 (6)	
2.64	1.02 (6)	
1.42	1.51 (8)	
1.84	0.72 (6)	
100.00		~6% in total

since the atoms are so big

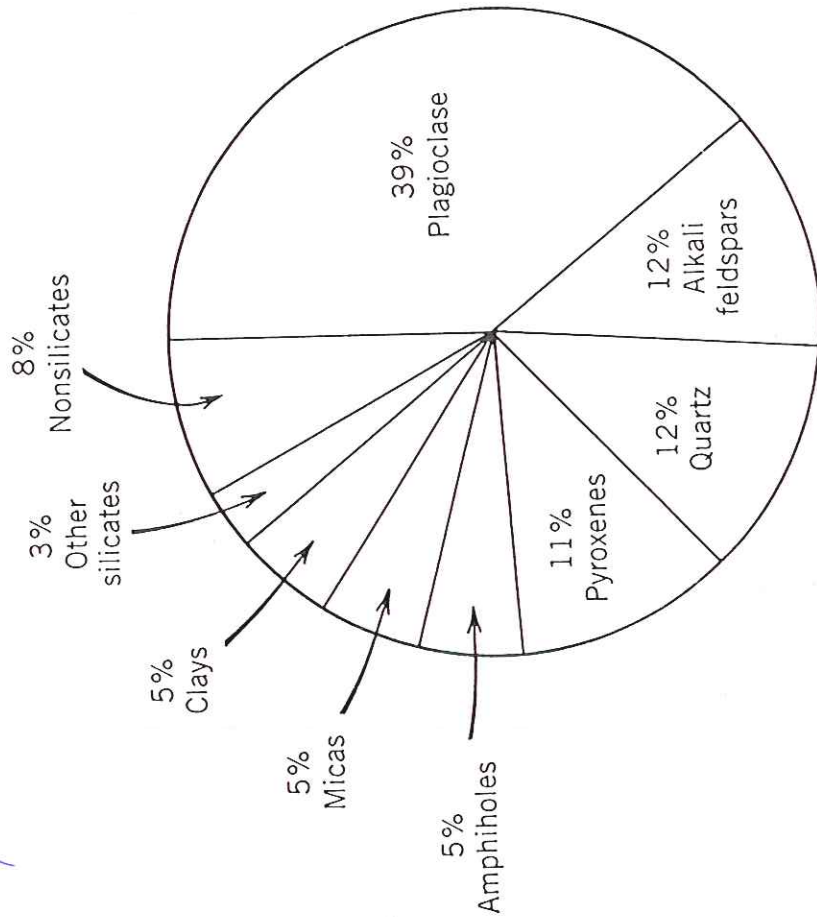
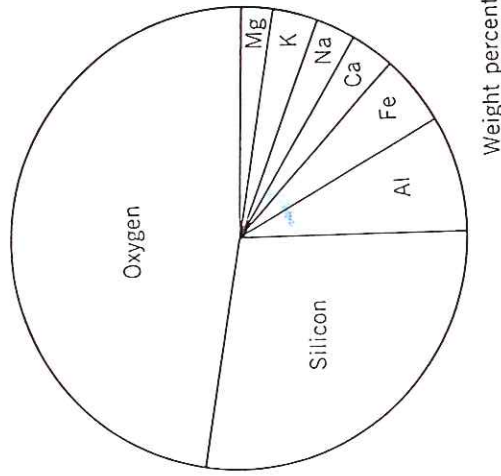


FIG. 13.1. Estimated volume percentages for the common minerals in the Earth's crust, inclusive of continental and oceanic crust. Ninety-two percent are silicates. (From Ronov, A. B. and Yaroshevsky, A. A., 1969, *Chemical composition of the Earth's crust*. American Geophysical Union Monograph no. 13, p. 50.)

Important minerals of crust (low pressure minerals)

silicates

dark colored silicates (Fe, Mg)

olivine Mg_2SiO_4 (Mg, Fe varieties) ($\rho = 3.3$)
(Si:O = 1:4 = 25% Si)

pyroxene (single-chain silicates)

(Mg, Fe) SiO_3 ($\rho = 3.3$) orthopyroxene

$\text{Ca}(\text{Mg, Fe})\text{Si}_2\text{O}_6$ ($\rho = 3.3$) clinopyroxene
(Si:O = 1:3 = 33% Si)

amphibole (double-chain silicates)

The simplest example is anthophyllite:

$\text{Mg}_7\text{Si}_8\text{O}_{22}(\text{OH})_2$ (Si:O = 4:11 = 36% Si)

but the most common is hornblende which has complex substitutions of Ca, Na, Fe and Al into this structure.

sheet silicates

micas

The simplest example is perhaps phlogopite:

$\text{KMg}_3(\text{AlSi}_3\text{O}_{10})(\text{OH})_2$ (Al/Si:O = 2:5 = 40% Si/Al)

but biotite and muscovite are more common varieties

clays

light colored silicates

quartz

SiO_2 ($\rho = 2.65$) (Si:O = 1:2 = 50% Si)

feldspar

$\text{CaAl}_2\text{Si}_2\text{O}_8$ (Na, K varieties) ($\rho = 2.76$)
(Al/Si:O = 1:2 = 50% Si/Al)

carbon-bearing compounds (bear the stamp of life)

carbonates

calcite CaCO_3 ($\rho = 2.72$)

organic matter

complex compounds

graphite C ($\rho = 2.23$)

other

evaporitic minerals

halite NaCl

gypsum $\text{CaSO}_4 \cdot 2\text{H}_2\text{O}$

water ice H_2O

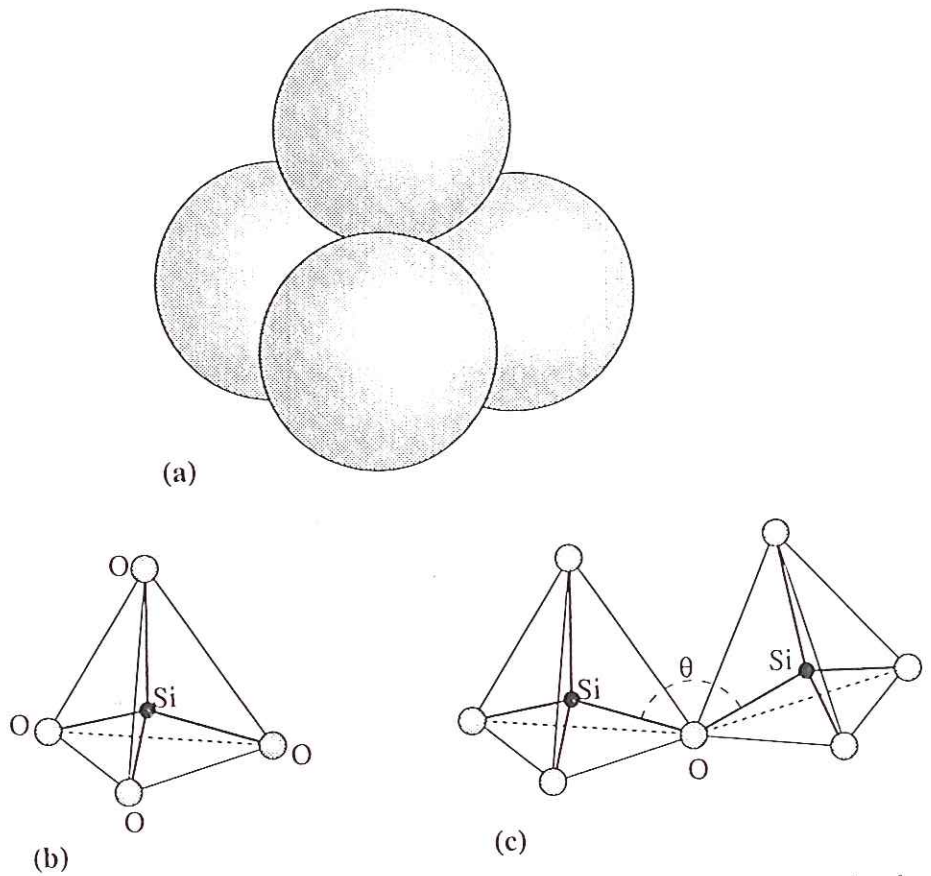
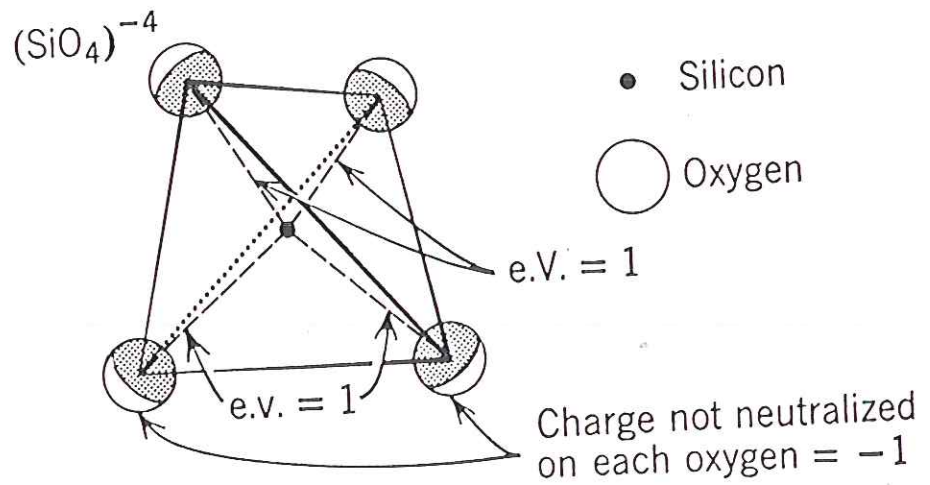


Figure 6.1. Silicate structures are built up from SiO_4 tetrahedra. (a) A space-filling model showing four oxygen atoms at the corners of a tetrahedron, obscuring the Si atom at the centre. (b) A less realistic, but clearer model of an SiO_4 tetrahedron, showing the Si-O bonds. (c) Two SiO_4 tetrahedra sharing a corner to form an Si_2O_7 pair. The angle θ is the Si-O-Si bond angle.



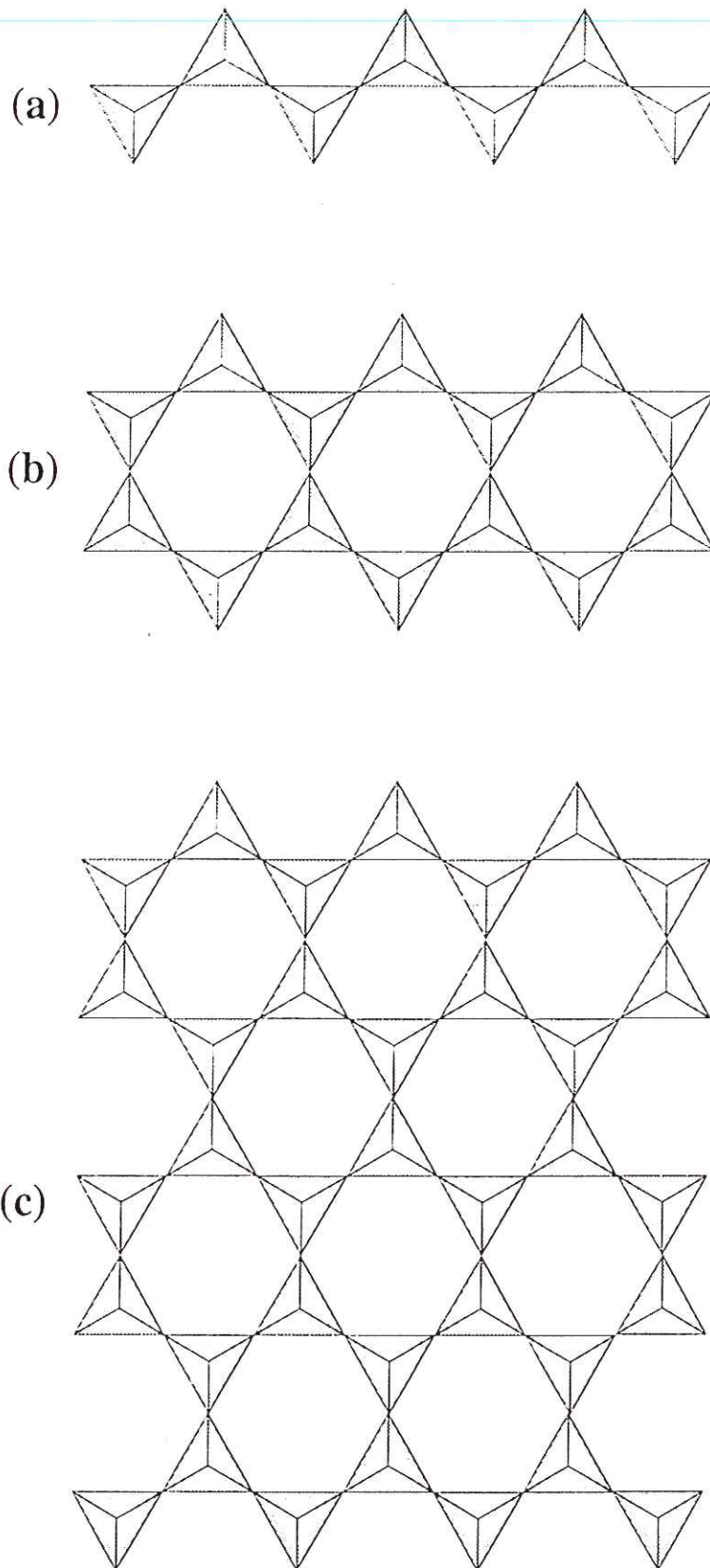


Figure 6.3. (a) Part of an infinite single chain of SiO_4 tetrahedra with each tetrahedron sharing two corners, as in the pyroxene structure. (b) Part of an infinite double chain of SiO_4 tetrahedra with half the tetrahedra sharing two corners, and the other half sharing three corners, as in the amphibole structure. (c) Part of an infinite sheet of SiO_4 tetrahedra, each tetrahedron sharing three corners, as in the sheet silicate structures.

Si:O

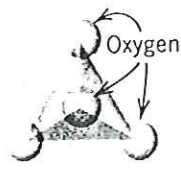

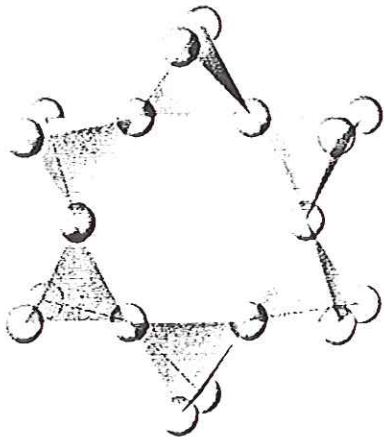
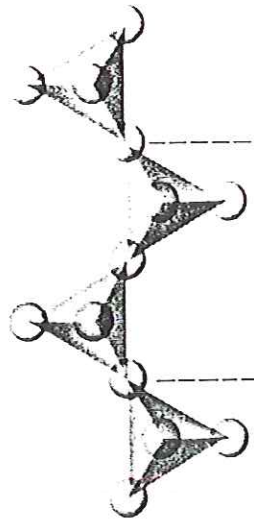
Class	Arrangement of SiO ₄ tetrahedra (central Si ⁴⁺ not shown)	Unit composition	Mineral example
Nesosilicates 1:4		(SiO ₄) ⁴⁻	Olivine, (Mg, Fe) ₂ SiO ₄
Sorosilicates 2:7		(Si ₂ O ₇) ⁶⁻	Hemimorphite, Zn ₄ Si ₂ O ₇ (OH)·H ₂ O
Cyclosilicates 1:3		(Si ₆ O ₁₈) ¹²⁻	Beryl, Be ₃ Al ₂ Si ₆ O ₁₈
Inosilicates (single chain) 1:3		(Si ₂ O ₆) ⁴⁻	Pyroxene e.g. Enstatite, MgSiO ₃

FIG. 13.3. Silicate classification.

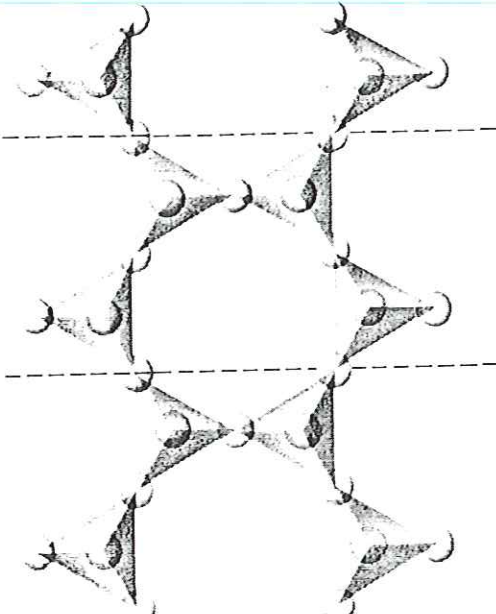
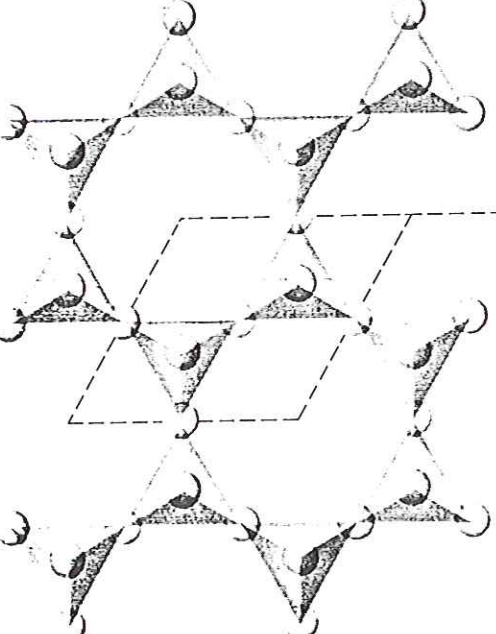
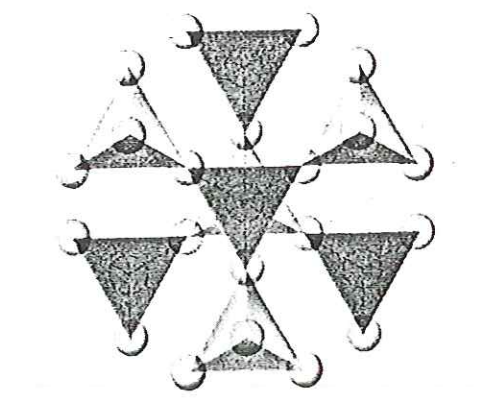
<p>Inosilicates (double chain)</p> <p>4:11</p>		<p>$(\text{Si}_4\text{O}_{11})^{6-}$</p>	<p>Amphibole e.g. Anthophyllite, $\text{Mg}_7\text{Si}_8\text{O}_{22}(\text{OH})_2$</p>
<p>Phyllosilicates</p> <p>2:5</p>		<p>$(\text{Si}_2\text{O}_5)^{2-}$</p>	<p>Mica e.g. Phlogopite, $\text{KMg}_3(\text{AlSi}_3\text{O}_{10})(\text{OH})_2$</p>
<p>Tectosilicates</p> <p>1:2</p>		<p>$(\text{SiO}_2)^0$</p>	<p>High cristobalite, SiO_2</p>

FIG. 13.3. (continued)

Table 4.9

SOME COMMON ELEMENTS (EXCLUSIVE OF HYDROGEN) THAT OCCUR IN ROCK-FORMING MINERALS, ARRANGED IN DECREASING IONIC SIZE

Ion	Coordination Number with Oxygen	Ionic Radius Å	
O ²⁻		1.36 (3)	
K ⁺	8-12	1.51 (8)-1.64 (12)	
Na ⁺	8-6	} cubic to } octahedral	
Ca ²⁺	8-6		1.18 (8)-1.02 (6)
Mn ²⁺	6	} octahedral	
Fe ²⁺	6		0.83 (6)
Mg ²⁺	6		0.78 (6)
Fe ³⁺	6		0.72 (6)
Ti ⁴⁺	6		0.65 (6)
Al ³⁺	6		0.61 (6)
Al ³⁺	4	} tetrahedral	
Si ⁴⁺	4		0.39 (4)
P ⁵⁺	4		0.26 (4)
S ⁶⁺	4		0.17 (4)
C ⁴⁺	3	triangular	0.12 (4)
			-0.08 (3)

*The first column lists the most common ionic (valency) states of the elements. The second column lists their most common coordination with respect to oxygen, and the third column lists ionic sizes for specific coordinations (the number in parentheses is **C.N.**). A complete listing of elemental abundances is given in Table 5.1.

Note the change in the ratio of Si to O depending upon the degree of polymerization

Ranging from SiO_4 to SiO_2

This is one reason there are many different silicate minerals with many different chemistries


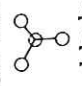
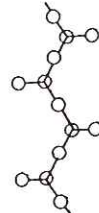
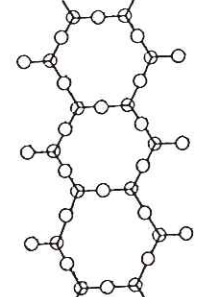
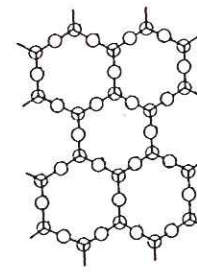

Another reason is the possibility of substitution

Table 4.9 — note, in particular, that Al^{3+} can substitute either for Mg^{2+} or Fe^{2+} , Fe^{3+} in octahedral cation sites or for Si^{4+} in the ~~silica~~ silica tetrahedra themselves.

This also allows for great variety. ~~The~~ Charge balance is achieved by addition or removal of other elements, including O^{2-}

Give examples of each category, increasing in degree of polymerization

Table 5.2
Classification of major silicate minerals

Type	Structure	Composition of tetrahedral groups	Si:O ratio	Mineral	Typical formula
Separate tetrahedron	 Plan view  used below	$[\text{SiO}_4]^{4-}$	1:4	Olivine	$(\text{Mg,Fe})_2\text{SiO}_4$
Chain		$[\text{SiO}_3]^{2-}$	1:3	Pyroxene	MgSiO_3
Double chain		$[\text{Si}_4\text{O}_{11}]^{6-}$	1:2.75	Amphiboles	$\text{Ca}_2(\text{Mg,Fe})_5[\text{Si}_8\text{O}_{22}](\text{OH,F})_2$
Sheet		$[\text{Si}_2\text{O}_5]^{2-}$ $[\text{AlSi}_3\text{O}_{10}]^{5-}$	1:2.5	Clay minerals —Kaolinite Mica	$\text{Al}_4[\text{Si}_4\text{O}_{10}](\text{OH})_8$ $\text{K}(\text{Mg,Al,Fe})_{2-3}[\text{AlSi}_3\text{O}_{10}](\text{OH})_8$
3-D framework	 (SiO_4) tetrahedron sharing all vertices	SiO_2 $[\text{AlSi}_3\text{O}_8]^{-}$	1:2	Quartz Feldspars —alkali —plagioclase	SiO_2 $(\text{Na,K})[\text{AlSi}_3\text{O}_8]$ $(\text{Na,Ca})[(\text{Al,Si})_4\text{O}_8]$

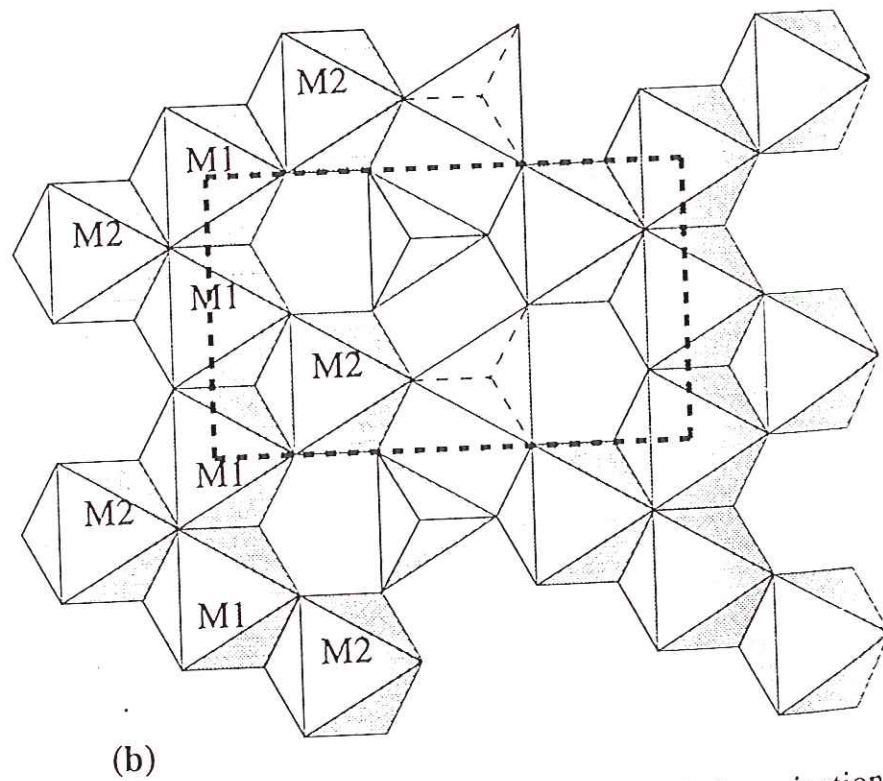
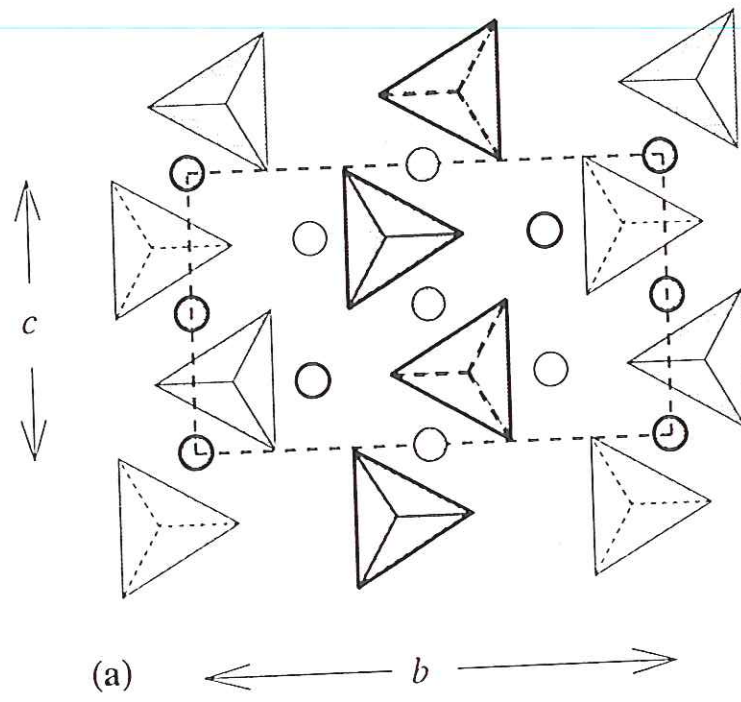


Figure 6.4. The structure of olivine, M_2SiO_4 . (a) A projection of the structure down the a axis of the orthorhombic unit cell (dashed line), showing isolated SiO_4 tetrahedra alternately pointing up and down and forming rows along the c axis. The tetrahedra are joined by the M cations (circles) also forming rows along c . These rows are at two levels within the unit cell: at height 0, indicated by the heavier line, and at height $a = 1/2$, in the lighter line. M1 cations are shown as filled circles, M2 cations as open circles. (b) The lower level of the unit cell shows the linkage between the M1 and M2 octahedra and the row of SiO_4 tetrahedra.

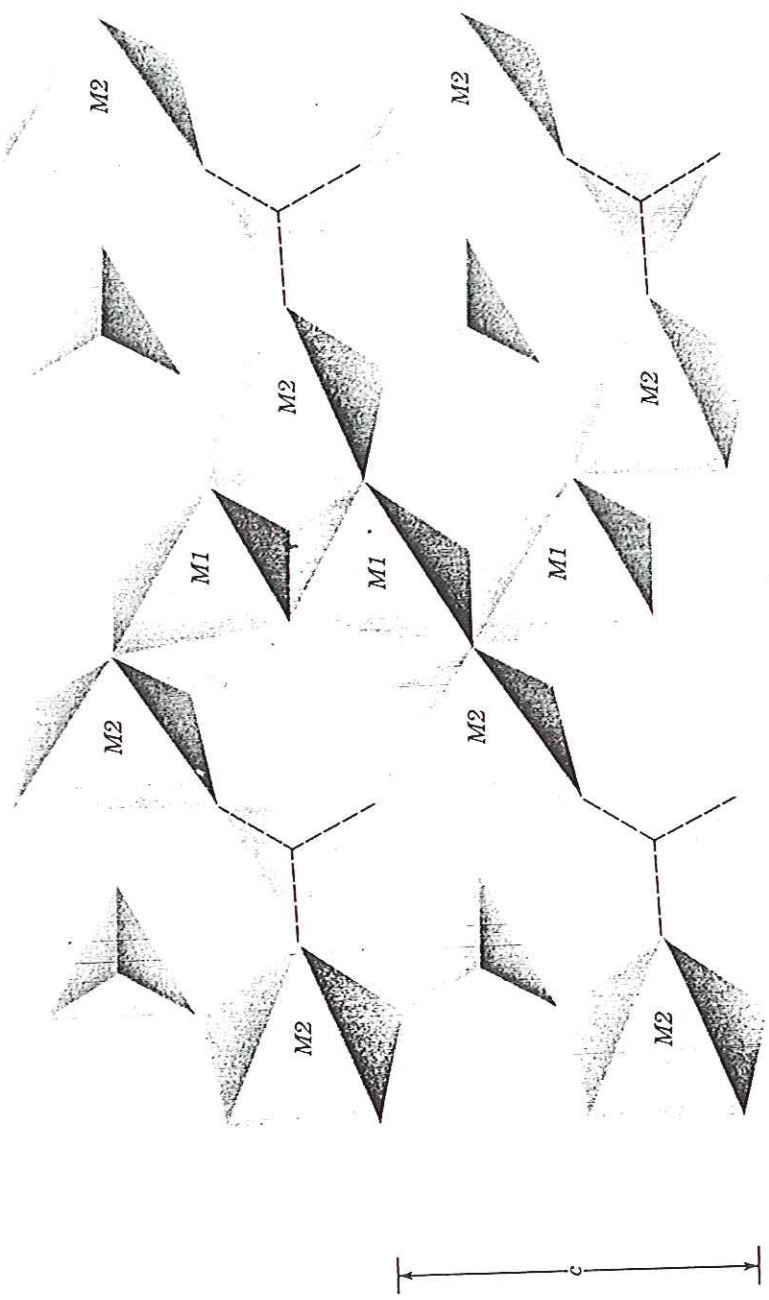
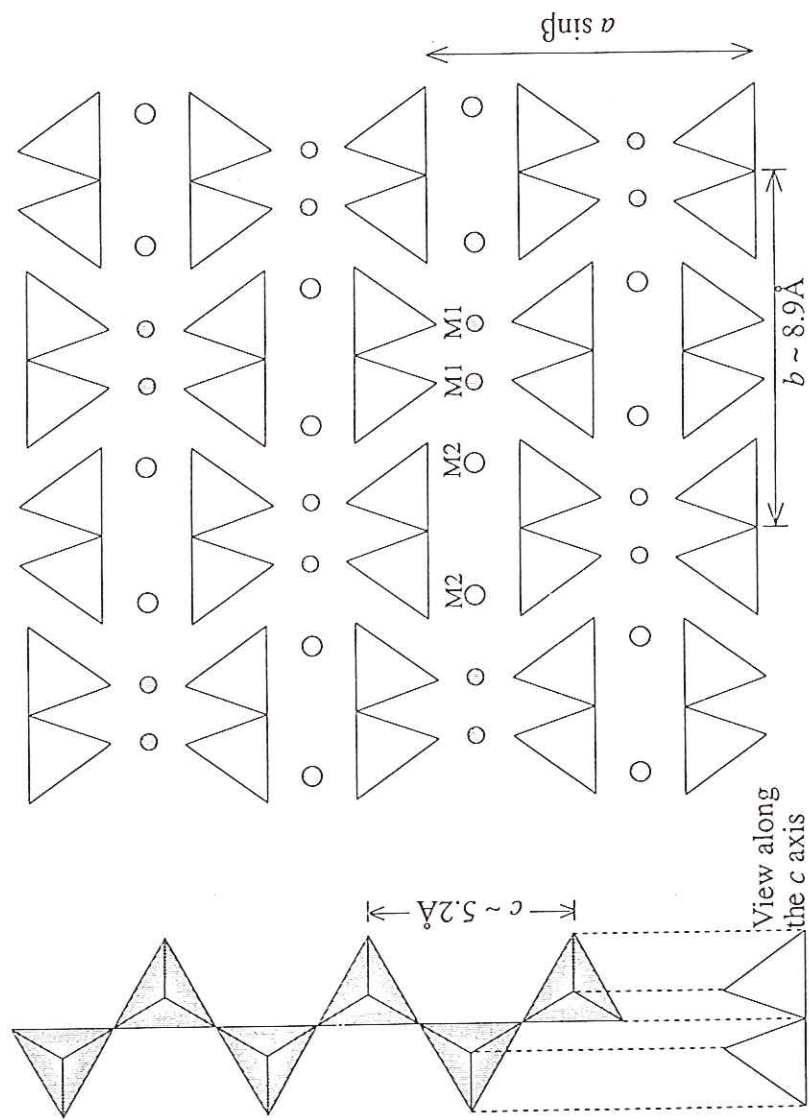


FIG. 13.4. Portion of the structure of olivine projected on (100). M1 and M2 are octahedral sites. The M1 site is most distorted and the M2 site is somewhat more regular. Extensive edge sharing among the polyhedra causes these distortions because shared edges are shortened as cations repel each other; see also page 197. (Redrawn after Papike, J. J. and Cameron, M., 1976, *Crystal chemistry of silicate minerals of geophysical interest. Reviews of Geophysics and Space Physics*, v. 14, pp. 37-80.)



(a)

(b)

Figure 6.11. (a) A single pyroxene chain which extends along the c axis and below, a schematic representation of this chain viewed end-on. (b) The arrangement of SiO_4 chains in the pyroxene structures, viewed along the c axis. The M1 cations form chains of edge-sharing tetrahedra between the apices of the tetrahedra, while the larger M2 octahedra form similar chains between the bases of the tetrahedra.

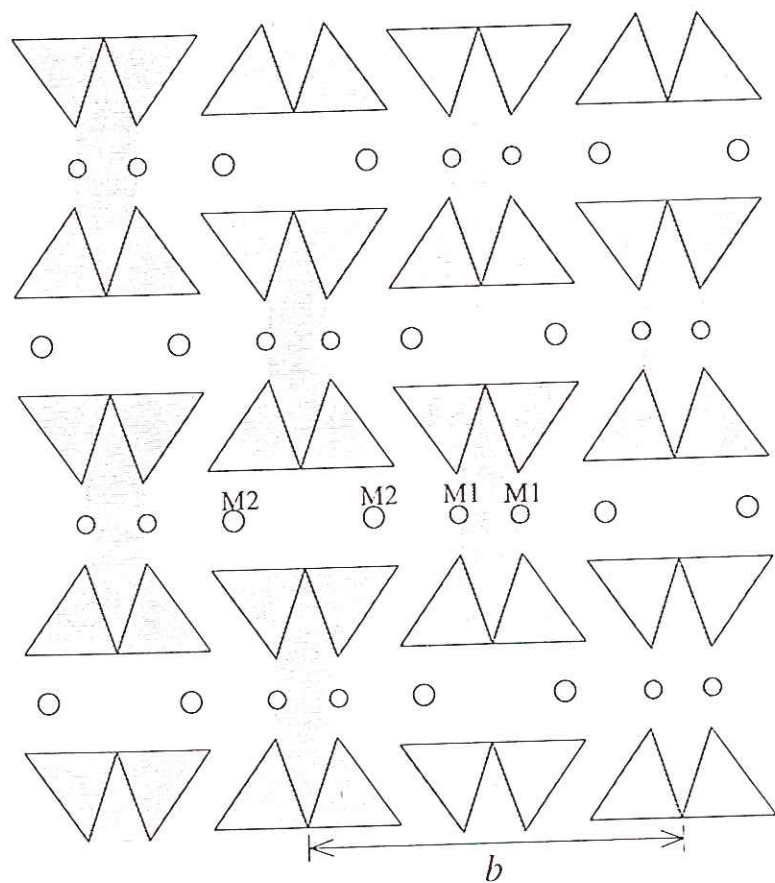
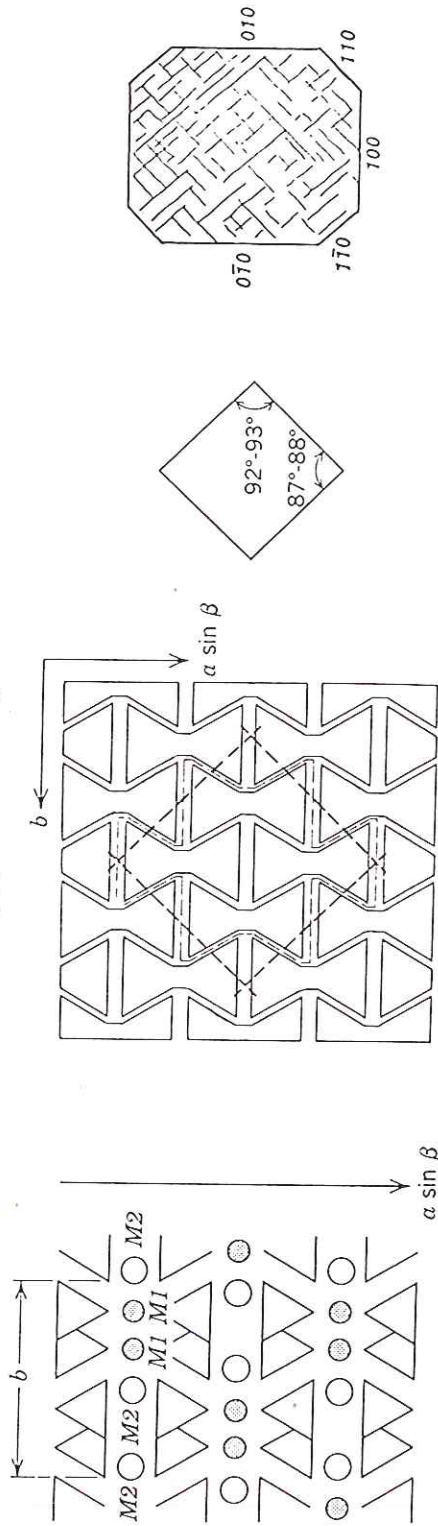


Figure 6.20. The I-beam representation of the pyroxene structure. Each pair of opposing tetrahedral chains, together with the M1 sites between them is shaded, and represents an I-beam, extending along the c axis. The various pyroxene structures can be conveniently represented in terms of such I-beams (see Figure 6.22).

FIG. 13.49. (a) Schematic projection of the monoclinic pyroxene structure on a plane perpendicular to the c axis. (b) Control of cleavage angles by t - o - t strips (also referred to as "l-beams") in the pyroxene structure, as compared with naturally occurring pyroxene cleavage.



(a)

(b)

~~XXXXXXXXXX~~ Show table 5.2 Cox each time

- isolated $[\text{SiO}_4]^{4-}$ tetrahedra

no bridging oxygens

e.g. olivine (forsterite)

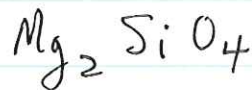


Fig 6.4 shows structure

Mg atoms fit in octahedrally coordinated sites between the Si tetrahedra

Also KH Fig 13.4

Cox 5.2 again

- single chain silicates

e.g. pyroxene MgSiO_3 (enstatite)

Figs. 6.11, 6.20 & KH 13.49

NB —
these are
looking
down the
chain

two types of octahedral sites

~~XXXXXXXXXX~~

referred to as M_1 & M_2

M_2 ~~///~~ bonds & interchain links are weaker than M_1 bonds

this controls the characteristic cleavage or fracture pattern of this black mafic mineral

Box J.2 again

- double chain silicates
e.g. amphibole

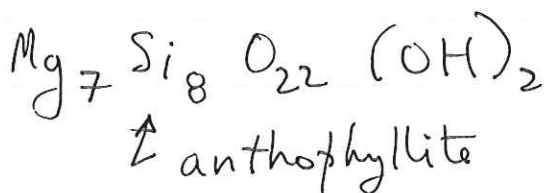


Fig 6.29 Patris

Now 4 types of octahedral sites
M1, M2, M3, M4

actually M4
either 6-fold
or 8-fold
A site is
always
8-fold
(biggest)

also room for two hydroxyl (OH) groups in each unit cell

Fig. 13.57 KH show cleavage controlled by weak A-M4 bonds

cleaves at 56° & 124°

amphibole
 90°
~cubic
hornblende
 52° &
 164°
prismatic

Cleavage an easy way in hand specimens to distinguish amphibole (double chain) from pyroxene (single chain) two dark minerals

such a substitution requires removing some O atoms according to the scheme $2\text{Al}^{3+} + \square = 2\text{Si}^{4+} + \text{O}^{2-}$, where \square represents a vacant oxygen site. The general formula for mullite is then written $\text{Al}_{4+2x}\text{Si}_{2-2x}\text{O}_{10-x}$ where x is the number of missing oxygen atoms per formula unit. The x value can vary between about 0.17 and 0.6, and so mullite can exist with a wide range of Al:Si ratios. The absence of these O atoms makes some of the tetrahedral sites effectively disappear and the extra Al atoms introduced by the substitution go into new tetrahedral positions as shown in Figure 6.9(b). Furthermore, the Al and Si atoms in the original tetrahedral double chain become disordered, and as the Al:Si alternation is lost the c axis repeat is reduced by half relative to that of sillimanite.

When sillimanite is heated to above 1545°C it is converted to mullite + melt while the mullite remains stable to $\sim 1850^\circ\text{C}$. The stability of mullite, in view of its apparently defective structure, will be a topic for further discussion in Section 12.5.1.

6.4 Single chain silicates

In this section we will describe two mineral groups in which the $[\text{SiO}_4]$ tetrahedra form linear single chains with two bridging oxygens per tetrahedron, as shown in Figure 6.10. The periodicity of the chains is every two tetrahedra for pyroxenoids and every three tetrahedra for pyroxenes. The Si:O ratio is 1:3 with a net charge of -2 for pyroxenoids and -4 for pyroxenes.

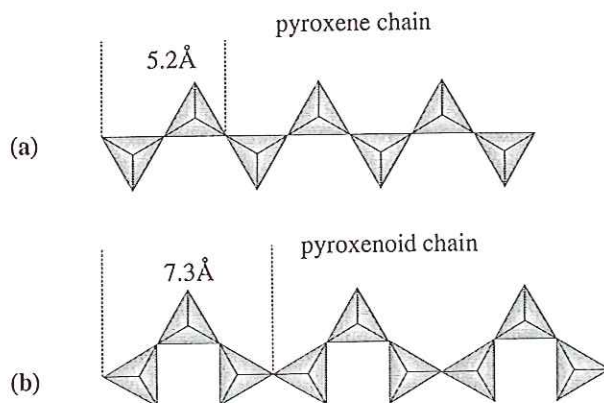


Figure 6.10. A comparison of the single SiO_4 chains in (a) pyroxenes with periodicity of 2 tetrahedra, and (b) pyroxenoids with periodicity 3 tetrahedra.

cross linked by cations, generally in octahedral sites. The flexibility of the chain is able to provide stable geometrical configurations with a very extensive range of cations and over a wide range of temperature and pressure conditions.

pyroxenes

6.4.1 The pyroxenes

The various modifications of the pyroxene structure are best understood by beginning with an idealized model which shows the basic topology, and then considering the effect of cation size and temperature on this topology. There are many analogies between single chain and double chain silicates in this respect so that an understanding of the behaviour of pyroxenes will be directly applicable to other chain silicates. The pyroxene structure will be therefore be described in some detail.

Figure 6.11(a) shows a straight single chain, which in all pyroxene structures extends along the c axis and defines the c parameter of the unit cell ($\sim 5.2\text{Å}$). The view of the structure down the c axis (Figure 6.11(b)) shows the chains end-on, and the way they are stacked back to back forming layers parallel to the (100) planes. The b axis repeat of pyroxene ($\sim 8.9\text{Å}$) is defined by this stacking arrangement. This projection of the structure is common to all pyroxenes but it does not show how the chains are arranged parallel to their length, nor does it show any differences between the chains. These two important features define the different pyroxene structural groups.

The cation positions in pyroxenes are of two types. The M1 sites lie between the apices of opposing tetrahedra; the M2 sites lie between their base (Figure 6.11(b)). The M1 sites are smaller, and are almost regular octahedra; M2 sites are larger, more distorted and may be octahedra when containing a smaller cation, or 8-fold sites when occupied by a larger cation. The M sites form edge-sharing chains which run parallel to the silicate chains.

The clinopyroxene structure

Figure 6.12 shows the arrangement of the silicate chains along their length in the clinopyroxenes and defines the orientation and repeat of the a axis ($\sim 9.7\text{Å}$). The unit cell is monoclinic with a β angle of around 106° , hence the term *clinopyroxene*. In this idealized structure the chains are all the same and are symmetrically related to one another. The

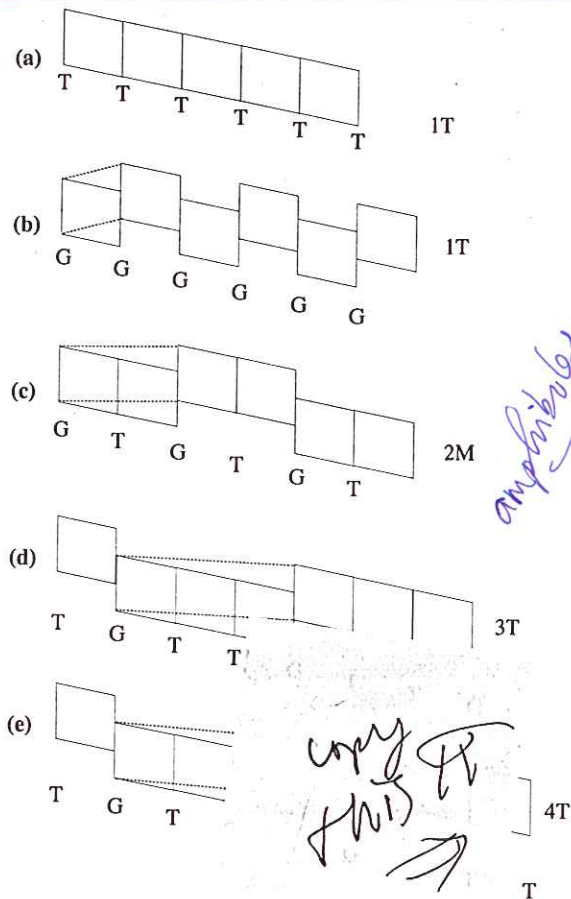


Figure 6.28. The polytypism of wollastonite is schematically shown in terms of the stacking of the tetrahedra as described in Figure 6.27. (a) Continuous chain of tetrahedra results in 1T wollastonite. (b) If every second tetrahedron is replaced by an octahedron, the structure is still 1T, but is twin related to the previous one, the structure is still 1T, but is twin related to (a). The twin related unit cell is shown by the dotted line. (c) 2M wollastonite (d) 3T wollastonite (e) 4T wollastonite. The unit cell is shown by the dotted line in each case. (After Henmi *et al.*, 1983.)

6.5 Double chain silicates – the amphiboles

The structure and the behaviour of the amphibole minerals are similar in many ways to the pyroxenes and we will make comparisons between the two mineral groups throughout this section. We will not therefore treat this group in as much detail, although the complexities, particularly due to the wider range of chemical compositions of the amphiboles are greater.

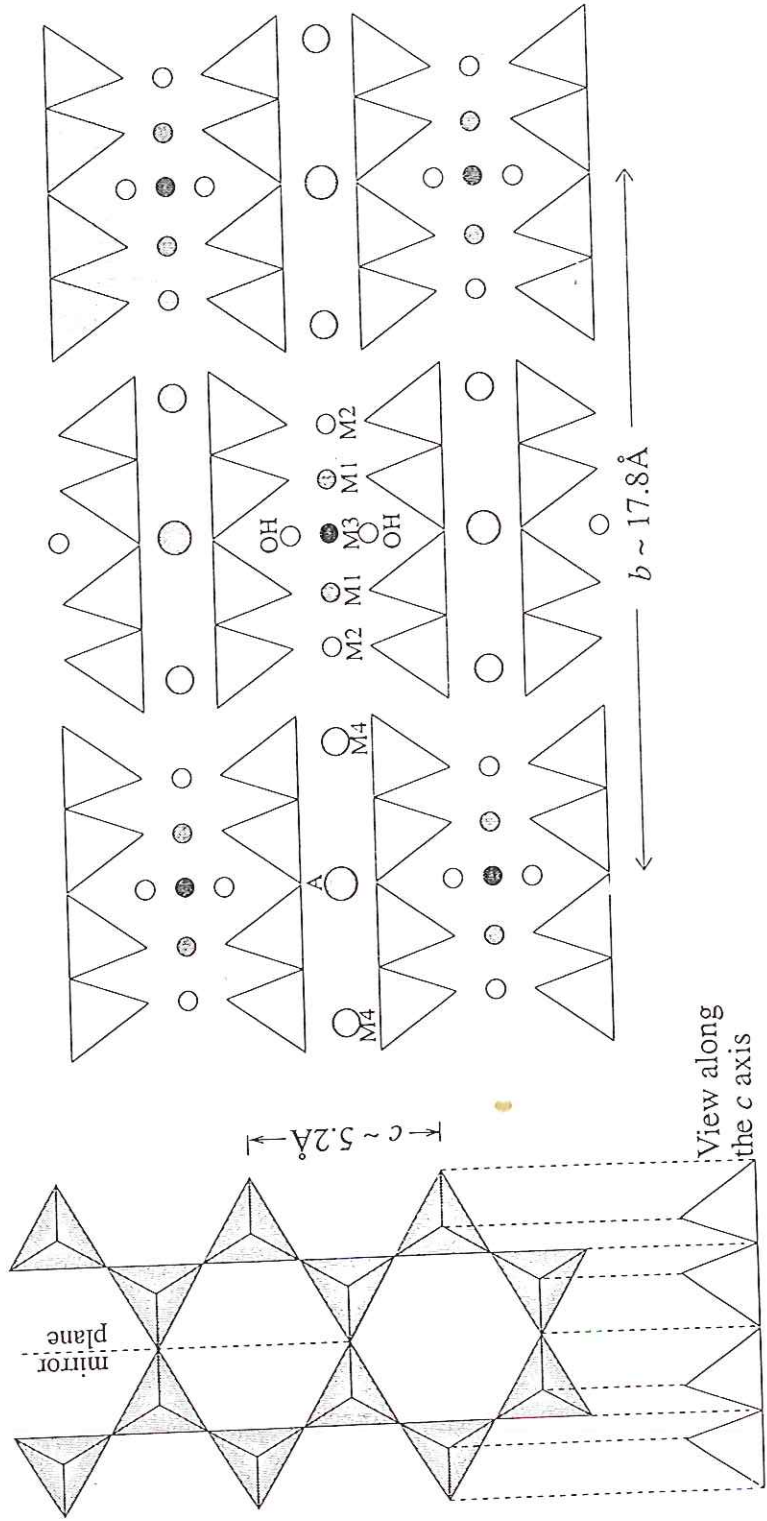
The essential feature of the amphibole minerals is the double chain of $[\text{SiO}_4]$ tetrahedra, which can be thought of as two single chains joined by corner-sharing, with a mirror plane along the join (Figure 6.29). The mirror plane is preserved in all amphi-

boles, even when the chains are not straight. Half of the tetrahedra have two bridging and two non-bridging oxygens; the other half have three bridging oxygens and one non-bridging. The general formula of the chain is therefore $(\text{Si}_4\text{O}_{11})_n^{6n-}$. The chains extend along the c axis defining the c axis repeat ($\sim 5.2\text{\AA}$) common to all amphibole structure types. The stacking of the chains is analogous to that in pyroxenes, forming (100) layers of chains with apices alternately pointing up and down, defining the b axis repeat (Figure 6.29(b)).

Again by analogy with the pyroxenes the cation sites in the structure are defined by their position relative to the apices and bases of the $[\text{SiO}_4]$ tetrahedra in the double chains. The sites between tetrahedral bases of adjacent chains are termed the M4 sites (cf. the M2 sites in pyroxenes), and the smaller sites between the opposed tetrahedral apices are the M1, M2 and M3 sites (cf. the M1 sites in pyroxenes). The coordination of the M4 sites is 8 when occupied by a larger cation such as Ca^{2+} , but reduces to 6 when occupied by a smaller cation such as Mg^{2+} or Fe^{2+} . The M1, M2 and M3 sites are octahedral. The double chains lead to a third type of cation site which lies between the rings formed by opposed tetrahedral bases in the chains. This large A site as it is called, may be vacant, partially filled, or fully occupied by Na and/or Ca in some amphiboles. Finally, $(\text{OH})^-$ or F^- lies in the centre of the hexagonal rings, at the level of the tetrahedral apices. All of these sites are shown in Figure 6.29(b). The space group of this ideal amphibole structure is $C2/m$. An I-beam, analogous to that in pyroxenes, is shaded.

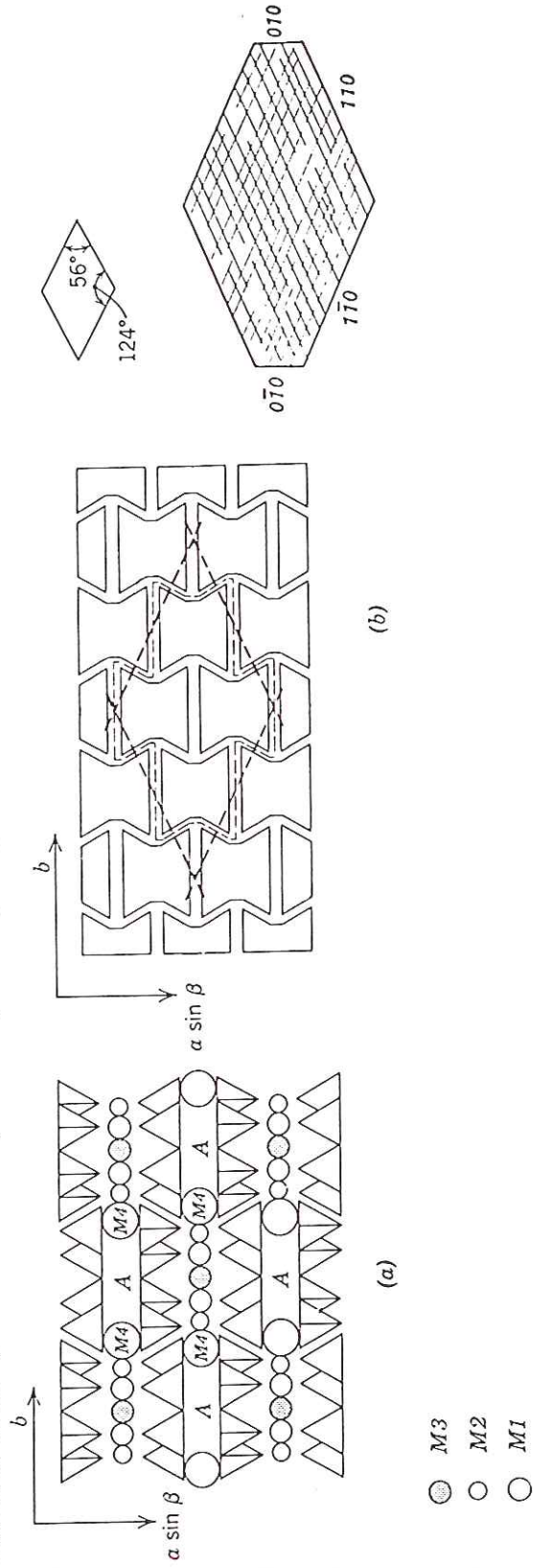
The basic relationships between the structure type, its composition and the temperature and pressure are analogous to the pyroxenes. Again the silica tetrahedra remain essentially inert during expansion or contraction of the cation sites, the linkage between the tetrahedral chain and the cation polyhedra being maintained by rotation of the individual tetrahedra which reduces the dimensions of the chain (Figure 6.30). Apart from the different mineral names, and their more complex chemistry, the structural modifications in the amphibole quadrilateral (Figure 6.31) can be interpreted in the same way as in pyroxenes.

1. In Ca-rich amphiboles the $C2/m$ structure exists over the whole temperature range and over a wide range of compositions. It also exists in Ca-poor amphiboles at high temperatures.

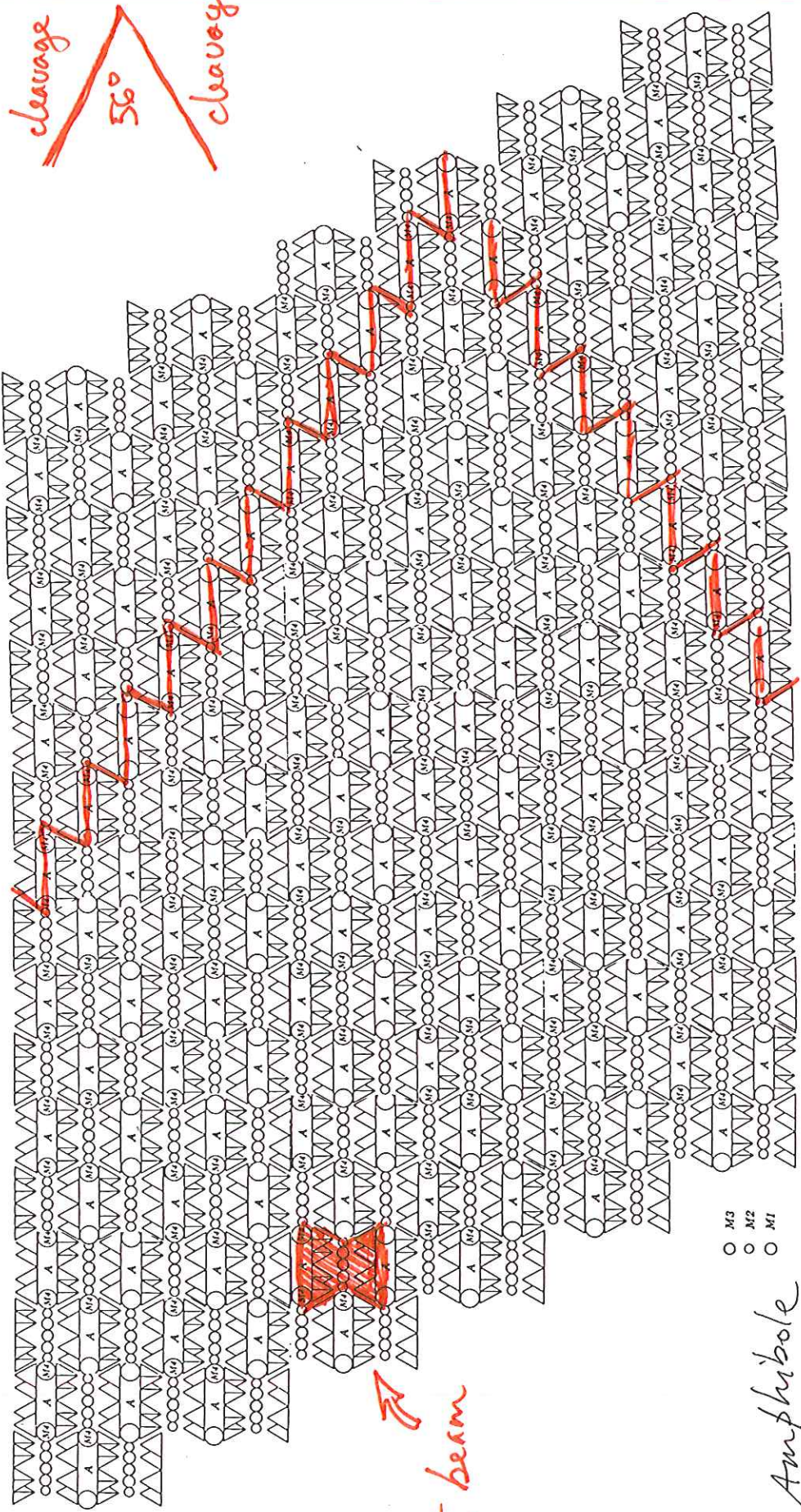


(a) A double chain of SiO_4 tetrahedra in amphiboles, extending along the c axis, and below, a schematic representation of this double chain viewed end-on. Here the chains are straight – in practice they are always slightly rotated as in Figure 6.30. (b) The arrangement of double chains in the amphibole structures, viewed along the c axis. The M1, M2 and M3 cations form chains of edge-sharing octahedra between the apices of the tetrahedra, while the larger M4 octahedra form similar chains between the bases of the tetrahedra. The A sites and the OH sites lie in the rings formed along the double chain. One I-beam, analogous to that in pyroxenes, has been shaded.

FIG. 13.67. (a) Schematic projection of the monoclinic amphibole structure on a plane perpendicular to the c axis (after Colville et al., 1966, *American Mineralogist*, v. 51, p. 1739). Compare with Fig. 13.49a. (b) Control of cleavage angles by t - o - t strips (also referred to as "l-beams") in the amphibole structure, as compared with naturally occurring cleavage angles.



cleavage
56°
cleavage



I beam

- M3
- M2
- M1

Amphibole

Cleavage Rules:

Weakest

Strongest

A plane < M4 M4 plane < M3 M2 M1 plane < tetrahedral planes

I beams

Table 13.3
**IONS IN COMMON
 PYROXENES AND
 AMPHIBOLES**

Pyroxenes			Amphiboles		
Atomic Sites	Name		Atomic Sites	Name	
M2	M1	A	M4	(M1 + M2 + M3)	Anthophyllite
Mg	Mg	<input type="checkbox"/> *	Mg	Mg	Cummingtonite
Fe	Mg	<input type="checkbox"/>	Fe	Fe	Grunerite
Ca	Mg	<input type="checkbox"/> other members of the orthopyroxene series	Ca	Mg	Tremolite
Ca	Fe		<input type="checkbox"/> Diopside	Fe	Fe
Ca	Mn	<input type="checkbox"/> Hedenbergite	Ca, Na	Mg, Fe ²⁺ , Mn,	Hornblende
Ca, Na	Mg, Fe, Mn, Al, Fe ³⁺ , Ti	<input type="checkbox"/> Johannsenite	Ca, Na	Al, Fe ³⁺ , Ti	
Na	Al	Augite	Na	Mg, Al	Glaucophane
Na	Fe ³⁺	Jadeite	Na	Fe ²⁺ , Fe ³⁺	Riebeckite
Li	Al	Aegirine	Li	Fe ²⁺ , Fe ³⁺	Afrvedsonite
		Spodumene		Mg, Fe ³⁺	Holmquistite
				Al, Fe ²⁺	

FIG. 13.49. (a) Schematic projection of the monoclinic pyroxene structure on a plane perpendicular to the c axis. (b) Control of cleavage angles by t - o - t strips (also referred to as "I-beams") in the pyroxene structure, as compared with naturally occurring pyroxene cleavage.

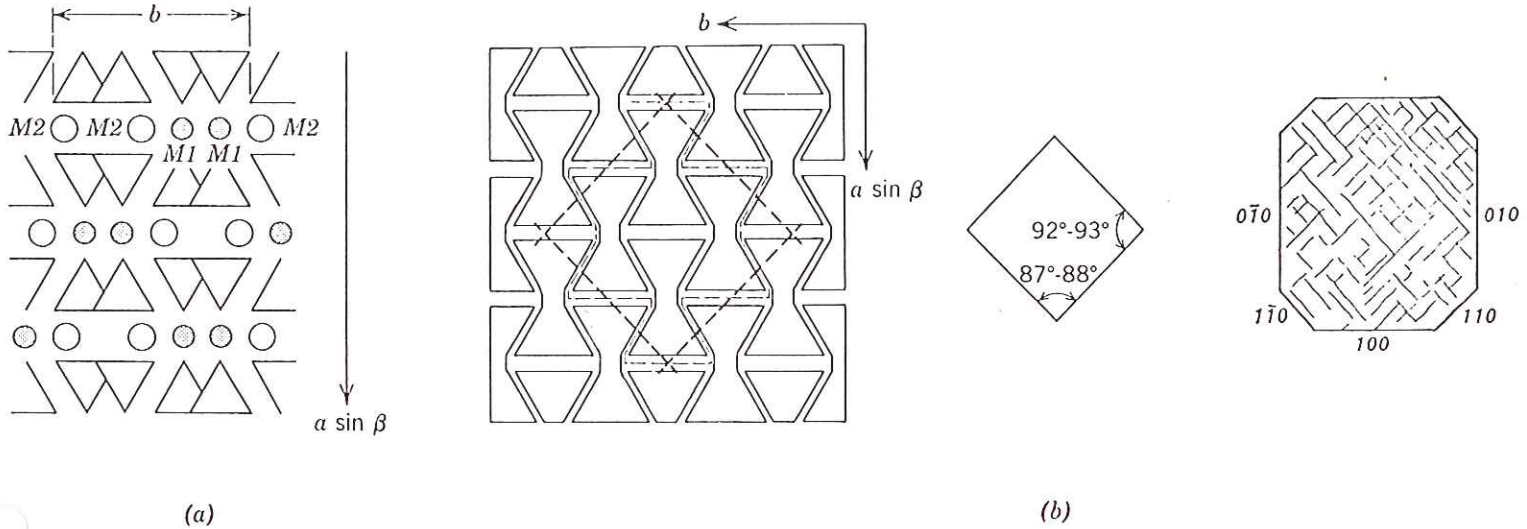
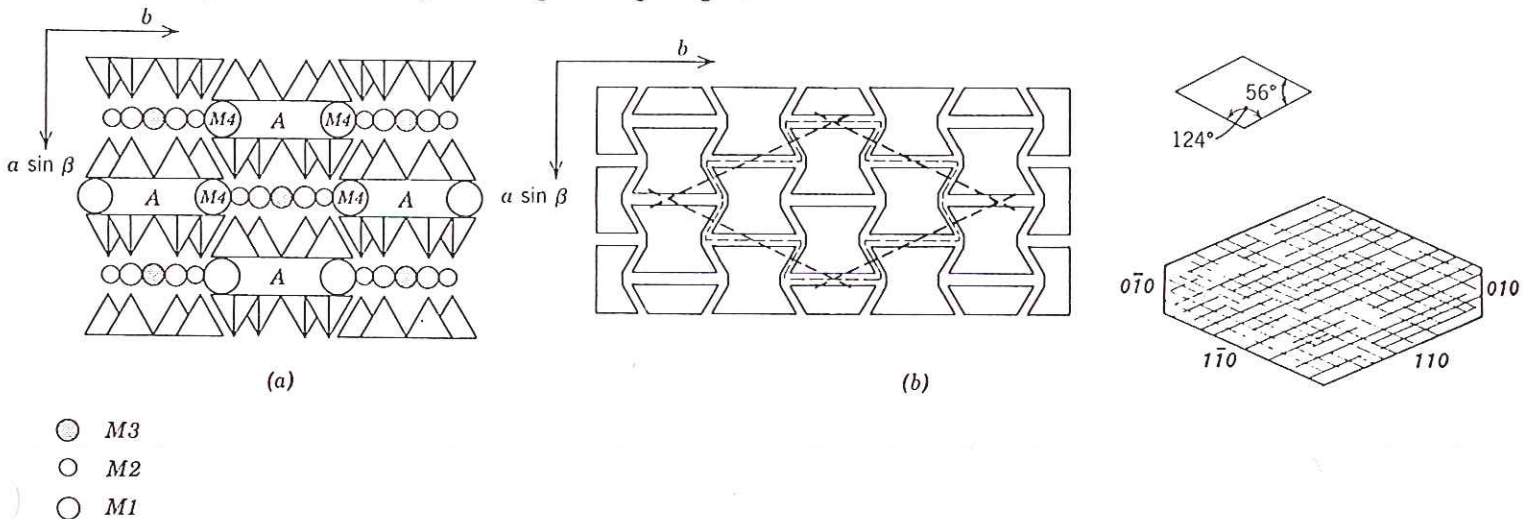


FIG. 13.67. (a) Schematic projection of the monoclinic amphibole structure on a plane perpendicular to the c axis (after Colville et al., 1966, *American Mineralogist*, v. 51, p. 1739). Compare with Fig. 13.49a. (b) Control of cleavage angles by t - o - t strips (also referred to as "I-beams") in the amphibole structure, as compared with naturally occurring cleavage angles.



not all sites necessarily occupied

Table 13.3 shows bewildering variety of pyroxenes & amphiboles, depending on what occupies the various sites

anorthite
& hornblende
are most common
anorthite -
pyroxene
hornblende -
amphibole

This kind of detail will NOT be on the exam - just to give you an idea of why there are so many different minerals

Cox 5.2 again

- sheet silicates - micas & clays

Fig 6.33 tetrahedral sheets
 Fig 6.34 2 types of octahedral sheets
 Fig 13.80 octahedral sheet
 (Mg or Al)₂O₆

Many different ways of putting these together

e.g. Fig. 13.83 muscovite
 $KAl_2(AlSi_3O_{10})(OH)_2$

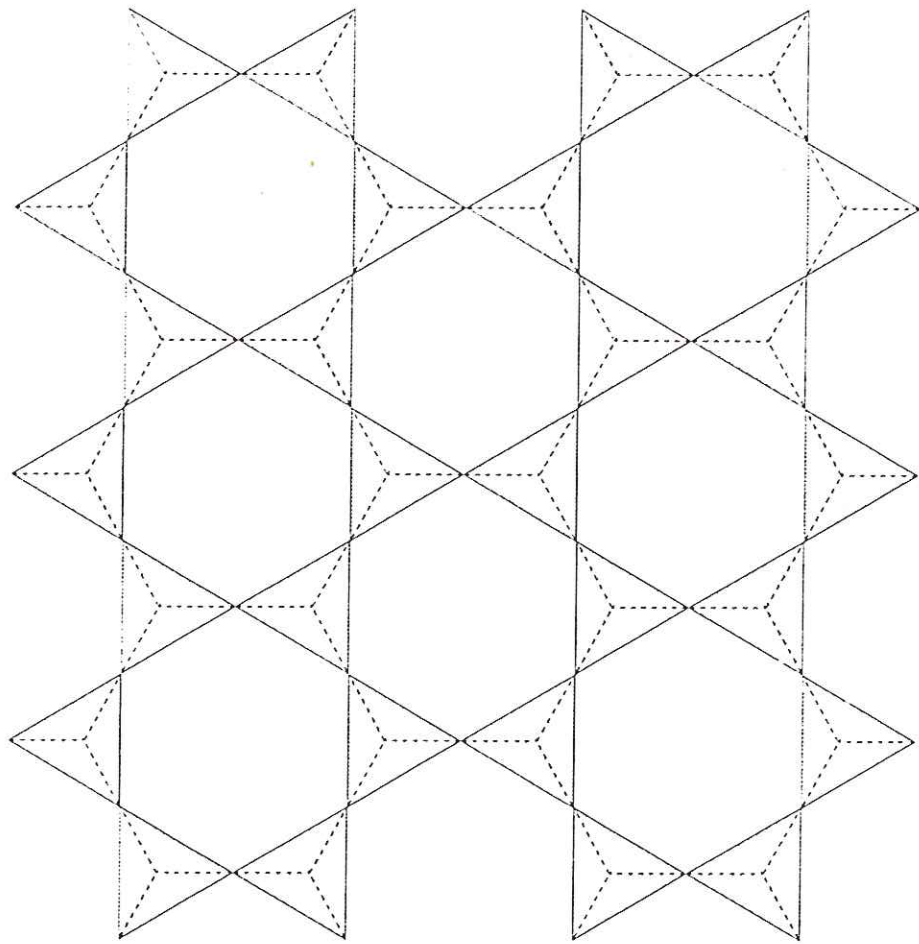
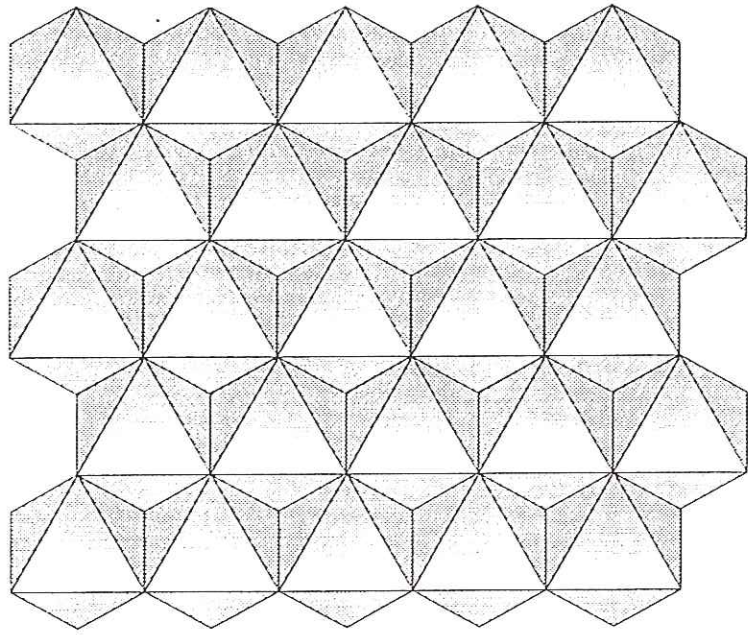
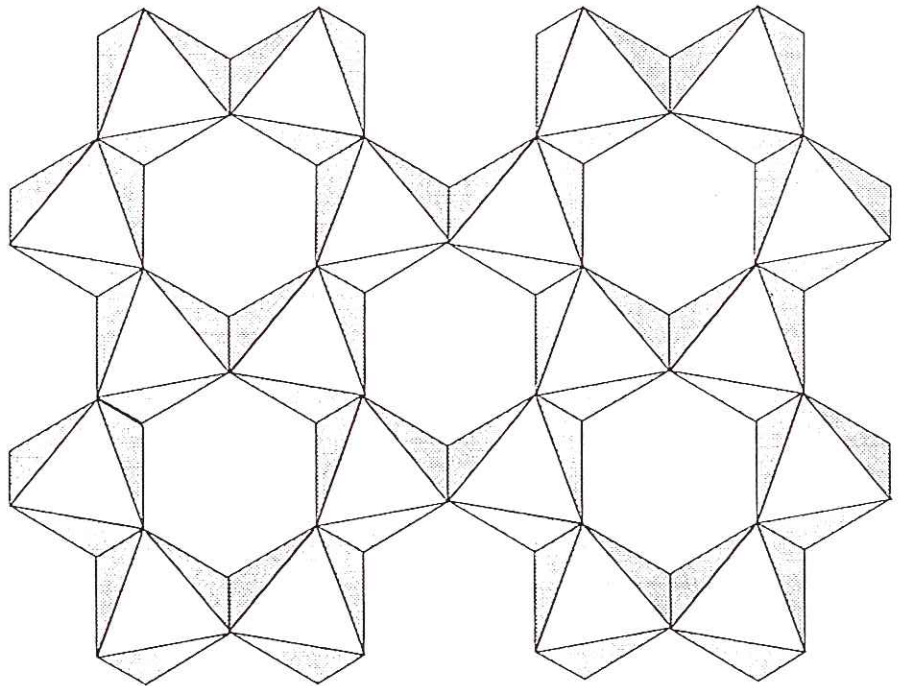


Figure 6.33. Part of an infinite tetrahedral sheet, made up of SiO_4 tetrahedra all pointing in the same direction, and sharing three corners. This sheet is one of the basic building units in the layer silicates.



(a)



(b)

Figure 6.34. (a) Part of an infinite sheet of edge-sharing octahedra. When all the octahedra are occupied the sheet is termed *trioctahedral*. (b) In a *dioctahedral* sheet one third of the octahedra are unfilled, and these vacant octahedra are ordered as shown. The distortion of the filled octahedra enlarges the vacant site.

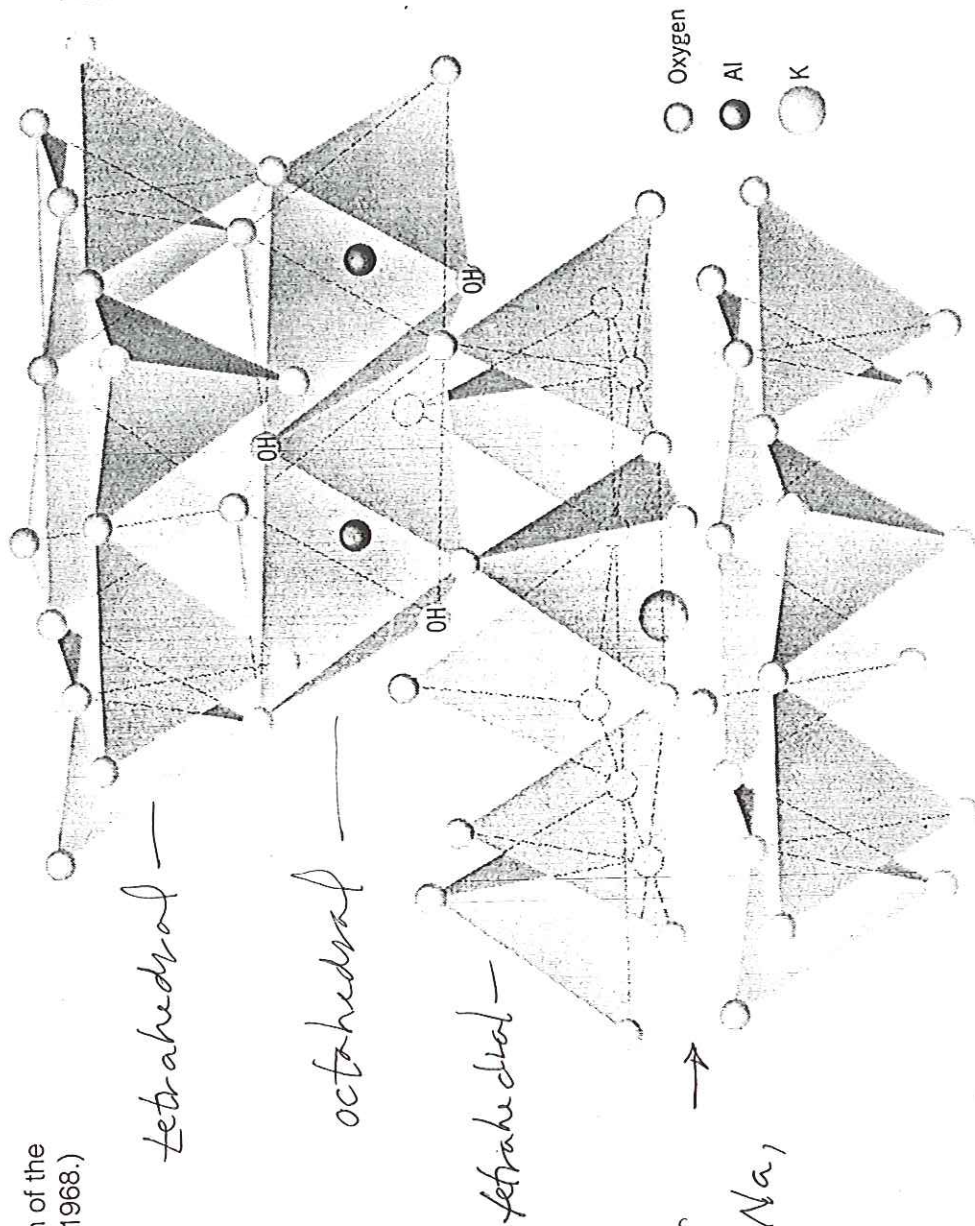


FIG. 13.83. Diagrammatic sketch of the muscovite structure. (After Grim, 1968.)

K 1.5 Å

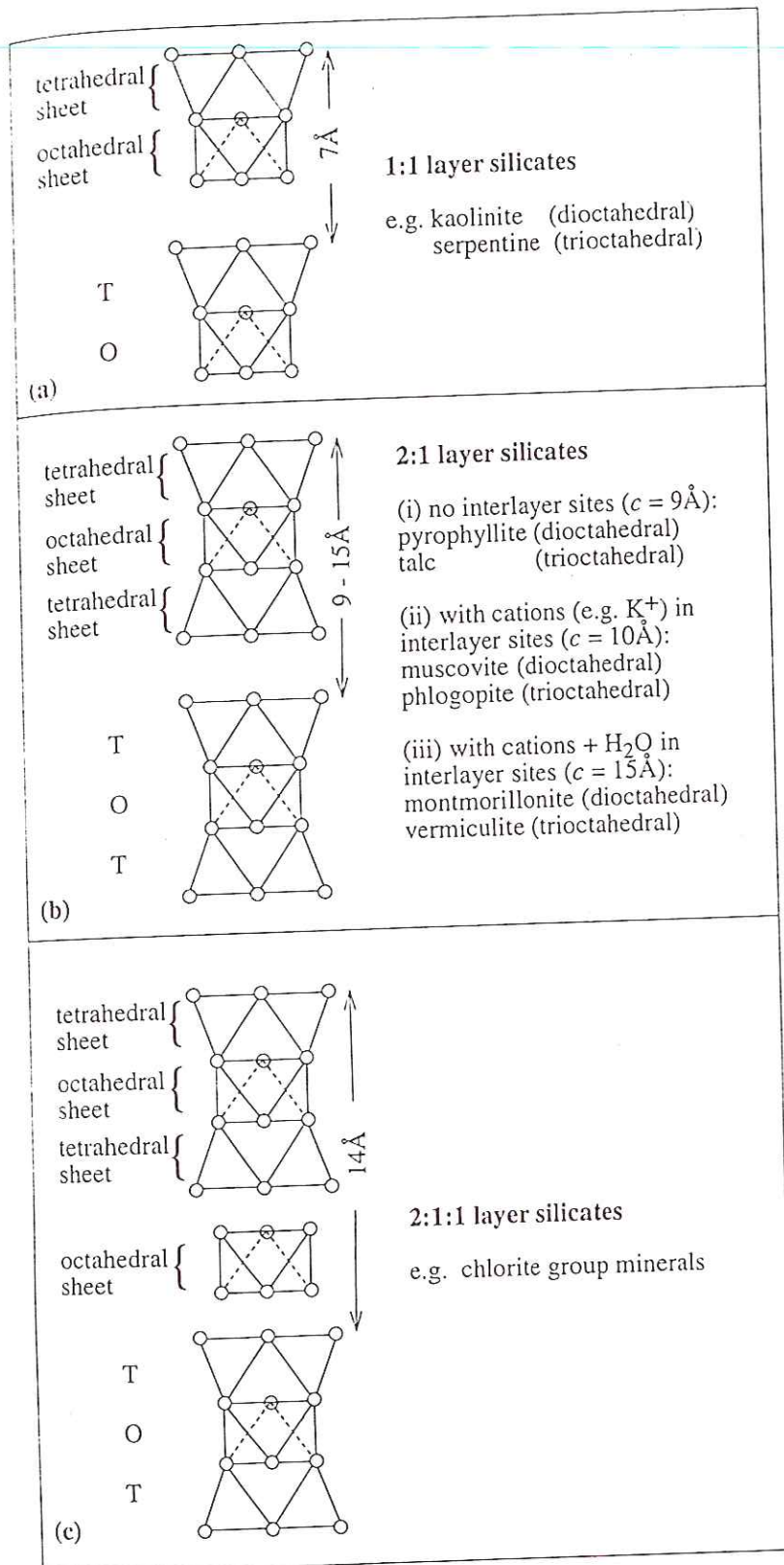
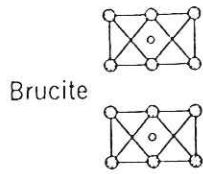


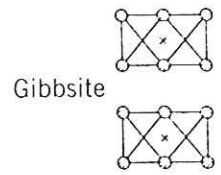
Figure 6.36. Schematic representations of the way in which (a) the 1:1 layer silicates (b) the 2:1 layer silicates and (c) the 2:1:1 layer silicates are built up from tetrahedral and octahedral sheets. The minerals within each group are named according to whether the octahedral sheet is dioctahedral or trioctahedral, and the nature of the interlayer cations.

Trioctahedral

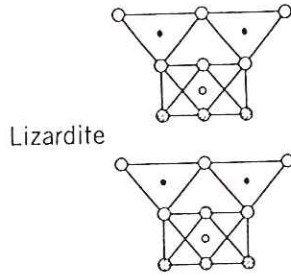
Dioctahedral



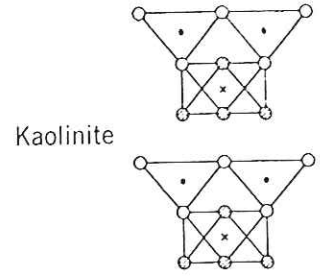
o



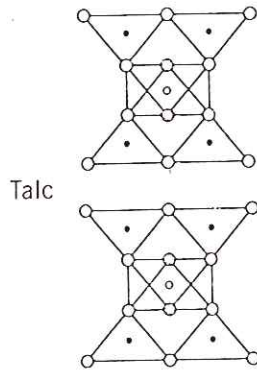
o



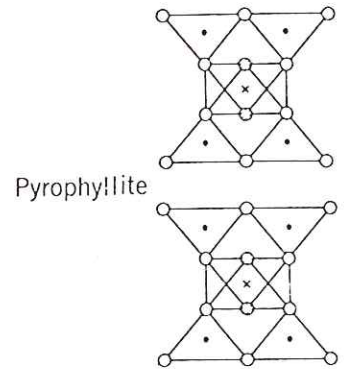
t
o



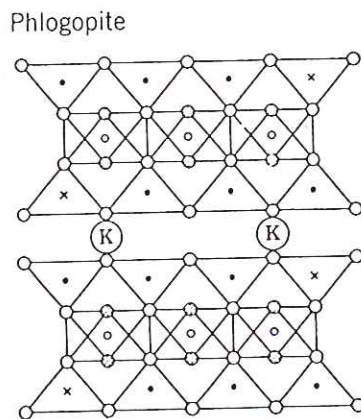
t
o



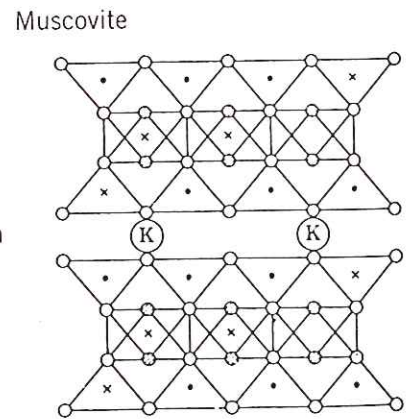
t
o
t



t
o
t



t
o
t
Interlayer cation



t
o
t

- = Oxygen
- ⊙ = Hydroxyl
- = Silicon
- × = Aluminum
- = Magnesium

FIG. 13.84. Schematic development of structure of the phyllosilicate structures (compare with Fig. 13.106).

o = octahedral
t = tetrahedral

a so-called 2:1 or t-o-t sheet

the bond between tetrahedral bases is van der Waals - very weak - filled with K atoms

K - 1.51 Å

responsible for sheet-like structure of muscovite & other micas

Fig 13.84 shows some other examples

Also Putnis Fig 6.36

Cox 5.2 again

• 3-d framework silicates

3 very important minerals see Fig 13.1 - crustal mineral abundance

almost 2/3 of crust	}	39% plagioclase Na, Ca feldspar
		12% quartz K, Na feldspar
		12% quartz

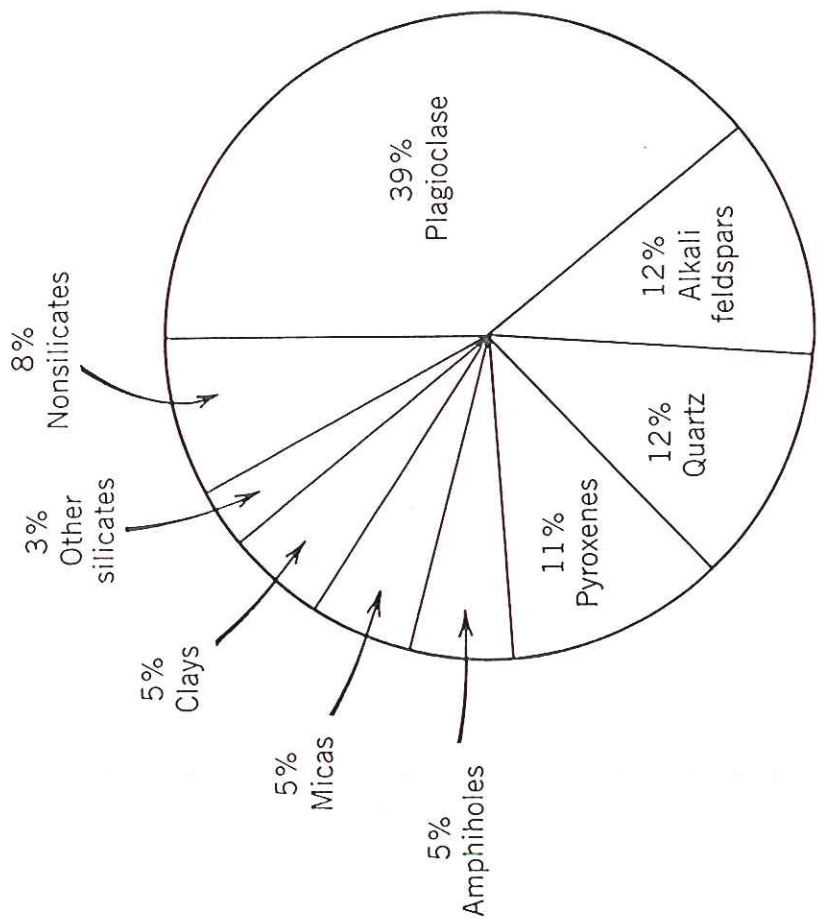


FIG. 13.1. Estimated volume percentages for the common minerals in the Earth's crust, inclusive of continental and oceanic crust. Ninety-two percent are silicates. (From Ronov, A. B. and Yaroshevsky, A. A., 1969, Chemical composition of the Earth's crust. American Geophysical Union Monograph no. 13, p. 50.)

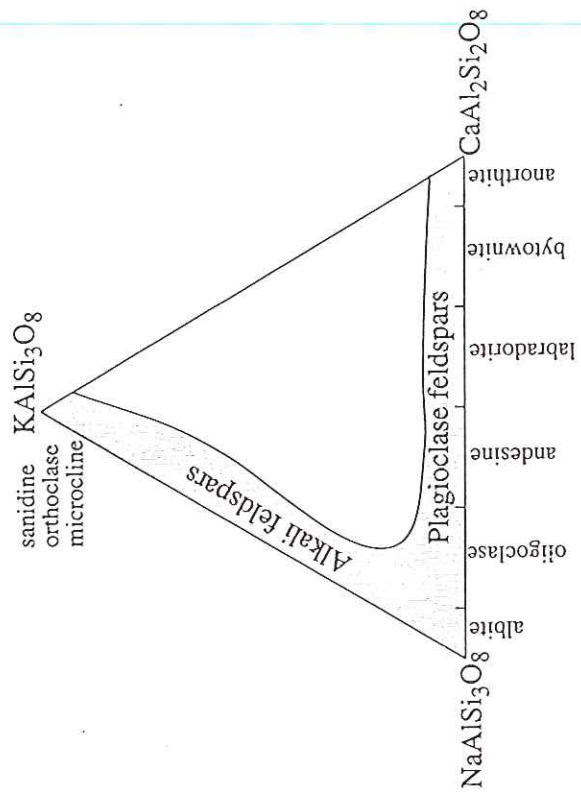


Figure 6.51. The extent of solid solution in alkali and plagioclase feldspars at high temperature. The plagioclase feldspars are subdivided according to composition, as indicated.

*With
described
structure*

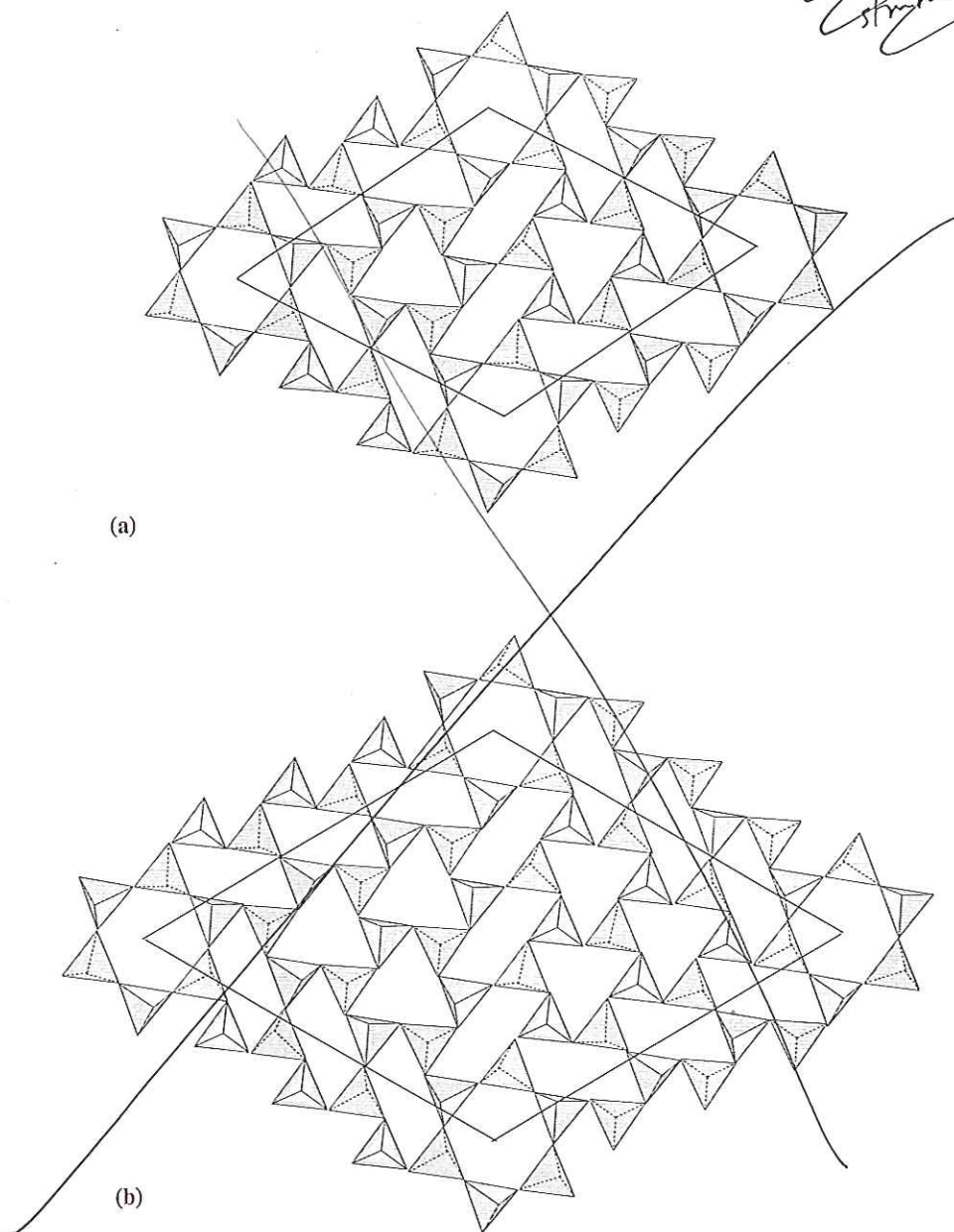


Figure 6.50. Structures such as (a) trikalsilite and (b) tetrakalsilite, are built up by alternating oval and trigonal rings in the tetrahedral layers. With K^+ in the hexagonal and trigonal rings and Na^+ in the oval rings, this scheme provides a mechanism for building structures with compositions between that of kalsilite and nepheline.

opportunity for studying the way a structure responds to a slowly changing geological environment.

We begin with the ideal high temperature feldspar structure of *sanidine* $KAlSi_3O_8$. The Al and Si are distributed at random so that the average occupancy of each tetrahedron is 25% Al, 50% Si. The structure is quite complicated and we will build it up from somewhat idealized units to describe its essential features. The basic construction of the framework is of rings of four tetrahedra with alternate pairs of

vertices pointing in opposite directions (Figure 6.52a). These rings are then joined in layers as shown in Figure 6.52b, in which the layers are viewed down the x axis.

In the third dimension, the rings are joined to one another by the apices, forming crankshaft-like chains parallel to the x axis (Figure 6.53). In Figure 6.53(b) the crankshafts are represented by lines joining the centres of the tetrahedra, and the way these crankshafts are related to each other by mirror

*feldspar
structure*

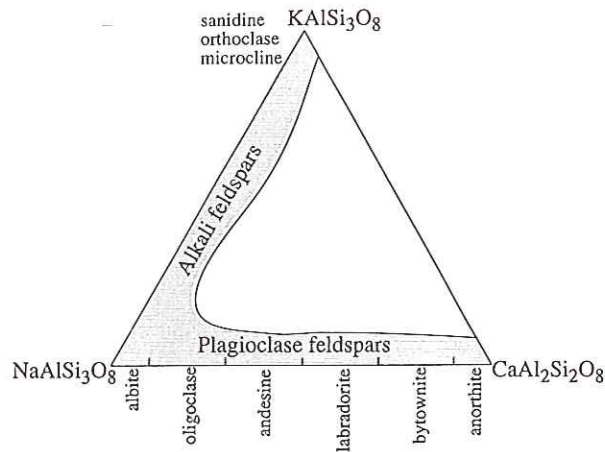


Figure 6.51. The extent of solid solution in alkali and plagioclase feldspars at high temperature. The plagioclase feldspars are subdivided according to composition, as indicated.

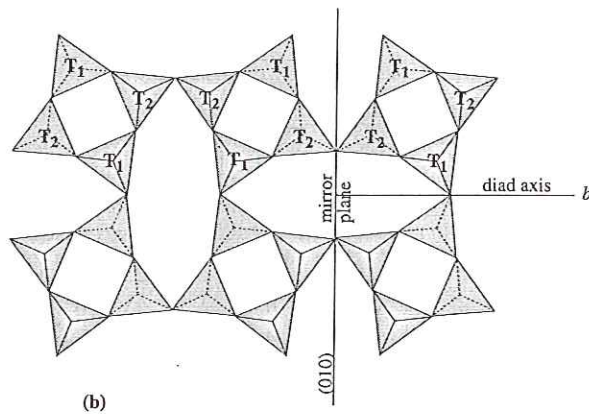
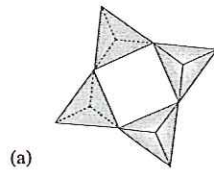


Figure 6.52. (a) The basic building unit of the feldspar structure is the four-membered ring of tetrahedra with a pair of tetrahedra pointing up and a pair pointing down. (b) The four-fold rings are joined to form a layer in which the rings are related by mirror planes parallel to (010) and diads parallel to the b axis. Two sets of individual tetrahedra are distinguishable in this layer, and are labelled T_1 and T_2 . The T_1 tetrahedra are all related to one another by symmetry, as are the T_2 tetrahedra. Cations occupy the large oval-shaped cavities between the rings.

planes is shown in Figure 6.54. The K atoms lie in the mirror planes between the crankshafts, occupying the largest cavities in the framework.

Although this is an idealized description, and in the real structure of high sanidine there is some

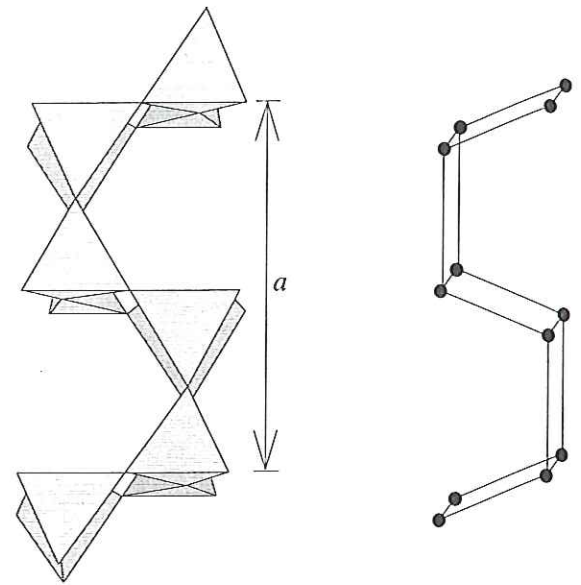


Figure 6.53. The linkage between the four-fold rings, shown at right angles to the view in Figure 6.52. The rings in one layer are linked by their apices to rings in the layers above and below, forming a crankshaft-like chain. In (b) this chain is abstracted further showing only the Si atoms at the centres of the tetrahedra.

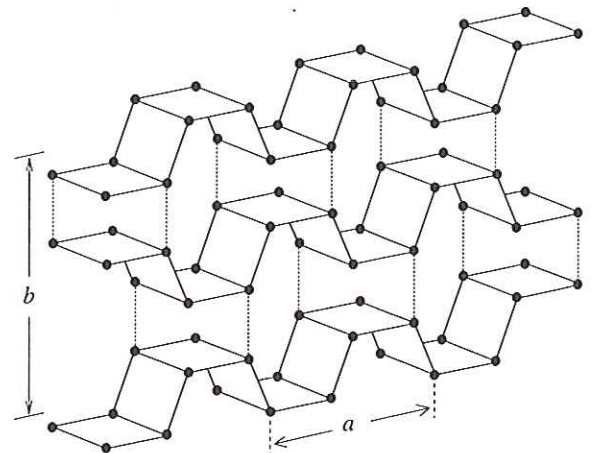


Figure 6.54. A perspective view of the feldspar structure showing the way the crankshafts described in Figure 6.53 are reflected by (010) mirror planes. The dotted lines are an aid to show some of the mirror-related atoms. The cations occupy the large open cavities between the crankshafts. (after Megaw, 1973)

rotation of the tetrahedra, the symmetry remains the same as in the figures above. The structure is monoclinic, space group $C2/m$ and has the highest symmetry possible in the feldspars. It will be treated as the parent structure from which all other feldspar structures can be derived. It is important to note that

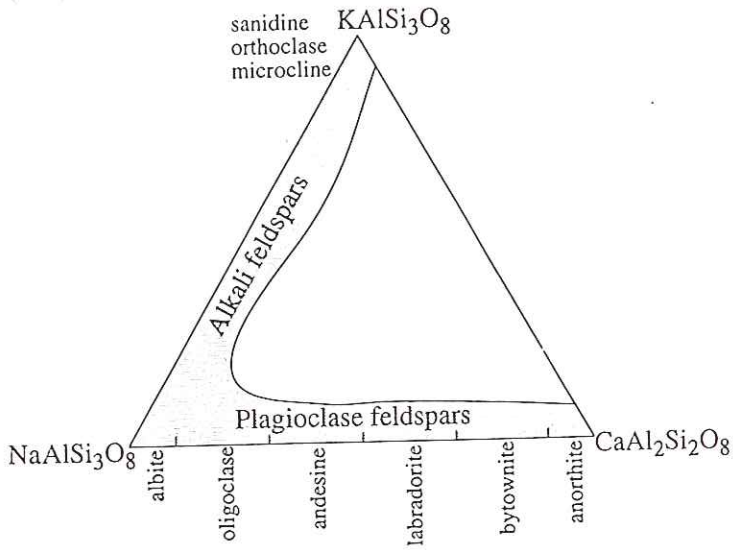


Figure 6.51. The extent of solid solution in alkali and plagioclase feldspars at high temperature. The plagioclase feldspars are subdivided according to composition, as indicated.

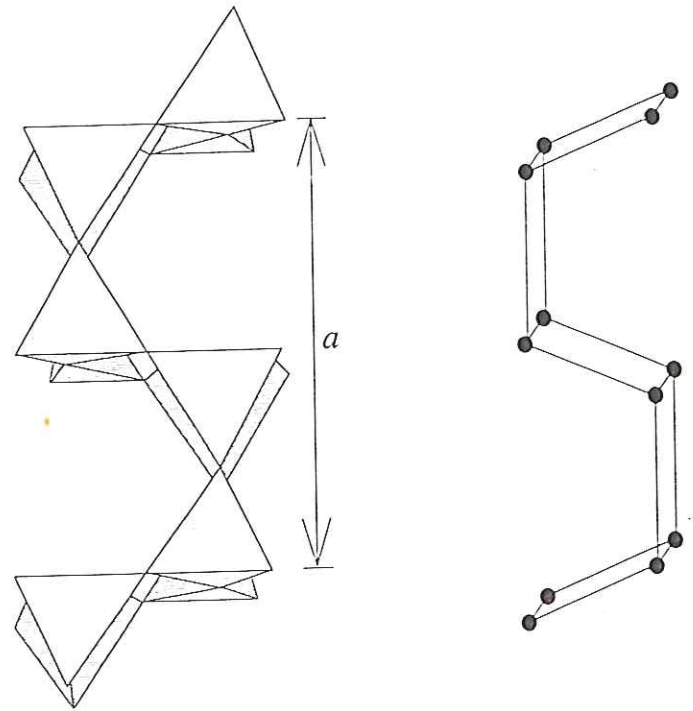


Figure 6.53. The linkage between the four-fold rings, shown at right angles to the view in Figure 6.52. The rings in one layer are linked by their apices to rings in the layers above and below, forming a crankshaft-like chain. In (b) this chain is abstracted further showing only the Si atoms at the centres of the tetrahedra.

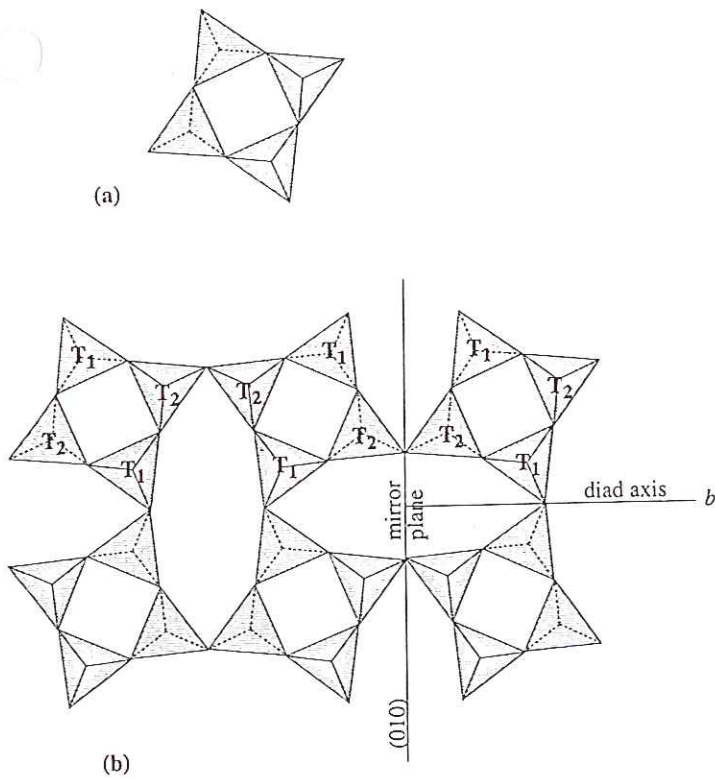


Figure 6.52. (a) The basic building unit of the feldspar structure is the four-membered ring of tetrahedra with a pair of tetrahedra pointing up and a pair pointing down. (b) The four-fold rings are joined to form a layer in which the rings are related by mirror planes parallel to (010) and diads parallel to the b axis. Two sets of individual tetrahedra are distinguishable in this layer, and are labelled T_1 and T_2 . The T_1 tetrahedra are all related to one another by symmetry, as are the T_2 tetrahedra. Cations occupy the large oval-shaped cavities between the rings.

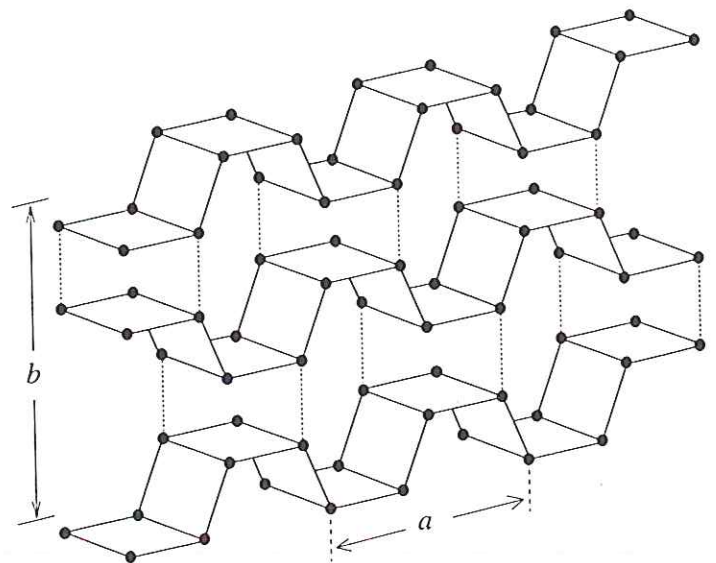
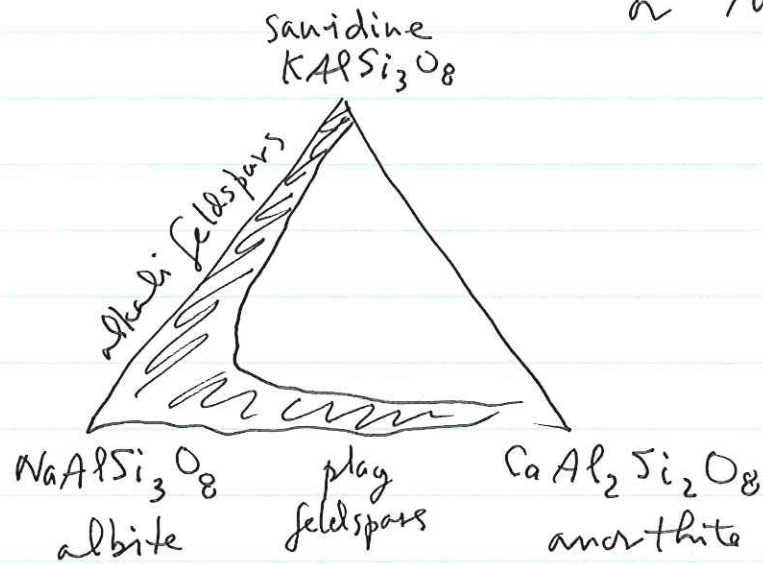


Figure 6.54. A perspective view of the feldspar structure showing the way the crankshafts described in Figure 6.53 are reflected by (010) mirror planes. The dotted lines are an aid to show some of the mirror-related atoms. The cations occupy the large open cavities between the crankshafts. (after Megaw, 1973)

see also KH Fig 13.117
or Putnis G.51



~~XXXXXXXXXXXX~~

Putnis Figs. 6.52 - 6.54 show
3-d structure

large (1.5 \AA) K atoms lie in
the large cavities between the
crankshafts

quartz SiO_2 - another framework
silicate - fig 6.46 Putnis
12% of crust

note the hexagonal symmetry

reason for hexagonal shape of xtal
Fig. 13.114

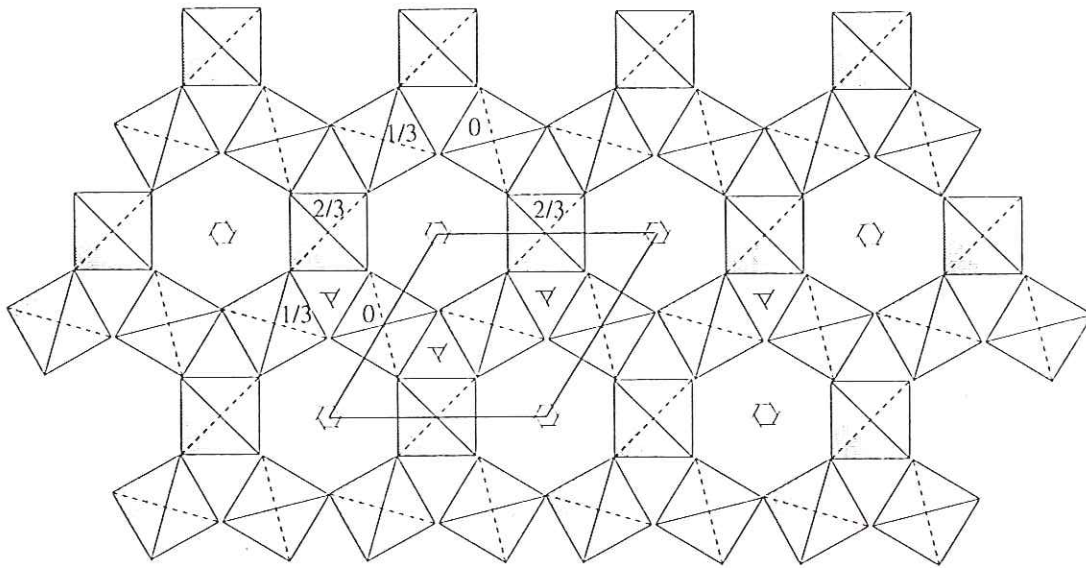


Figure 6.46. The structure of high quartz projected on the ab plane. SiO_4 tetrahedra at vertical heights $0, 1/3, 2/3$ form three-fold spirals, and these spirals are arranged in an hexagonal array to give a framework structure, each tetrahedron sharing four corners. A unit cell is outlined.

FIG. 13.114. Quartz crystals.

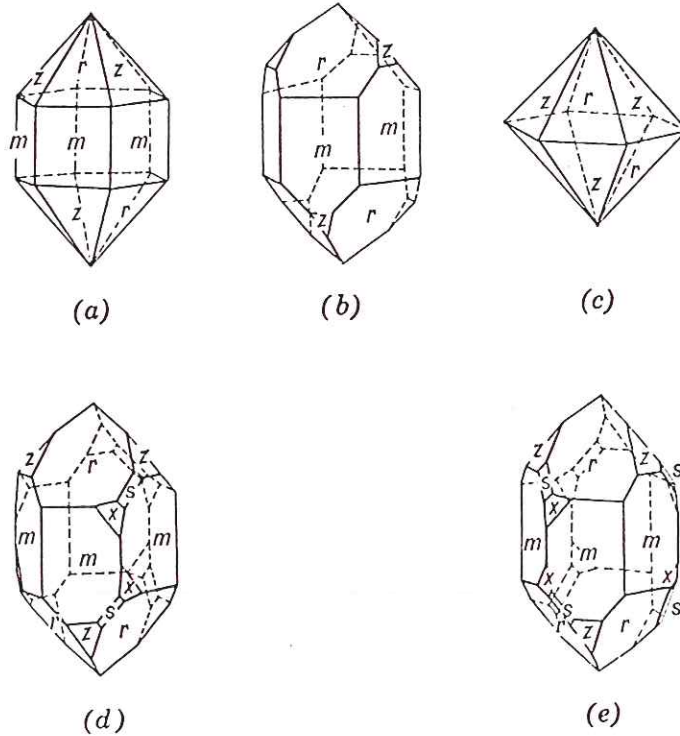


FIG. 13.114. Quartz crystals.

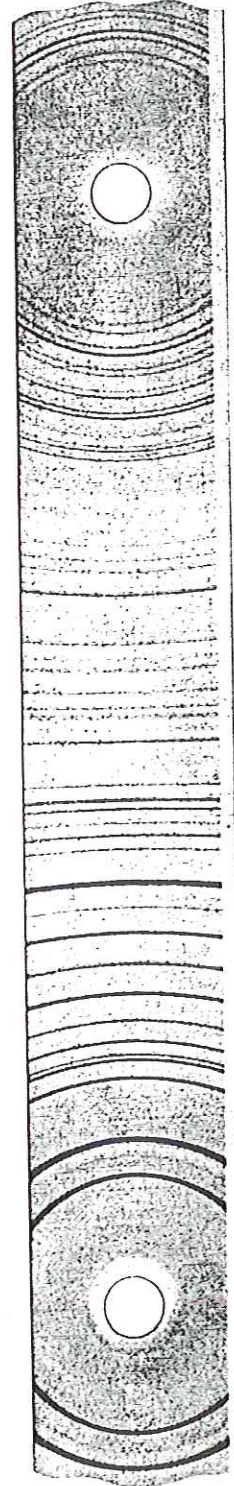
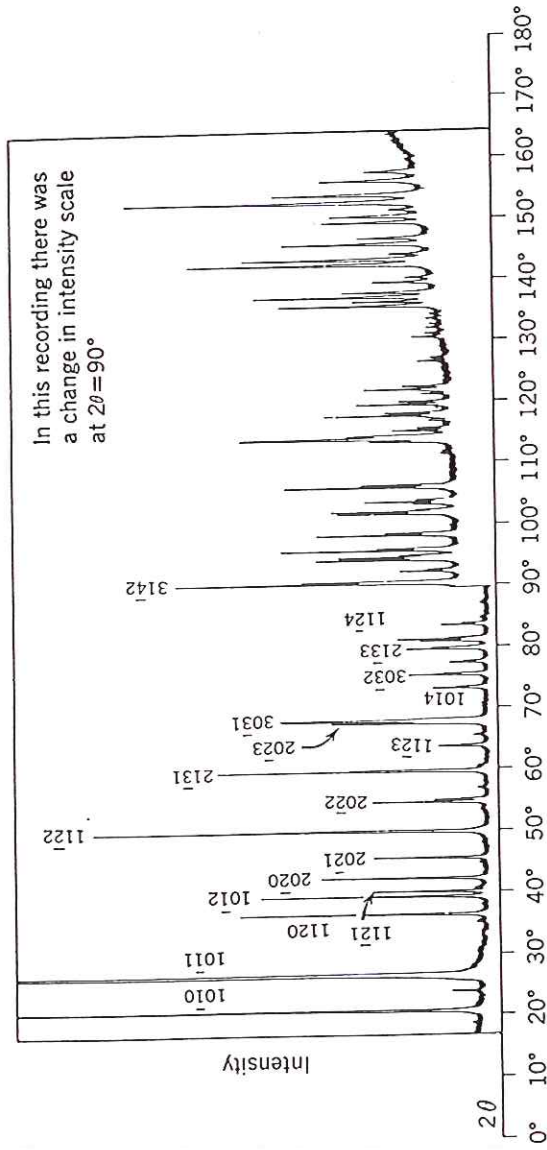
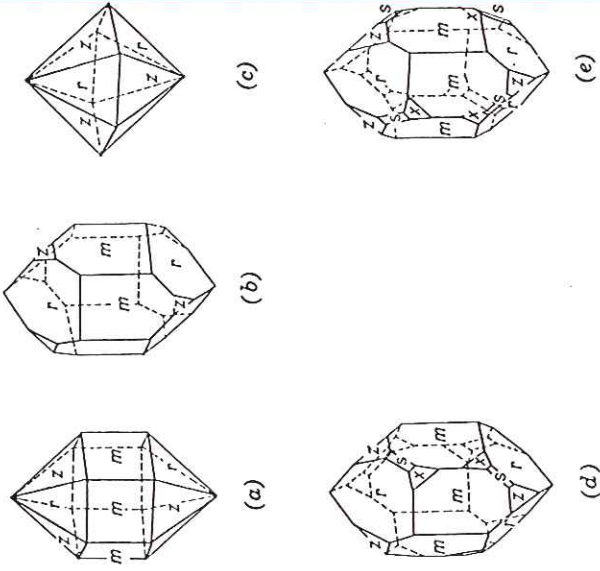


FIG. 7.19. Comparison of diffractometer record and powder film of quartz. On the diffractometer recording are given the Miller indices of the crystal planes that gave rise to the various low-angle diffraction peaks. (Courtesy of Philips Electronic Instruments, Inc., Mahwah, N.J.)

Fig 13.113 shows the phase diagram for SiO_2

Like C it can exist in a variety of phases

Common form so-called low quartz

At high T (above $\sim 600^\circ\text{C}$)
transforms to less symmetric
~~low quartz~~ high quartz

Fig 6.47

above
 1750°C
quartz
melts

Also two high pressure phases

- coesite — above 25–40 kbars
- stishovite — above 80–100 kbars
- coesite — above 2.5–4.0 GPa
- stishovite — above 8–10 GPa

Structures Fig 13.112 — more compact
with no open holes

densities:	quartz	2700	2700	kg/m^3
	coesite		3000	kg/m^3
	stishovite		4400	kg/m^3

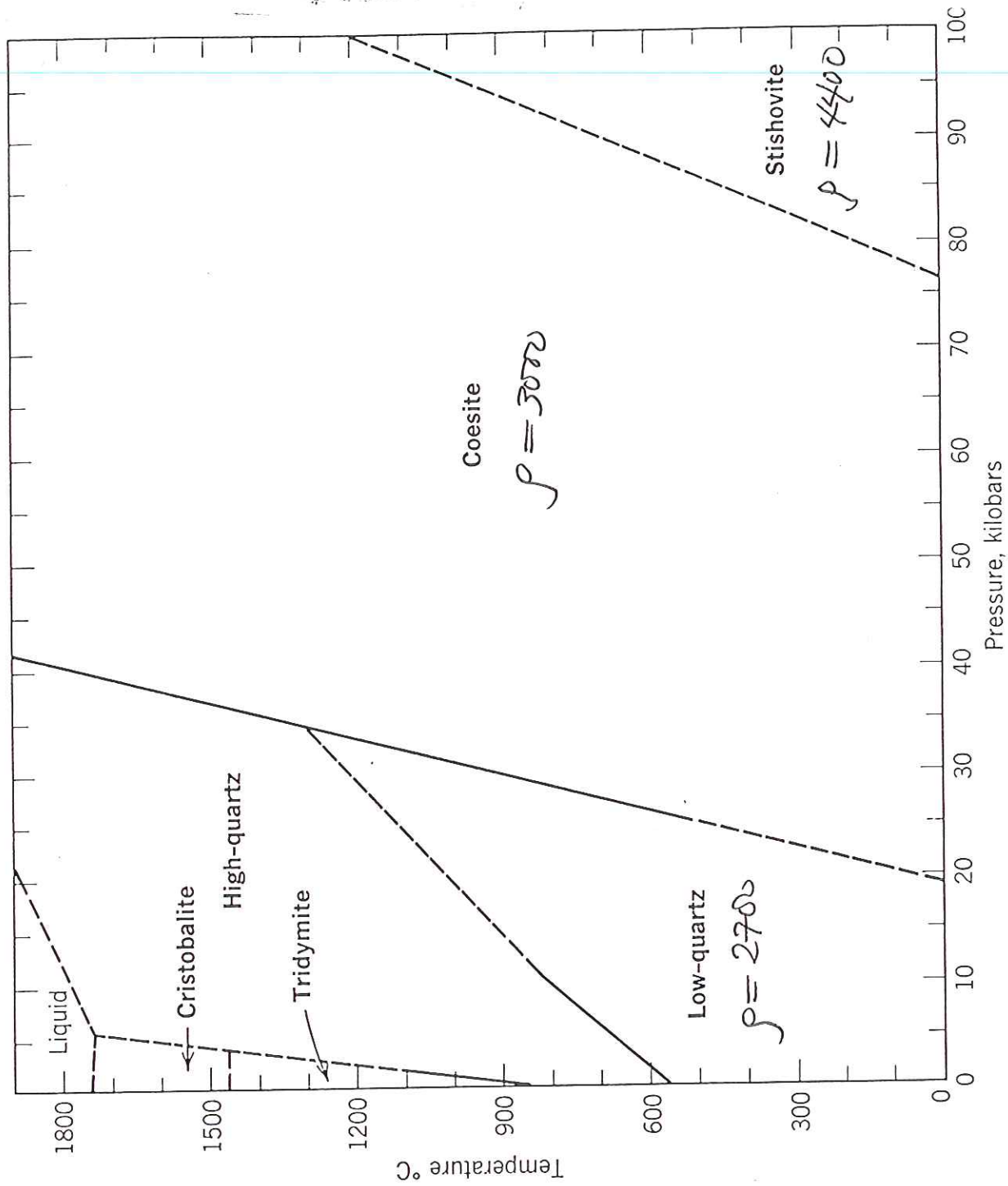


FIG. 13.113. Stability relations of the SiO₂ polymorphs.

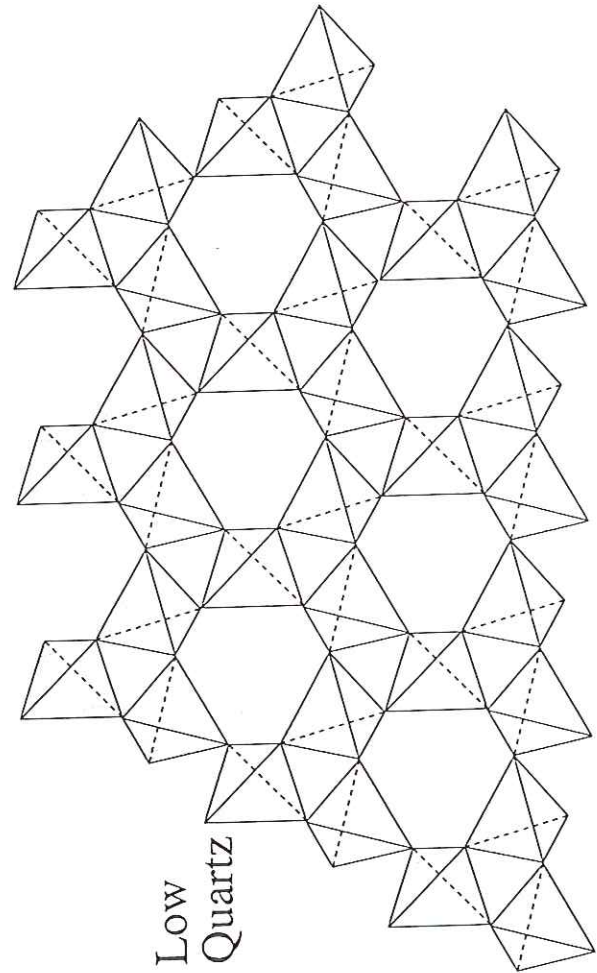
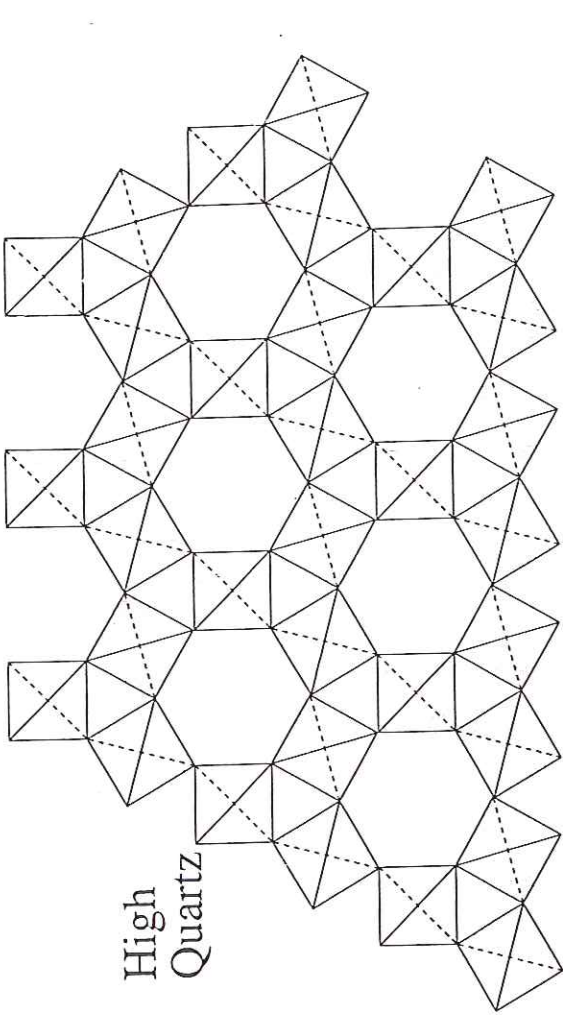


Figure 12.16. The structures of high and low quartz. The rotation of the relatively rigid tetrahedra reduces the symmetry from hexagonal to trigonal. Note how the distortion changes the shape of the six-membered ring of SiO_4 tetrahedra.

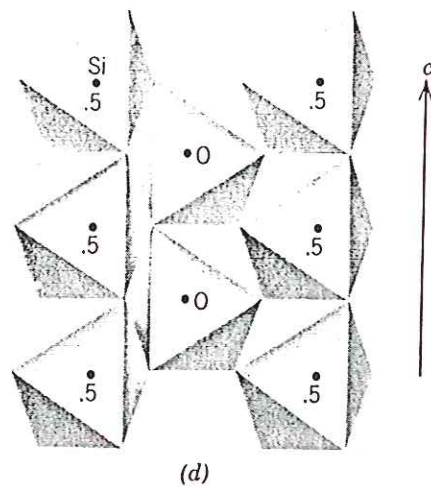
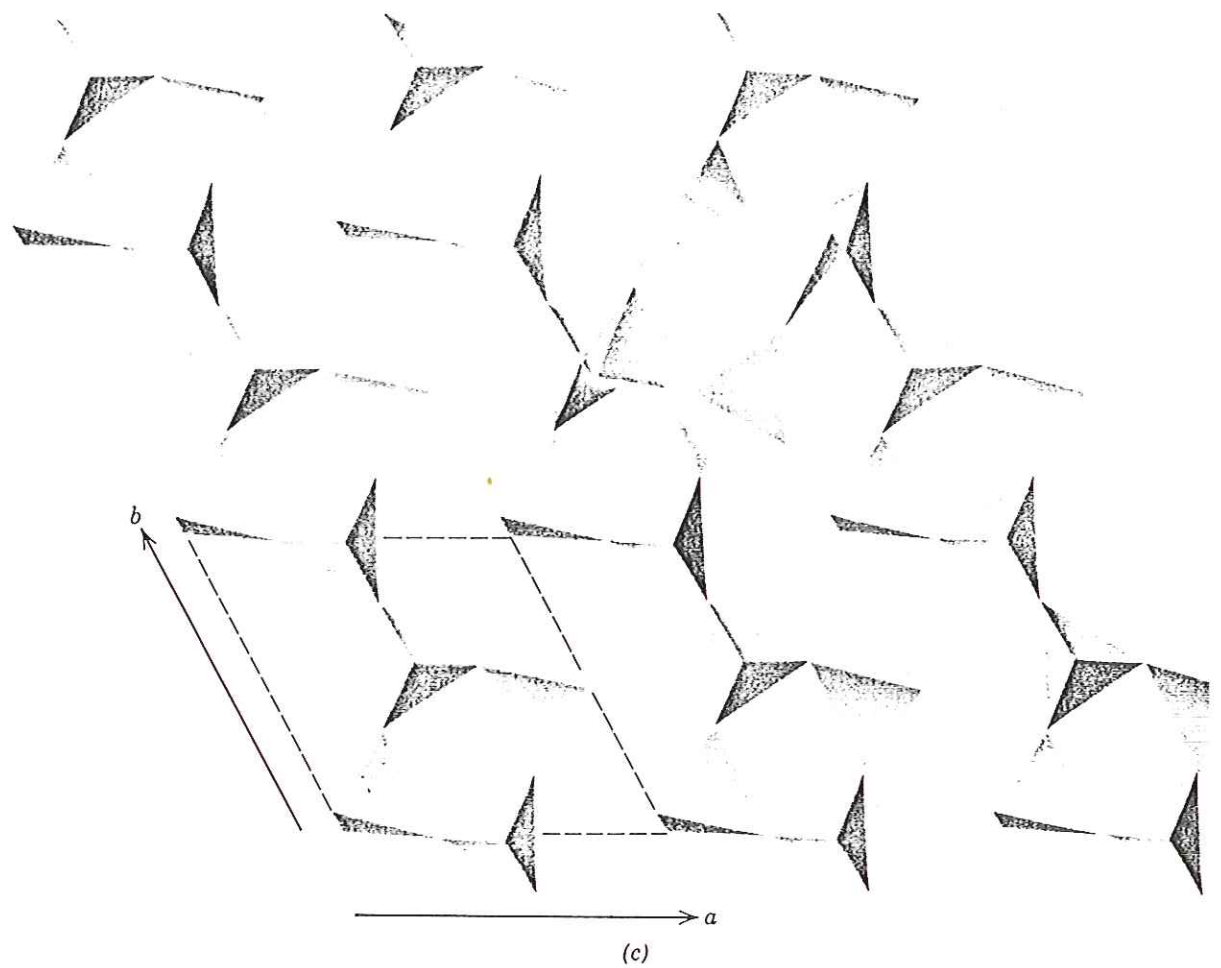


FIG. 13.112. (continued) (c) Coesite structure showing four-membered tetrahedral rings that lie parallel to (001). (d) Structure of stishovite, with Si in octahedral coordination with oxygen, projected on (100) (a, b, c, and d after Papike, J. J. and Cameron, M., 1976, Crystal chemistry of silicate minerals of geophysical interest, *Reviews of Geophysics and Space Physics*, v. 14, pp. 37-80.)

text μ
SiO₂

It is clear from this notation that kyanite represents the closest atomic packing of the three polymorphs.

The diagram in Fig. 9.4b shows two independent sets of equilibrium boundaries that radiate from a triple point. These are marked (R) and (H) and represent two sets of independent experimental results on this system. Both results are shown because they illustrate the experimental difficulties in determining the exact equilibrium boundaries in a highly refractory system (refractory meaning that, in this chemical system, the transformation reactions are difficult to delineate because of the sluggishness of the reactions, causing metastability of a specific polymorph into another polymorphic phase region). Recent work by Bohlen et al. (1991) has largely confirmed the triple point location marked (H); this configuration will therefore be used in Chapters 13 and 14 as well.

In the case of the experimental study of the stability fields of the three polymorphs of Al₂SiO₅, very high purity minerals may be used for the experiments although most commonly the starting materials are high purity chemicals. For example, gem grade and inclusion-free kyanite may be found at increasing *T* to react to form sillimanite (see Fig. 9.4b). The position of the curve separating the kyanite and sillimanite fields is based on the first evidence of sillimanite forming at the expense of kyanite with increasing *T* and on evidence of the reverse reaction, namely sillimanite giving way to kyanite at decreasing *T* or increasing *P*. The determination of the beginning of such reactions is generally based on a combination of X-ray powder diffraction and optical microscopic techniques. Because of uncertainties in various aspects of the experimental techniques in locating specific reaction boundaries, the reaction curves, defined in *P* and *T* values, may represent relatively broad reaction zones, although they are commonly shown as narrow lines or curves.

Kyanite, or sillimanite, or andalusite, without any textural indication of reaction to another Al₂SiO₅ polymorph, can be found in metamorphic rocks of all geological ages, including early Precambrian. This observation signifies that the activation energy necessary to transform a high-temperature or high-pressure polymorph into the lower *P-T* polymorph stable at atmospheric conditions has not been provided. However, in many other metamorphic rocks that contain Al₂SiO₅ polymorphs, the following rimming reactions have been observed:

- a center of kyanite rimmed by sillimanite;
- a center of sillimanite rimmed by kyanite;
- a center of sillimanite rimmed by andalusite;
- a center of andalusite rimmed by kyanite.

All of the above textural occurrences delineate various *P-T* paths across the different equilibrium boundaries in Fig. 9.4b.

Figure 9.4c outlines the stability fields of phases in the system SiO₂. This diagram was also discussed in Chapter 3, under "Polymorphism" (Fig. 3.38). All the equilibrium boundaries between solids (except for the line separating high and low quartz) are boundaries of reconstructive polymorphic transformations. The low to high quartz boundary is a displacive transformation boundary. Quartz, as low quartz, is the SiO₂ phase in plutonic, metamorphic, and sedimentary rocks, reflecting their general temperature of origin below 1000°C. Tridymite and cristobalite are found in volcanic assemblages of many geological ages. This means that these minerals exist metastably for long geological time periods. In other volcanic occurrences, the original cristobalite or tridymite may have been converted to low quartz, but still preserving the crystal form of cristobalite or tridymite (these occurrences, therefore, represent pseudomorphs of low quartz after higher-temperature SiO₂ polymorphs). Such pseudomorphic occurrences suggest that the activation energy necessary for the reconstructive transformations (from cristobalite or tridymite to low quartz) was possibly provided by some reheating due to later metamorphism of the original volcanics. The high-pressure polymorphs of SiO₂, coesite and stishovite, have been found in meteorite impact craters. Coesite also occurs as inclusions in diamonds, and inside pyrope garnets in very pyrope-rich high-grade metamorphic rocks from Parigi, Northern Italy (Chopin, 1984; for complete reference see reference list at end of this chapter). Coesite has also been found in a xenolith nodule (a xenolith is a foreign inclusion) in a kimberlite pipe (see Fig. 4.52). This kimberlite pipe originated at a depth of about 170 to 200 km in the mantle, at pressures of approximately 60 to 70 kilobars (a pressure region in Figs. 9.4a and c where both diamond and coesite are stable). Coesite-diamond coexistences have also been reported from very high-pressure metamorphism of crustal rocks in eastern China (Shutong et al., 1992; for complete reference see reference list at end of this chapter). The coesite-diamond-jadeite (another high-pressure mineral) assemblage is considered the result of burial of the crust to great depths, metamorphism, and subsequent exhumation back toward the Earth's surface.

Figure 9.4d shows the stability diagram for CaCO₃, with two polymorphic forms, calcite and aragonite. By far the most common carbonate, be it sedimentary, metamorphic, or igneous in origin, is calcite. The phase diagram in Fig. 9.4c suggests that CaCO₃ that is formed at normal temperatures and

coesite
&
stishovite
metastable
occurrences



Figure 4.4

Meteor Crater, Arizona, is a recent impact crater similar to those found on the Moon. It is one of the youngest impact craters found on Earth. This small crater formed about 25,000 years ago when an iron meteorite struck Earth. The bowl-shaped crater is a little over 1 km in diameter and is 200 m deep. Its floor is covered by younger lake sediments. An extensive blanket of ejecta surrounds the crater. The polygonal outline of the crater is probably the result of a fracture system that predates the excavation of the crater.

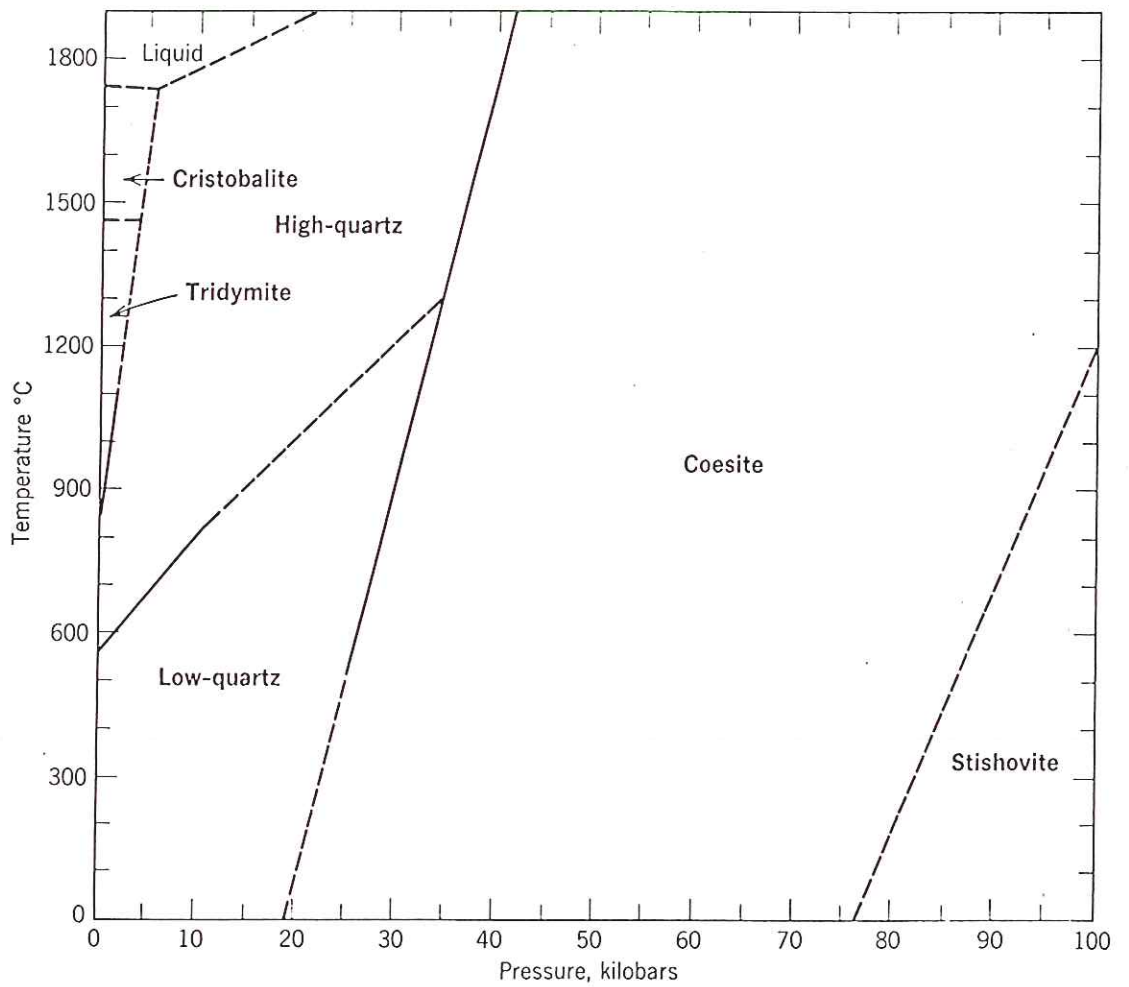
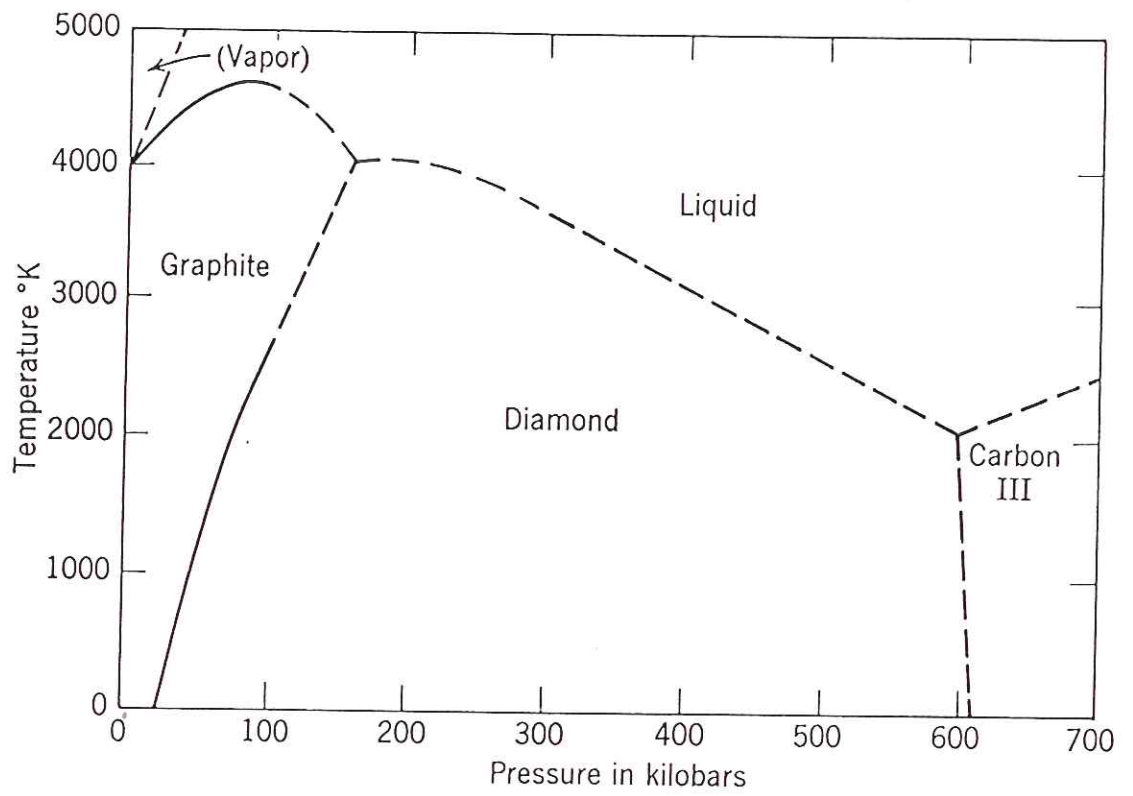
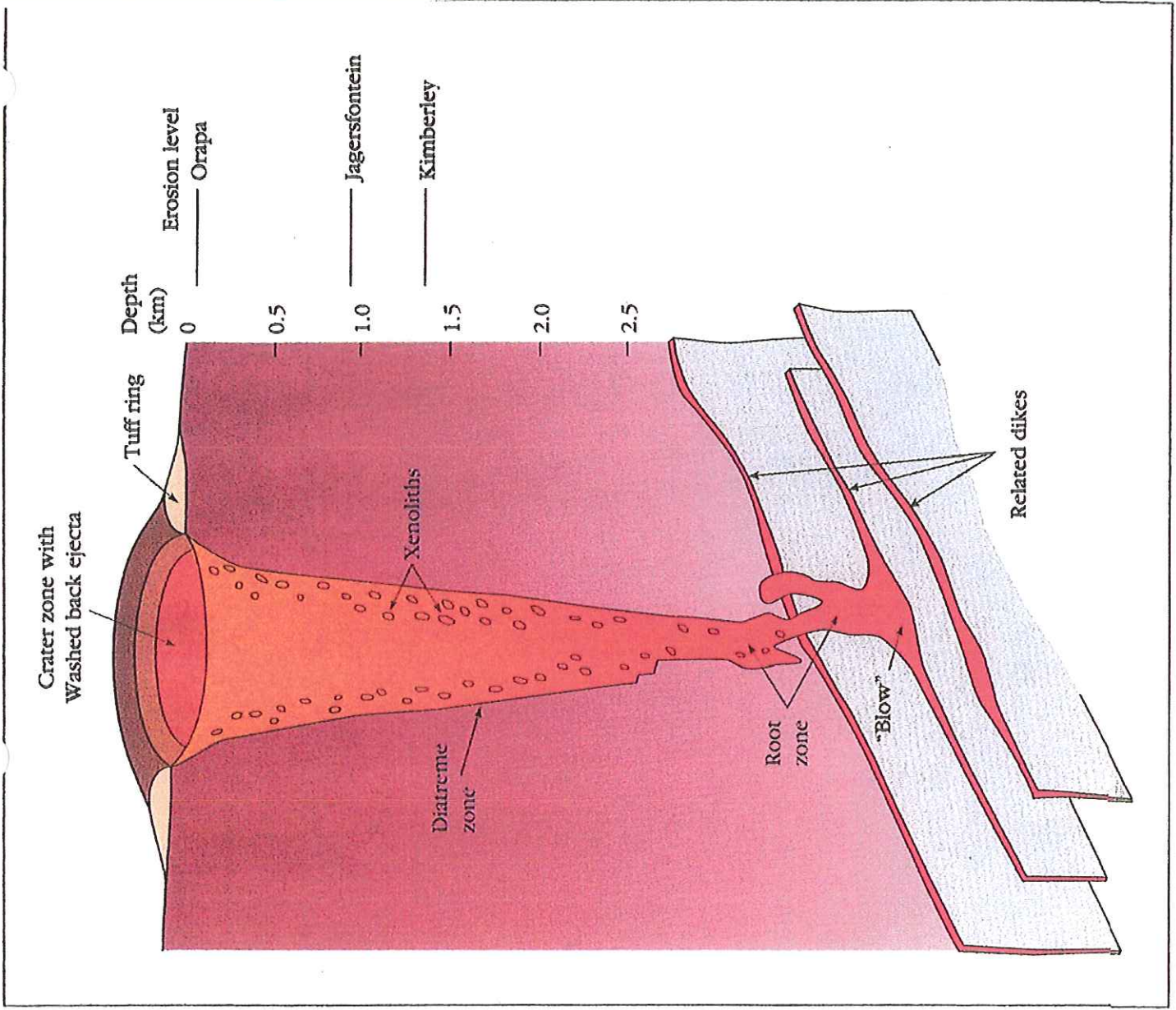


Figure 3. This cross section sketch of a typical kimberlite pipe shows the carrot-shaped profile. The root zone is the point where the high velocity eruption commences, in which exsolved gases blow out the fragmented kimberlite (tuff breccia) including volcanoclastics that form the volcano's tuff ring. The crater zone partially refills with ejecta that falls or washes into the crater. Depth measurements show the levels of erosion for various kimberlite pipes in South Africa. (Adapted from Hawthorne, 1975, and Mitchell, 1995.)



Both coesite and stishovite found at Meteor Crater — produced by high P, T associated with the impact (Fig. 4.4)

J&R call this shock metamorphism

Fig. 3 ↗

Coesite also found in association with diamonds in kimberlite pipes

Both were synthesized before being found in natural rocks.